EXPERIMENTS USING A WILSON CLOUD-CHAMBER TO INVESTIGATE THE NATURE OF THE RADIATION PRODUCING THE HIGH-ENERGY SCINTILLATIONS OBSERVED IN AN ACTIVATED PHOSPHOR.

Thesis

submitted by

Robert Michael Hudson

B.Sc., (London)

for the Degree of

Doctor of Philosophy

University of Edinburgh

October, 1958.

PREFACE

The research described in this thesis has been carried out in the Department of Natural Philosophy of the University of Edinburgh, under the joint direction of Professor N. Feather, F.R.S. and Dr. G.R. Evans.

CONTENTS

	Page
Preface	i
Chapter 1.	
INTRODUCTION.	1
Chapter 2.	
DESCRIPTION OF CLOUD CHAMBER AND ASSOCIATED ELECTRONICS.	
2.1. Introduction	7
2.2. Description of chamber.	7
2.3. The electric clearing field.	9
2.4. The chamber valves and associated mechanism.	9
2.4.1. The expansion valve	9
2.4.2. The filling valve	10
2.4.3. The slow expansion valve	10
2.4.4. The recompression cylinder and valve	11
2.4.5. The reservoir pressure control system	12
2.4.6. Summary of mechanical details	13
2.5. The photographic mechanism.	
2.5.1. The cameras	14
2.5.2. The chamber illumination system	16
2.6. The chamber hut and thermostatic control.	
2.6.1. The chamber hut	17
2.6.2. The thermostatting arrangement	17
2.7. The electronic control system.	18
2.7.1. The original system	
2.7.2. The present system	19
2.8. Summary.	27
Chapter 3.	
EXPERIMENTAL BEHAVIOUR OF CHAMBER.	
3.1. Introduction	

Page

3.1.1. Application of fast recompression to reduce the recycling time of a cloud chamber 28
3.1.2. Filling gas and physical operation of chamber 31

3.2. Experimental work to try to discover the reason why clearing expansions are required.

3.2.1. Effects due to the rubber diaphragm 32
3.2.2. Temperature effects 36
3.2.3. Other effects possibly present 36

3.3. Chamber recycling time.

3.3.1. Original recycling time 37
3.3.2. Recycling time with fast recompression 38

3.4. Optical problems. 39

Chapter 4.

DESCRIPTION OF SCINTILLATION COUNTERS AND ORIGINAL COINCIDENCE SYSTEM.

4.1. General. 40

4.2. The scintillation counter.

4.2.1. Theoretical 40
4.2.2. The large counter 49
4.2.3. The small counter 50

4.3. The cathode followers. 51

4.4. The pulse amplifiers. 51

4.5. The descrimination system. 52

4.6. The coincidence circuit. 53

4.7. Summary of coincidence arrangements used. 53

Chapter 5.

CONSTRUCTION AND CALIBRATION OF A SINGLE-CHANNEL PULSE HEIGHT ANALYSER.

5.1. Theory of operation. 55

Page

5.2. Constructional details. 57

5.3. Calibration of analyser.

5.3.1. The lower level 58
5.3.2. Channel width 58

5.4. Uses of analyser. 59

Chapter 6.

INTRODUCTION TO MILLIMICROSECOND PULSE TECHNIQUES.

6.1. General 60

6.2. Definition of resolving time of coincidence circuits. 60

6.3. Applications of fast coincidence circuits. 61

6.3.1. Time of flight measurements 62
6.3.2. Reduction of chance coincidence rate 63
6.3.3. Measurement of very short half lives 63

6.4. Components of a fast coincidence system.

6.4.1. General 64
6.4.2. Counters 64
6.4.3. Amplifiers 65
6.4.4. Pulse-shaping circuits 66
6.4.5. Discriminator and trigger circuits 66
6.4.6. Coincidence mixers 66

6.5. The complete coincidence system. 68

Chapter 7.

CONSTRUCTION AND THEORETICAL OPERATION OF A FAST COINCIDENCE UNIT.

7.1. General introduction to the apparatus. 69

7.2. Theoretical description of operation of each channel.

7.2.1. General 70
7.2.2. The photomultiplier 70
7.2.3. The cathode follower 75
7.2.4. The pulse shaping circuit 77

		Page
7.2.5.	The amplifier stage	79
7.2.6.	The discriminator and trigger circuit	82
7.2.7.	Summary of channel description	84
7.3.	Theoretical description of operation of coincidence mixer.	84
7.4.	Concluding remarks.	87
7.5.	Constructional details and auxiliary apparatus.	
7.5.1.	General	87
7.5.2.	Voltage distribution chassis	87
7.5.3.	Preamplifier	89
7.5.4.	Delay-line box	89
7.5.5.	Conclusion	91

Chapter 8.

EXPERIMENTAL TESTS OF FAST COINCIDENCE UNIT.

8.1.	Determination of resolving time of unit.	
8.1.1.	Introduction	92
8.1.2.	Theory of delayed coincidence method and shape of curves obtained	92
8.1.3.	Experimental arrangement	97
8.1.4.	Method of measuring resolving time of circuit using a double pulse generator	99
8.1.5.	Conclusions	100
8.2.	Time of flight measurements for gamma-rays from Cobalt 60, using coincidence unit.	
8.2.1.	Introduction	101
8.2.2.	Experimental arrangement	102
8.2.3.	Preliminary experiments	103
8.2.4.	Measurements on the chance coincidence rate for the coincidence unit	108
8.2.5.	Successful time of flight measurements	110
8.3.	Delayed coincidence curves using cosmic rays.	115
8.4.	Summary	116

Chapter 9.

THE RESPONSE OF THE PLASTIC PHOSPHOR TO COLLISION ENERGY LOSS, AND THE COUNTING EXPERIMENTS WITH THE LARGE COUNTER

		Page
9.1.	Introduction.	117
9.2.	Consideration of the phosphor response to particles of different energies and different kinds.	
9.2.1.	Theoretical response of phosphor	117
9.2.2.	Collision loss and range of particles in the plastic phosphor	118
9.2.3.	Linearity of response of phosphor to different energy losses	121
9.3.	Pulse height - Frequency distribution curves for large scintillator for γ -rays and μ -mesons.	
9.3.1.	Distribution for Rd Th γ -rays	123
9.3.2.	The cosmic-ray spectrum	124
9.4.	Detection of showers occurring in lead.	
9.4.1.	General introduction	125
9.4.2.	Experimental Rossi curve	127

Chapter 10.

THE CLOUD CHAMBER WITH COUNTER CONTROL

10.1.	General Introduction.	129
10.2.	The photographs.	136
10.2.1.	The large scintillator and Geiger counters in coincidence	136
10.2.2.	The large scintillator only	138
10.2.3.	The large and small counters in coincidence	144
10.2.4.	Photographs taken with the small counter only, with 15 cm of lead above the counter	144
10.3.	Conclusions.	145

Chapter 1.

INTRODUCTION

In recent years, the scintillation counter has been proved to be of great value in those experiments in which nuclear particles and electrons are involved. The counter makes use of the fact that short bursts of light, or scintillations are observed whenever a charged particle passes through, or stops in, certain materials such as, for example, activated sodium iodide crystals. The amount of light emitted is a function of the energy lost by the particle in the scintillating material (or scintillator) which in turn is a function of its velocity and charge. It is therefore possible to use the scintillator to differentiate between similar particles having different velocities, or different particles having the same momentum.

In the majority of these applications the light output corresponds to the dissipation in the scintillator of only a few MeV. However, there are observed occasionally large bursts of light corresponding to a total energy loss of several hundred MeV. In the experiments to be described later, pulses corresponding to an energy loss in a plastic scintillator of over 1 GeV have been recorded but only at a frequency of not more than one per 40 hours. These large pulses can only be due to cosmic ray events, and it has been the aim of this work to study these large pulses, to investigate what type of process could produce them.

As long ago as 1932, Blackett and Occhialini using Geiger counters discovered cosmic ray showers. They were able to unravel the nature of the particles in these showers by using a pulse from the counter system to trigger a cloud chamber. Rossi, too, in 1933,

by counting coincidences between three trays of counters, investigated the production of showers in lead, giving the so-called "Rossi Curve" relating frequency of shower production to thickness of absorber. Since then, a great variety of arrangements have been used, with or without the cloud chamber. Those arrangements described by Rochester (1946) and by Butler et al (1950) are typical of the many systems in use in cosmic ray investigations during the past twenty-five years.

There are three distinct types of cosmic ray showers:

(i) Cascade (or electron) shower,

(ii) "Knock-on" showers

and (iii) penetrating showers.

Any or all of these showers may occur as part of large "air showers" covering areas of several hundred square metres.

Of greater interest and importance are the penetrating showers, consisting of relatively small numbers of light and heavy mesons produced by the nuclear component of cosmic rays in and near the apparatus. This nuclear component represents only a small fraction (of 1%) of the total radiation even at an altitude of 7,000 ft. and hence penetrating showers occur only infrequently.

In June 1953, an experiment run jointly by two groups, one from the University of Edinburgh and the other from University College, London, was set up at a mountain station in the Dolomites at 7,000 ft. to study the heavy mesons. Coincidences from two trays of Geiger counters were used to trigger a cloud chamber. The electronic circuit, which in its ultimate state was designed by Mr. A. Metheringham, triggered the chamber on five-fold

coincidences made up in various ways i.e. 4-1, 3-2 ... etc., two of these alternatives being operated simultaneously. A detailed analysis of the cloud chamber photographs gave a 15% detection efficiency for penetrating showers containing three or more penetrating particles, produced in single events in or near the chamber. The majority of the remaining photographs showed only electron or knock-on showers. The difficulties which are encountered in the operation of such a system can best be treated by referring to the details of the Marmolada system.

One tray of counters was placed immediately above the chamber, the other one below the chamber. Generally, each tray was covered top and sides with lead of thickness 10 cm, the top layer acting as the target for the fast nucleons striking the system. Since the interaction length of these particles in an absorber is about 100 gm/cm^2, about two thirds of the particles would interact in the lead. On account of the geometry of the system only a fraction of these events, about 25%, would trigger the lower tray of counters, partly because the secondary particles may not be travelling vertically and partly because the smaller showers would be unable to discharge the required number of counters in the tray. If the lower tray is set for n-fold coincidences where $n \geqslant 2$, more than n particles are required,(on the average,) to make certain that a coincidence is recorded.

The lower lead shield helps to reduce the number of electron showers recorded by the system. These showers are a nuisance and are extremely difficult to avoid. A fast electron striking the top lead shield multiplies, producing electrons and photons in a

cascade process. These secondary electrons are absorbed in the lead but unfortunately the photons are not so easily absorbed and some of these may eventually reach the lower tray. One very striking example of this was taken at Marmolada; a photograph showing about 20 tracks of low energy Compton recoil electrons was obtained but no other tracks although the hodoscope reading showed a 10-10 coincidence in the counter trays.

"Knock-on" showers are also difficult to avoid. A fast μ-meson producing a small knock-on shower can trigger the top tray, and a second shower in the lower lead shield triggering the lower tray even although all of the electrons in the first shower are completely absorbed in the lead shielding. Increasing the amount of lead makes no difference to the number of such showers due to the great penetrating power of these mesons.

After awhile it seemed that there would be no advantage to be gained by any re-arrangement of the counter system. Any further improvement could only be gained by exploring the possibilities of using a different type of counter.

In most interactions or "stars" involving nucleons, low energy nuclear particles ("evaporation" particles) are emitted in addition to the meson secondaries. Hence if a detection technique, sensitive only to these slow particles were used in conjunction with the conventional system, a more efficient system should result. Interesting and encouraging results had been reported by Salvini(1951) and Ascoli(1952) using scintillation counters. It was therefore decided to set up at sea-level a pilot scheme to explore the best and most efficient way of using these counters, and to decide whether or not it would be better to use only scintillation

counters or to use a mixed system.

In the new system, two scintillators were to be used, to replace the original Geiger counters. One of these would also, in addition, replace the top lead shield and act as the target for the incident nucleons. If a high energy star was produced in this scintillator, the evaporation particles having only small range would be stopped giving a large light output. The secondary particles, most π -mesons escaping from this scintillator would be recorded by the second scintillator, the chamber being triggered by a 2-fold coincidence. This second scintillator is necessary because only about 10% of the stars occurring in the top scintillator contain fast meson secondaries, the other 90% being due to the capture of relatively low energy nucleons. The question of size of scintillator is important. A large scintillator is sensitive to electron showers of all kinds, giving a total light output similar to that obtained from a star. This difficulty can be avoided by using several small Sodium Iodide crystals, each having its own photomultiplier, and arranging that the chamber be triggered by a 2-fold coincidence between any one of these counters and the lower counter. This second counter should have a large area and for this a slab of plastic scintillator is ideal.

Since only 2-fold coincidences are required, it is necessary to have a coincidence unit of small resolving time and for this a resolving time of not more than 20 milliμsec. was aimed at.

This ideal arrangement is not a very practical one to use as a pilot scheme, particularly at sea-level owing to the very low intensity of the star producing radiation. Accordingly attention

was concentrated on an investigation of the large pulses of light which were observed using a piece of plastic scintillator, to make sure in the first place that these were due entirely to cosmic ray events.

To assist in the interpretation of these observations, an automatic cloud chamber was constructed. Also a new coincidence system was constructed. The details of these experiments will be described in the following chapters, giving first of all information about the cloud chamber and followed in later chapters by a description of the various electronic circuits which have been constructed and tested. Finally, a chapter is devoted to pictures taken with various counters arrangements, consisting of one and then two scintillation counters and also of a mixed system consisting of one scintillation counter and one tray of Geiger counters.

Chapter 2.

DESCRIPTION OF CLOUD-CHAMBER AND ASSOCIATED ELECTRONICS

2.1. Introduction.

The cloud chamber described here is based on a design by E.J. Williams (1939). The original form of the present apparatus has been described by D.N. Davies, with whom the writer was working during his first year of research. The chamber itself will therefore only be described briefly.

The modifications made by the writer, including adaptation of the chamber to automatic working, and the design and construction of a new control system to operate it will be described later in this chapter. Fast recompression of the cloud chamber is used, and one to three clearing expansions can be done automatically after a fast expansion, in order to clean the chamber.

In addition to investigating the improvement in recycling time produced by the recompression, an automatic chamber was desirable so that long runs of photographs could be taken without attention. This was particularly necessary for the experiments using a fast coincidence system for chamber triggering to be described in Chapter 10, where fairly fast repetition rates were used.

2.2. Description of chamber.

The main features of the chamber are shown in figure 1. The working volume, V, has a diameter of 13 inches and a depth of 4 inches, consisting of the volume between the plate P, the pyrex cylinder B, and the chamber window A. The plate P has holes of diameter $\frac{1}{4}$ inch drilled in it, at a separation of 1 inch. The

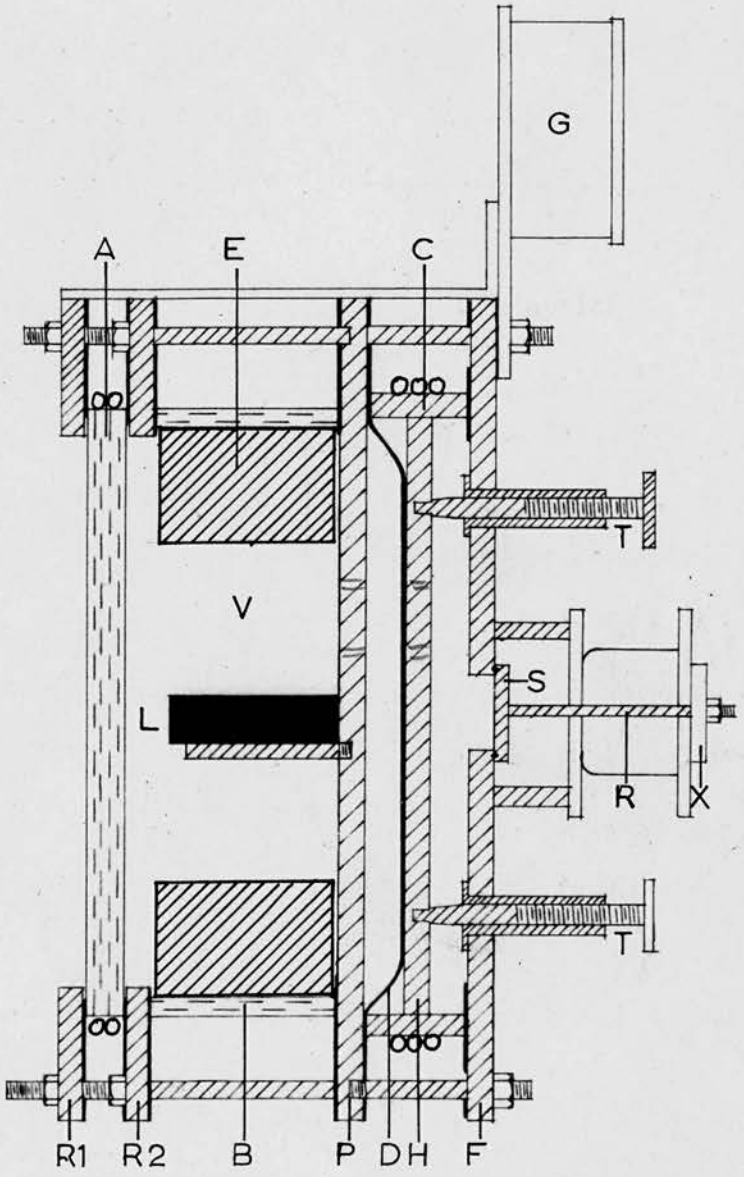

Figure 1. Side view of the cloud chamber

front surface of this plate is covered by a circular piece of black velveteen stitched to the plate, to provide a suitable background for photography. The rubber diaphragm D is held to the back of the plate P, and the movement of this diaphragm between P, and a moveable perforated plate H determines the expansion ratio of the chamber. The plate H can be moved away from or towards P; the two plates remaining parallel, by means of three symmetrically placed screws T, projecting from the back of the chamber. The volume between the diaphragm, the brass ring C and the chamber back plate F can be pressurised, forcing the diaphragm forward against the pressure in the working volume.

Pressure gauges G are connected to the working volume and the back volume of the chamber. They are used to measure the pressure in the working volume, and to ensure that the diaphragm has been pumped hard forward against this pressure when the chamber is being operated.

A hole $1\frac{3}{8}$ inch in diameter is drilled in the centre of the chamber back plate F. This is normally closed by the expansion valve (see section 2.4.1.) Two Klinger stop-cocks are screwed into the plate F. One is for admitting gas to force the diaphragm forward, and the other one which communicates with the atmosphere, is for performing slow expansions.

Thin copper pipes are wound round the front window and round the brass ring C. Cold water circulates through them, and helps to keep the chamber at an even temperature.

2.3. The electric clearing field.

An electric field is used to remove any ions from the sensitive volume which are formed while the chamber is waiting to be expanded. If these ions were not removed, drops would be formed on them during the fast expansion, increasing the background cloud.

The field electrodes E (figure 1), originally consisted of copper gauze and were each supported by three bakelite rods threaded into the plate P. For reasons to be mentioned later, the electrodes were eventually made from thin copper sheet, in contact with the chamber wall B, and held in position by vacuum grease. The electrical connections to the electrodes are introduced through holes in the ring R_2, which are sealed at each end by rubber bungs to act as pressure seals and to insulate the input leads.

A lead block L, $11\frac{1}{2}$ inches x $3\frac{1}{2}$ inches x 1 inch is supported horizontally at the centre of the chamber by means of two $\frac{1}{2}$ inch diameter threaded rods which are screwed into the plate P. This acts as the second clearing electrode for each half of the chamber, as the other electrodes are both at the same positive potential. It is also used to estimate the energy of particles forming tracks, as the energy loss in passing through it can be computed.

2.4. The chamber valves and associated mechanism.

2.4.1. The expansion valve.

The expansion valve can be seen in figure 1 . The hole in plate F is sealed by the brass disc S, which has an O-ring embedded in a groove in its front face, and can be held against the plate by the electromagnet M. A brass rod R is hard soldered to S, and has a disc of soft iron X threaded onto it. The electromagnet

coil is wound with 40 gauge wire and energised by an ex-government rectifier giving 120V D.C. When the disc X is in contact with the flat face of the magnet, sufficient holding power is available to keep the valve closed against the pressure in the back volume of the chamber. As the back volume pressure may be as great as 25 lb. per sq. in. above atmospheric, and the area of the valve is 2 sq. in., the maximum force needed is 50 lb. wt.

2.4.2. The filling valve.

The front of the chamber can be filled with gas through a filling valve, which is connected to a hole drilled in the side of the plate P, and connecting with the front of the chamber. This hole can be sealed off from the outside, by means of a needle valve, the point of which seats into it. This prevents any pockets of gas in the filling valve from interfering with the chamber action, by introducing gas into the front volume at a different temperature from the rest.

A Klinger stop-cock is connected to the filling valve, to which a gas cylinder can be attached. When filling the chamber, alcohol is put in the valve, and is then carried into the front volume with the gas entering from the cylinder.

2.4.3. The slow expansion valve.

In order to introduce cleaning expansions into the automatic cycle, a slow expansion valve was required. This is fixed to the back of the chamber, and can be operated magnetically to let out the gas in the back volume slowly.

Figure 2 shows the construction of this valve. The hole A, $\frac{3}{8}$ inch in diameter can be sealed by the rubber bung B. The outlet C

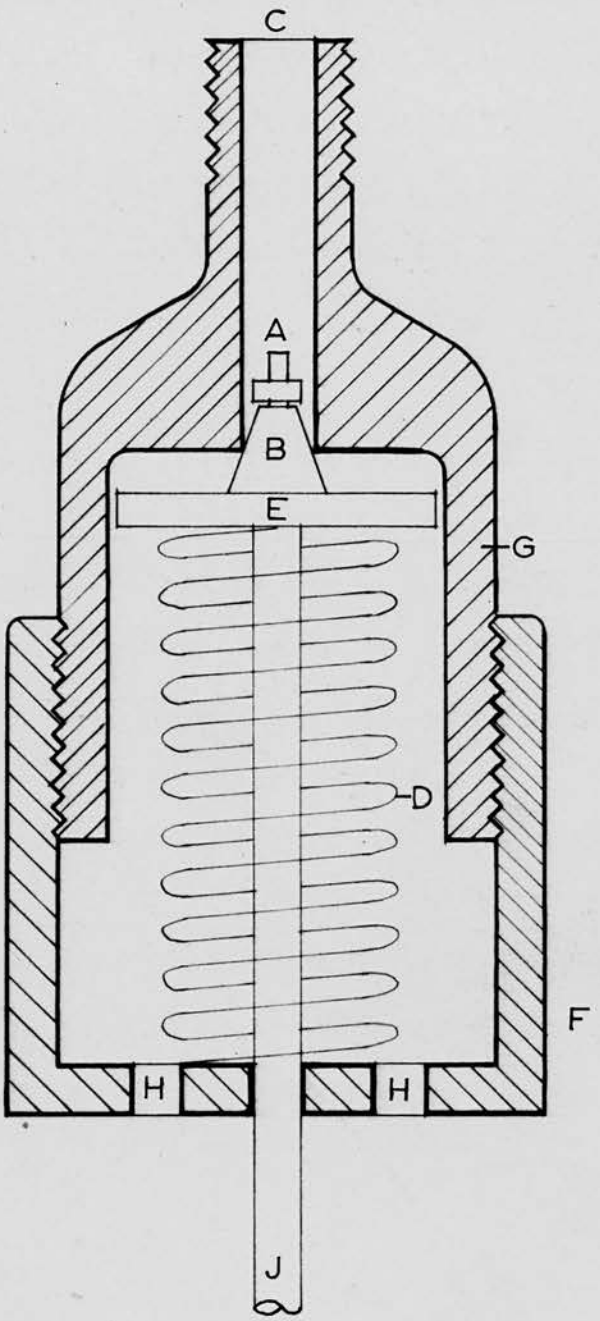

Slow Expansion Valve

Figure 2

is connected to the back volume of the chamber by rubber pressure tubing. The valve can be kept closed against the back volume pressure by means of the spring D which bears against the disc E. The tension of this spring is adjusted by varying the position of the valve cap F, which is threaded onto the valve body G. Holes H in the flat face of F allow gas to escape from the back volume when the valve is opened.

The shaft J is connected to an electromagnet, which is a modified version of an ex U.S. Navy bomb release mechanism. The coil has been rewound to operate at 120V D.C. With a back volume pressure of 25 lb. per sq. in., a force of about 3 lb. wt. is required to keep the valve shut. In order to open the valve, the electromagnet is energised, and the valve is then opened against the spring.

2.4.4. The recompression cylinder and valve.

After each chamber expansion (slow or fast) the back volume of the chamber needs to be re-compressed, in order to be ready for the next expansion. This is done by opening a valve and connecting a large pressure reservoir to the back volume of the chamber. The reservoir is maintained at a pressure of about 25 lb. per sq. in. When the valve is opened, the pressures equalize at about 22 lb. per sq. in.

The pressure reservoir consists of a modified Calor gas cylinder and has a volume of about 11/12 cubic ft. The re-compression valve is mounted directly on the top of the reservoir cylinder, the base of the valve assembly screwing into the top of the cylinder. The lower part of the valve, which is turned from

a single piece of brass, also carries inlet connections for the pump and for the pressure control switch. These inlets communicate directly with the reservoir.

The valve is shown in figure 3 . The hole A of diameter 1½ inches communicates directly with the reservoir pressure, the threaded portion of B being screwed into the top of the reservoir. The valve can be closed by the moveable piston C, the O-ring D making the pressure seal. C is hard soldered to a steel shaft E, which passes through a hole in the top part of the valve F. The pressure seal is made by the O-ring G. An O-ring H makes the seal between B and F. A tendency for the O-ring in the piston to blow out when the valve opened was corrected by drilling some small radial holes J, which equalize the pressures at the inside and outside parts of the O-ring.

The shaft E then passes through a hole in the centre of the iron core K of the electromagnet L. A circular iron disc M is threaded into the top of the shaft to complete the magnetic circuit. The position of M can be adjusted to obtain the most efficient sealing action. The magnet coil N is of 40 gauge copper wire, wound on an insulating former P. The magnet is energized by a supply of 120V D.C.

The outlet R is connected to the back of the chamber by pressure tubing of diameter 1½ inches. This tubing, and the gas passage inside the valve, were made as large as possible in order to obtain maximum speed of recompression.

2.4.5. <u>The reservoir pressure control system</u>.

The pressure in the reservoir is maintained approximately

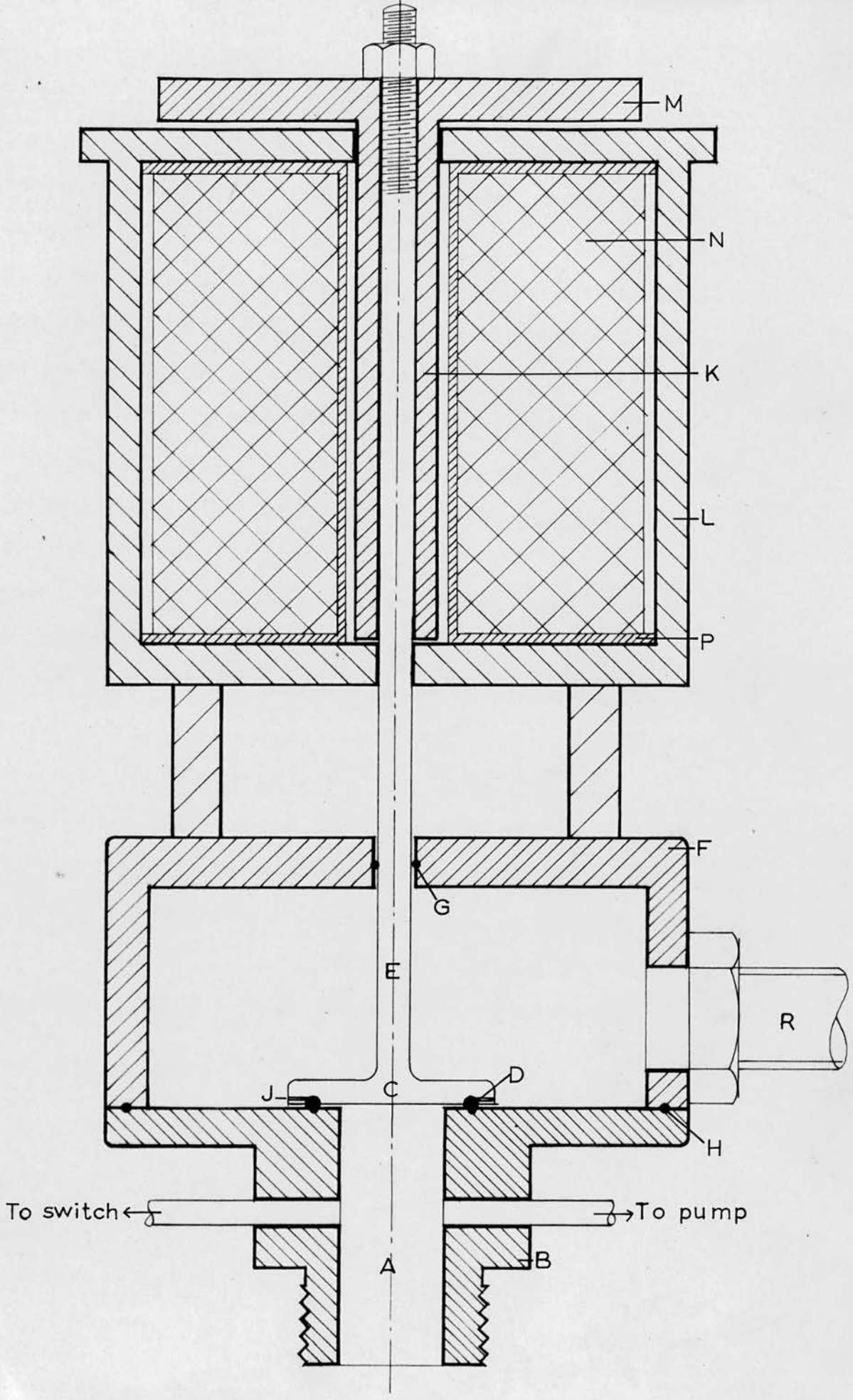

Recompression Valve

Figure 3

constant by means of a pump controlled by a pressure switch. This switch is so arranged that the pump is switched on whenever the pressure in the reservoir falls below about 24 lb. per sq. in., and is switched off again when the pressure has risen to 25.5 lb. per sq. in.

The pressure control is a type K6/TIE/2 manufactured by Teddington Industrial Equipment Ltd. The operating element of this control consists of a flexible metallic bellows unit, which is connected directly to the reservoir. The movement of the bellows resulting from pressure changes is employed to operate a mercury tube switch. The bellows movement is opposed by a spring, the compression of which can be varied manually to raise or lower the operating point (10 - 55 lb. per sq. in.) The differential pressure (the difference in pressure between the point at which the switch makes the circuit on fall of pressure, and the point at which it breaks the circuit on rise of pressure) is also adjustable and this is used at its minimum value of 1.5 lb. in^{-2}. The switch is set to operate at 24 lb. in^{-2} and pump to 25.5 lb. in^{-2}. It is ensured that the diaphragm will still be pushed hard forward even if the reservoir pressure is at its lower limit when re-compression takes place.

2.4.6. Summary of chamber mechanical details.

The layout of the chamber, and the valves described in the last few sections is shown in figure 4. The volume A represents the back volume of the chamber, R is the pressure reservoir, V_1 the fast expansion valve, V_2 the recompression valve and V_3 the slow expansion valve. B is the compressor pump and P the pressure control.

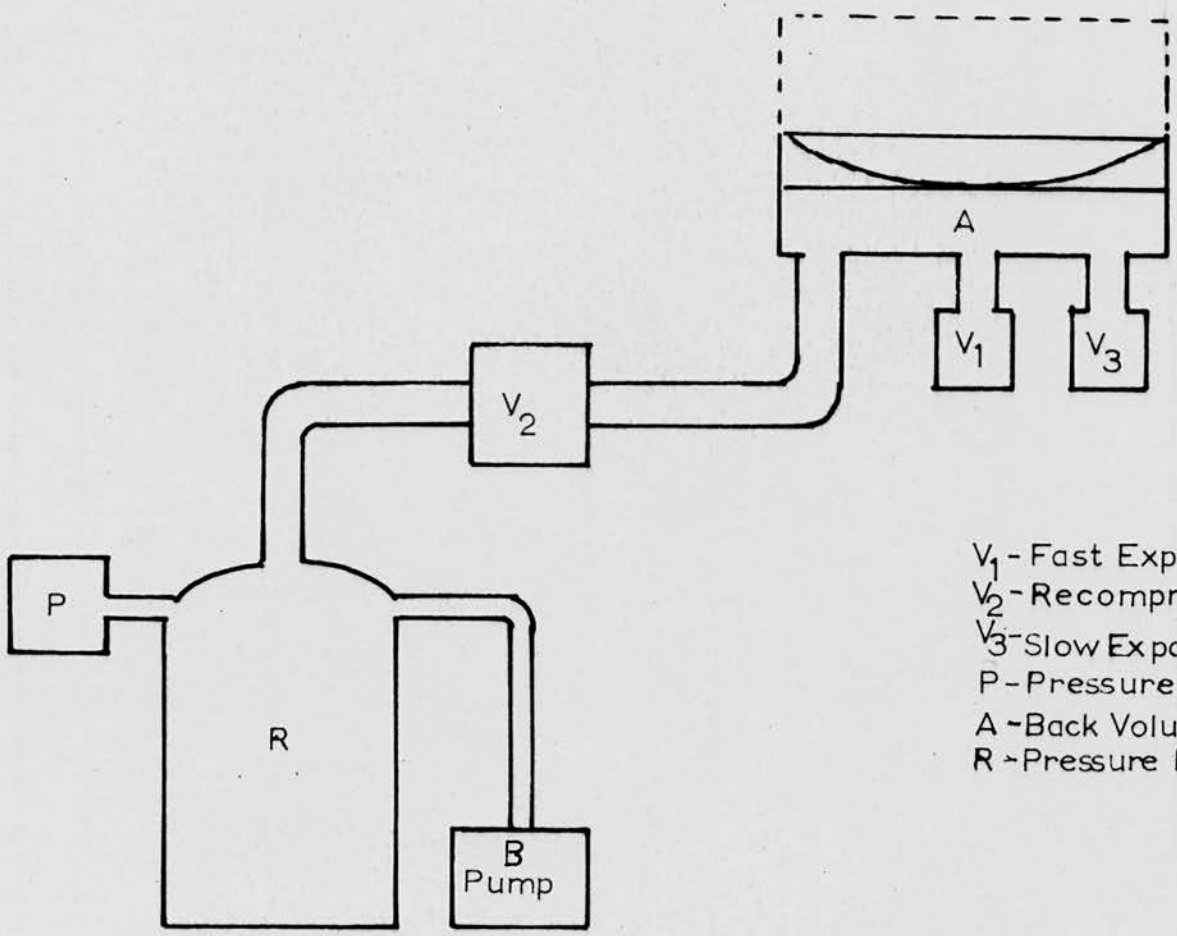

V_1 - Fast Expansion Valve
V_2 - Recompression Valve
V_3 - Slow Expansion Valve
P - Pressure Control
A - Back Volume of Chamber
R - Pressure Reservoir.

Arrangement of the Mechanical Valves for the Cloud Chamber. Figure 4

2.5. The photographic mechanism.

2.5.1. The cameras.

Two cameras have been used with the chamber. The original plate camera was replaced when the chamber was made automatic, as a camera using 35 mm. film was much more convenient. This can easily be wound on automatically after a picture has been taken.

(a) The original camera

The original camera used with the chamber was a plate camera taking plates $3\frac{1}{4}$ in x $4\frac{1}{4}$ in. Photographs were taken in stereoscopic pairs, the camera having two Zeiss lenses, focal length f = 5 cm. and maximum aperture of f 4.5. The horizontal separation of the lens axes was 2 inches. The camera was mounted on a wooden platform at such a height that the line joining the lens axes was on the same level as, and parallel to, the horizontal diameter of the cloud-chamber. By inserting a ground glass screen in the camera, tests could be made to determine the position of the plane of best focus. The distance between a convenient point on the camera, when in position on its stand, and the centre of the sensitive volume of the chamber was measured. The camera was then mounted away from the chamber and focussed on a steel rule, being adjusted until the plane of best focus occurred at the measured distance. Allowance was made for the shift of the apparent position of the object due to the thick front window of the chamber.

(b) The present camera

This camera uses two Dallmeyer anastigmatic lenses, of maximum aperture f 3.5 and focal length 35 mm. These lenses

have been matched by the makers for use as a stereoscopic pair. The lenses are mounted in the front of the camera with a horizontal separation of their axes of two inches. Photographs are taken on 35 mm recording film, Ilford Type 5G91. The lenses are placed at such a distance from the film as to enable the whole chamber to be included in a photograph, with the plane of best focus approximately at the centre of the illuminated part of the sensitive volume. This necessitates the camera being considerably farther from the chamber front window than had been the case with the plate camera.

The camera is mounted on a horizontal wooden platform so that the line joining the centres of the lenses is horizontal and passes through the chamber horizontal axis. It is also symmetrical with respect to the chamber, when viewed from above. A shaft in the bottom of the camera, which operates the wind-on sprocket and take-up spool in the camera through suitable gearing, passes through a hole in the wooden platform and engages with a vertical shaft. This shaft is coupled, through suitable reduction gearing, to a small A.C. motor, which winds on the film. A switch operated by a cam, which is also rotated by the motor, serves to switch it on for a suitable time to wind on the film a sufficient amount. As there is a fairly large space between the two photographs in a given pair, the next pair is taken with one photograph between the two images of the succeeding pair. Thus, the cam is arranged to wind on lengths of film in the ratio three to one at alternate operations.

The cam operates the motor by pushing down a relay, the motor circuit being made by the relay contacts. In order to start the

operation, the relay is brought down by passing a current through its coil, until the cam has rotated far enough to hold it down mechanically. The relay coil circuit is made by one of the uniselector contacts (see later), the wind on taking place soon after the photograph has been taken.

It is possible to load 100 feet of film into the camera at one time, although the take-up spool can only hold film equivalent to 60-80 pictures. At fast rates of photography, therefore, development of exposed film must be done fairly often.

2.5.2. The chamber illumination system.

(a) The photoflash tubes

Two straight photoflash tubes are used to illuminate the sensitive valume of the chamber. These are Siemens type SF5 and have an effective length of about 7.5 inches. The tubes are enclosed in lamphouses made of Tufnol sheet. The power for the lamps is obtained from photoflash condensers of total capacity 99 F for each lamp, and charged to a potential of about 2,300 volts. These condensers can be placed across the lamps for a short period without discharging through them. A small coil of bare copper wire is wound round each flash tube, about 3 inches from the end of the tube which is at earth potential. The coils from both lamps are connected to the secondary of a spark coil, and when the primary is excited, the insulation in the flash tubes breaks down. The condensers then discharge, dissipating about 260 joules in each lamp. A general arrangement drawing of the front view of the cloud chamber showing the lamps is given in figure 5 . The condenser circuit is given in section 2.7.2.(g). The camera shutters are left open while waiting for a photograph.

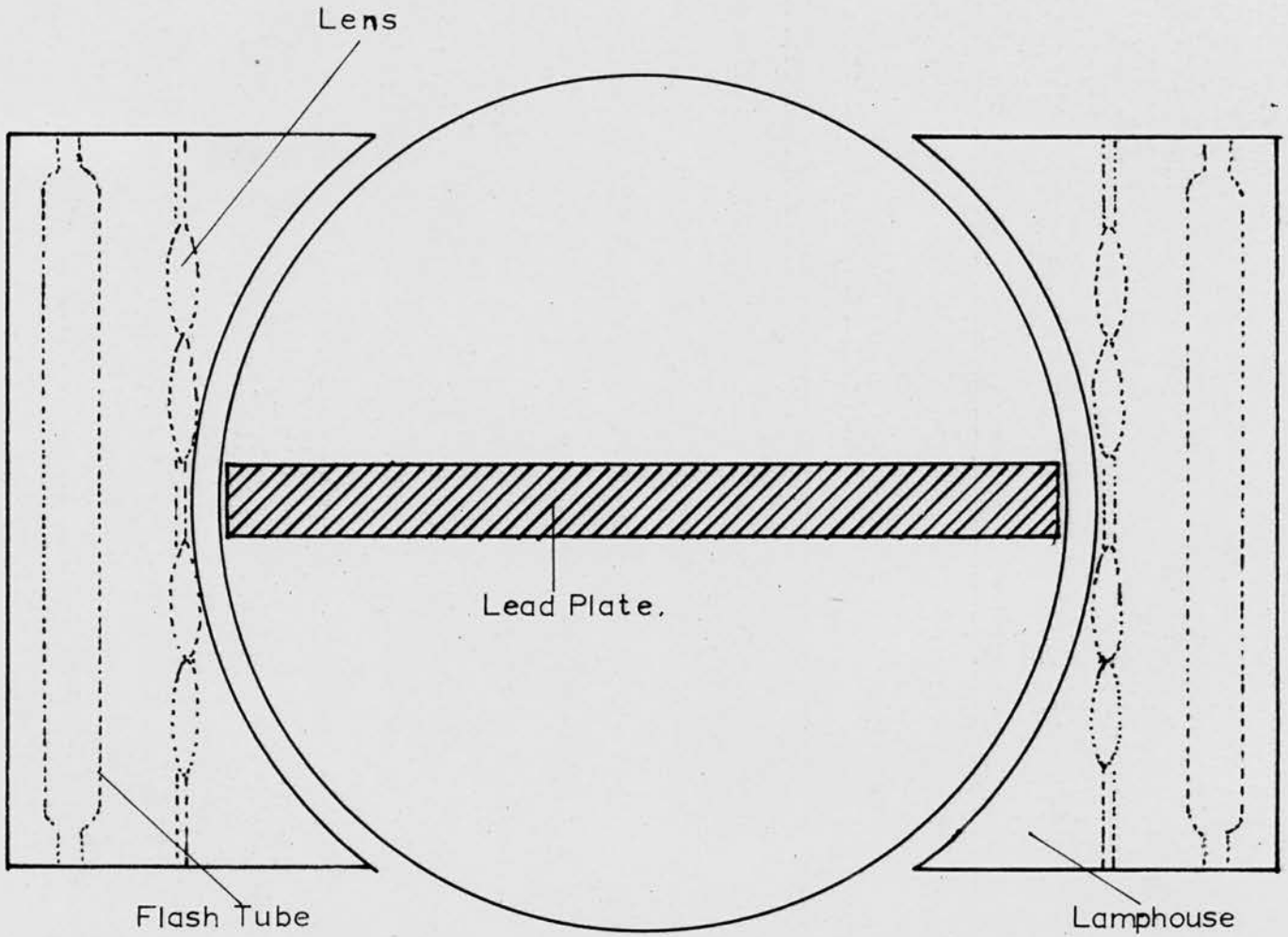

General Arrangement Drawing of the Front View of the Cloud Chamber, Showing the Illumination System.

Figure 5

(b) The lamp lens system

Originally, two plano-convex lenses were used to produce an approximately parallel beam of light from the flash tubes. A length of 2 inch diameter perspex rod was cut down a diameter, one half being fixed to the front of each flash tube, the flat surface of the lens being in contact with the tube. Together with stops in front of the lamp, this system worked reasonably well while the plate camera was in use.

When the present camera was brought into use, the photographic background was much worse, partly because of the smaller size of the negatives. The original lenses were removed, and a system of short-focal length convex lenses substituted. This system is described in the next chapter (section 3.4.)

2.6. The chamber hut and thermostatic control.

2.6.1. The chamber hut.

The chamber, and the associated equipment including the pump and the recompression reservoir, is enclosed in a fibreboard hut. This serves two purposes:-

(i) It enables the chamber to be kept at an even temperature by means of thermostatting,

(ii) As the hut is light-tight, the camera can be left with the shutters open for long periods without fogging the film.

2.6.2. The thermostatting arrangement.

This consists of a fan and three tubular electric heaters. The fan is fixed to the inside wall of the hut and blows air past a coiled copper pipe through which cold water flows. Its

function is to circulate cold air throughout the hut. The three heaters are placed along three walls of the hut, and are operated by a bimetallic thermostat. An indicator light outside the hut shows when the heaters are on. The thermostat temperature setting is adjusted until the indicator light shows that the heaters are being turned on and off regularly, so that an equilibrium hut temperature is being maintained. This temperature is usually about 65°F.

2.7. The electronic control system.

2.7.1. The original system.

The control system used before the chamber was made automatic will only be described very briefly.

When the chamber was triggered, either manually or by a pulse from a counter system, a thyratron conducted and tripped a relay. This opened the expansion valve circuit, shorted out the clearing field and operated a second relay which changed over the photoflash condensers from the charging position, to across the flash tubes.

After a variable delay, produced by charging a condenser through a variable resistance, a thyratron conducted and operated a relay which discharged a condenser through the spark coil primary, flashing the lamps. A photograph was then taken. The purpose of the delay was to allow time for the drops to grow to visible size before being photographed.

Before taking another photograph, the electronics had to be reset, when the photoflash condensers were re-charged. Hence,

a second photograph could not be taken accidentally on the same plate if the chamber was left overnight.

2.7.2. The present system.

(a) Control Sequence

The sequence of operations in the automatic cycle is given below. The number of clearing expansions performed can vary from zero to three, according to the necessity. The stages are:-

(1) Open expansion valve and short clearing field to earth. Change over photoflash condenser relay.

(2) Make variable photographic delay (0.1 - 0.2 sec.)

(3) Trigger flash tubes to take photograph, and open recompression valve.

(4) Close recompression valve, wind on camera and make delay (about 15 sec.) to allow temperature equilibrium to be reached.

(5) Open clearing expansion valve and make delay (about 15 sec.) to allow cloud formed in clearing expansion to fall to the foot of the chamber.

(6) Close clearing expansion valve and recompress.

If more than one clearing expansion is done, the stages 4 - 6 are repeated each time.

After the final clearing expansion a delay of up to two minutes can be made to allow the chamber to settle down. During the whole cycle after the chamber is first triggered, the input is disconnected until the cycle has been completed. The clearing field is put back on after stage 6.

(b) The uniselector

A uniselector is used to carry out the cycle sequence. This consists of a multiposition switch, having fixed contacts arranged in banks around a semicircular arc. Moving wiper arms (one for each bank) make contact with each pin of the bank in turn. The operation is electromagnetic, the selector moving round by one contact when current is passed through its coil for a short time. The selector used in this case has four banks with separate wiper arms. These instruments are sometimes arranged so that the banks are associated in pairs - one bank for each half of a complete 360° rotation. In this case the selector reaches its initial position after every 180° rotation.

One bank is used to make the connections necessary in order to rotate the selector with appropriate delays. The other three banks are used either to switch in connections directly, or to operate relays. In addition to the new functions, the uniselector also performs the operations originally done by a separate timing circuit in the non-automatic chamber.

(c) The uniselector driving circuit.

The uniselector is driven by a circuit containing a thyratron V_4 (type EN91). The time delays are obtained by charging a condenser connected to the grid from about -80 V to the thyratron striking voltage (between -2 V and earth). The driving circuit is shown in figure 6 .

When the selector is stationary, the thyratron is prevented from conducting by the bias potential of -84 volts on the condenser C, connected to the grid. This bias potential is obtained from a stabilizer, type CV449, having a burning voltage of 84 volts. The same bias potential is also used to bias off the other thyratrons

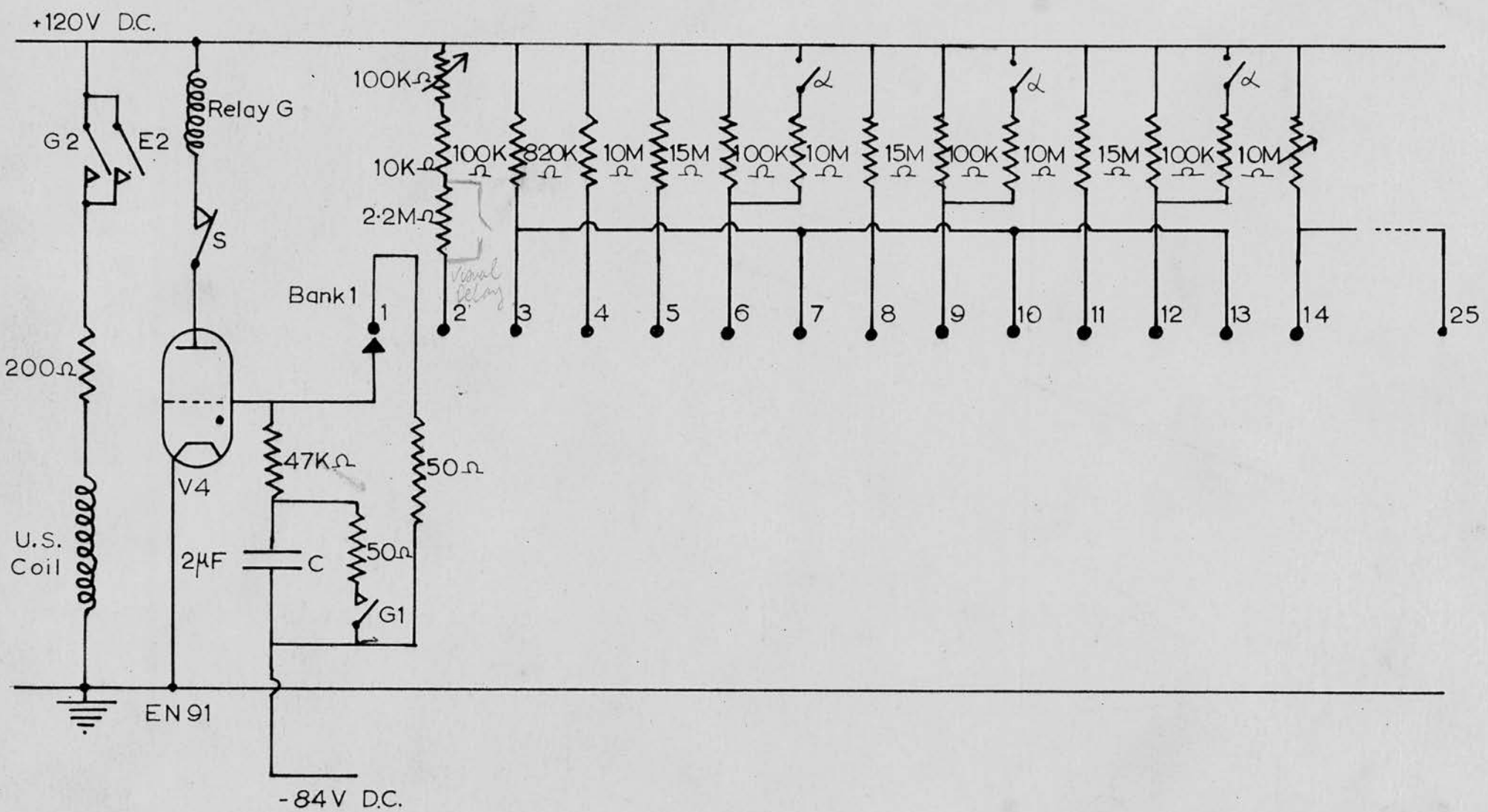

Uniselector Drive Circuit

(See also text and figures 7, 8 and 10)

Figure 6

in the control circuit. In order to trigger the thyratron, it is necessary to remove this bias voltage.

When the uniselector wiper arm is in contact with pin 1 of the contact bank, the grid of the thyratron is connected to the bias voltage directly, through a 50Ω resistance. This ensures that the thyratron remains non-conducting during the chamber waiting period.

The thyratron anode circuit contains a relay, relay G, and there is a switch S in the anode circuit. The operation is as follows. With the wiper arm in contact with a pin other than pin 1, the condenser C (2 μF) charges through a resistance R, the other end of the resistance being connected to the +120V D.C. line. The condenser then charges towards +120 V at a rate determined by the value of the time constant RC. When the grid reaches about -2V to 0V with respect to earth, the thyratron conducts, causing relay G to be energized. A contact on relay G connects the +120V supply to the uniselector coil through a suitable dropping resistance, causing the selector to move on one contact. A second contact on relay G discharges condenser C through a 50Ω resistance, returning the grid potential to -84V ready for the next operation. The switch in the thyratron anode circuit is operated when the uniselector coil is energized, removing the H.T. voltage from the thyratron, and ensuring that the discharge is extinguished. When the selector has moved on one contact, the H.T. voltage is re-applied, but conduction is prevented by the grid bias voltage. The condenser is now re-charged through a different resistance and the cycle is repeated. The uniselector thus completes a full 180°

rotation, until the wiper arm comes round again to position 1. As the same condenser is used for all the delays, different delay times are obtained by varying the value of the resistance through which it is charged.

(d) Uniselector triggering and fast expansion circuit.

The cycle is initiated by the discharge of a thyratron V_1 having a relay in its anode circuit. The anode of the thyratron is connected to about 350 V D.C., supplied by a small metal rectifier It is connected at the junction of a 1 MΩ resistor in series with the rectifier as a current limiter, and a 4μF condenser connected between H.T. and earth. When the thyratron is triggered, the condenser discharges through it, bringing the relay into operation. As no relay holding voltage is supplied the relay goes down, and then comes up again rapidly as soon as the condenser is discharged. The D.C. current through the 1 MΩ resistor is insufficient to keep the relay down.

When the relay is triggered it opens the expansion valve circuit, causing a fast expansion. In addition to this, a make contact connected in parallel with contact 2 on relay G (G_2) makes the uniselector coil circuit, so that the selector moves from pin 1 to pin 2. Thereafter the cycle continues as already described. It is necessary that the relay should stay down for the minimum time, as otherwise the expansion valve would remain open, so that recompression could not take place, and also the uniselector coil would remain energized for this period. The circuit is shown in figure 7.

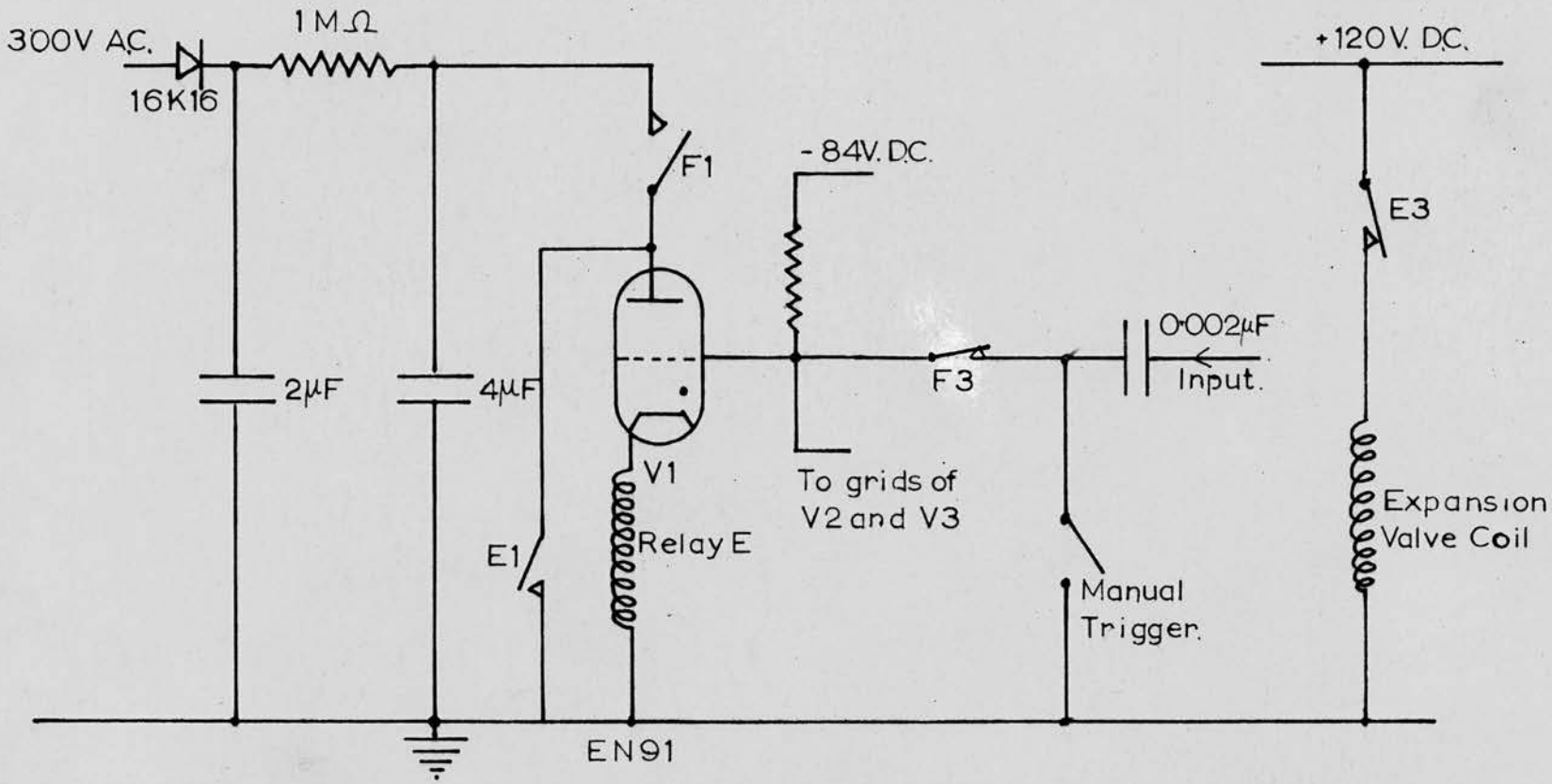

Uniselector and Expansion Valve Triggering Circuit.
(See also text and figures 6, 8 and 10)

Figure 7

(e) Clearing field circuit.

Problems in connection with clearing field.

At the pressure of operation of the cloud chamber, considerable field separation of counter controlled tracks would take place unless the clearing field was removed very rapidly after the chamber has been expanded. The mobility of argon ions at the pressure used (about 1 atmosphere above atmospheric) is about 1 cm/sec per volt/cm. The field strength is about 25 volts/cm. Therefore, a delay of 0.01 sec in switching off the field would lead to motion of each ion column (+ and -) through a distance of 2.5 mm, i.e. a track separation of 5 mm. This is a maximum value, for tracks perpendicular to the electrostatic field. Hence the field must be removed as quickly as possible.

Circuit - See figure 8.

The positive clearing field is about 400V D.C., obtained from a small metal rectifier. The same field is applied to both the upper and lower electrodes, the earthed lead plate forming the second electrode for each half of the chamber. A 1 MΩ resistor in series with the rectifier is connected to the anode of a third thyratron (V_2). When the valve is triggered, its anode potential rapidly falls to about 8V, which is the value when conducting. If this residual clearing field was left on for too long, it would be sufficient to cause some field separation of the tracks. With this voltage, the field strength is about 0.5 volts/cm, giving a separation in 0.1 sec of 1 mm. It was thus also necessary to remove the residual field rapidly.

In order to do this, a high speed Siemens type relay is used. This is connected in the anode circuit of a fourth thyratron (V_3),

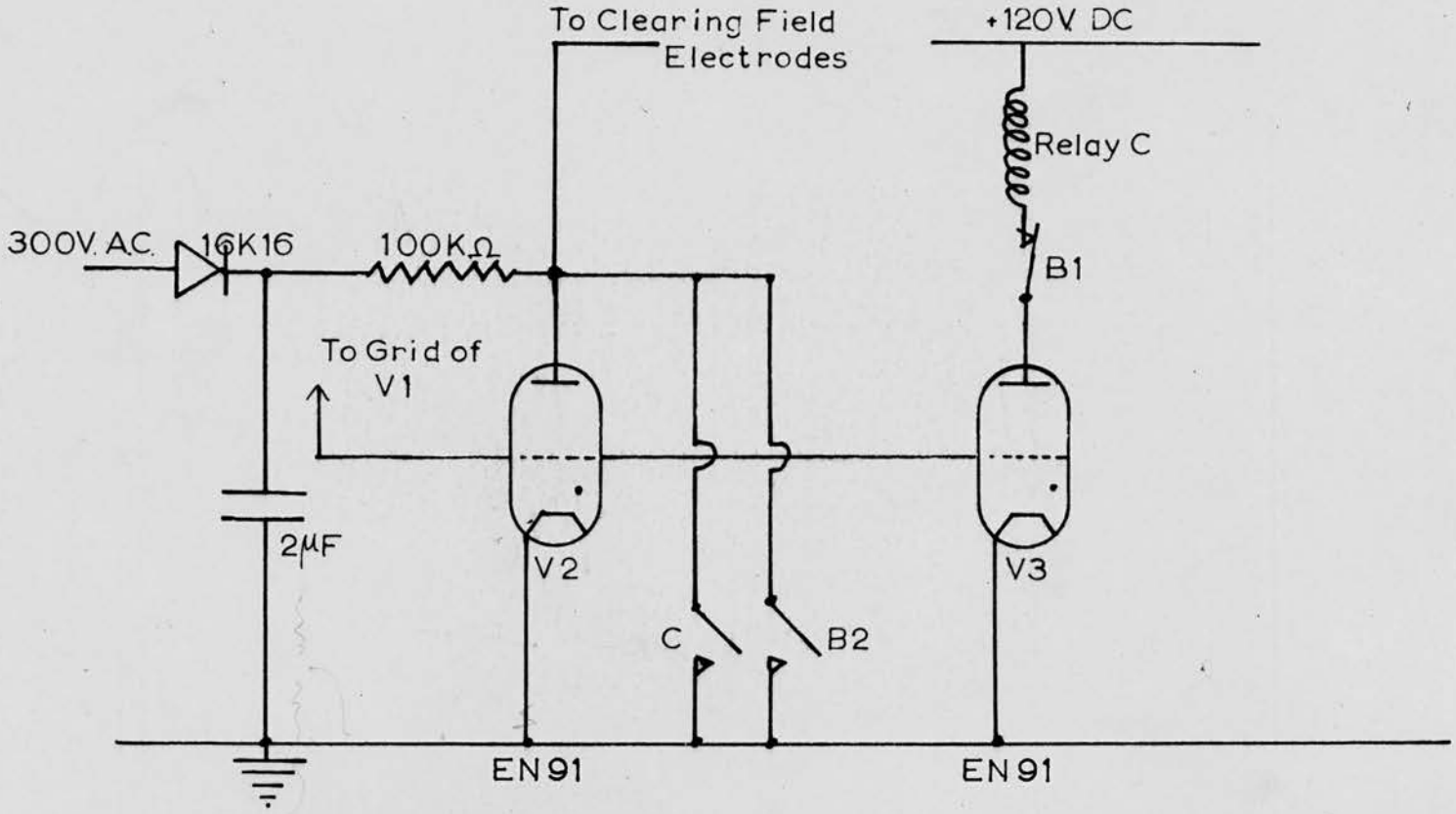

Clearing Field Circuit
(See also text and figures 6, 7 and 10)

Figure 8

one end of the relay coil being connected to +120V D.C. When the thyratron conducts, the relay shorts out the residual voltage across the clearing field thyratron, at the same time extinguishing it. No dropping resistance is connected in series with the relay coil, so that the relay operates as quickly as possible, and the thyratron continues to conduct when its grid becomes negative again. The shorting out of the clearing field during the period of the clearing expansions is taken over by another relay, so that the relatively high current through the high-speed relay, and conduction of V_3, take place for the minimum time. A separate thyratron is used to operate the high-speed relay, so that the majority of the clearing field is removed from the chamber as quickly as possible. The presence of an inductive relay coil in the thyratron circuit would reduce the speed at which equilibrium was reached with the thyratron anode potential at its conducting value (about 8 volts).

(f) General remarks on foregoing circuits.

The grids of valves V_1, V_2 and V_3 are all connected together so that they are all triggered simultaneously by an applied pulse. Cut-off bias is obtained by connecting them to the -84V supply through a grid stopper resistance.

(g) Electronic flash circuit.

This unit is mounted on a separate chassis from the rest of the chamber control electronics. A circuit diagram is given in figure 9 . The flash tubes are energized by discharging condensers with a total capacity of 99 μF, and at a potential of about 2,300 volts through each one. The valve V_1 is a high voltage rectifier, type CV261, and valve V_2 is a beam tetrode,

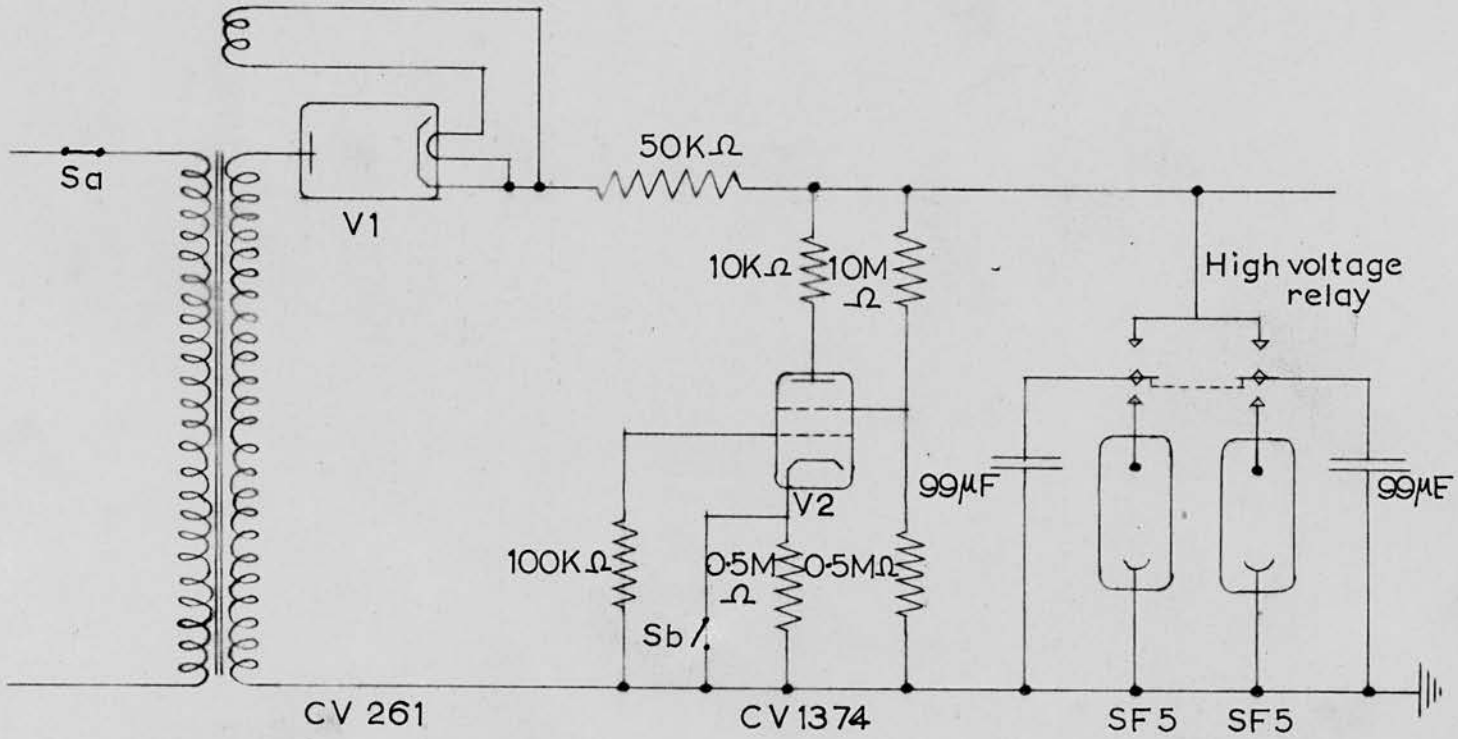

Figure 9 Circuit diagram for the discharge lamps.

type CV1374 (807). The switch S is a double bank toggle switch, consisting of sections S_a and S_b. S_a is in series with the A.C. mains and the high voltage transformer, and S_b is connected across the grid bias resistor of V_2. When it is required to charge the condensers, S_a is closed and S_b is open. The valve V_2 is then so biassed that it only conducts about 40 μA. The high voltage relay is so energised that it connects the two condenser banks across the charging supply. This relay has two separate coils. When one coil is energised the armature is held in contact with the charging supply. Breaking this circuit, and energising the other coil connects the condensers across the flash tubes. The holding and triggering voltage supplies (about 12V each) for this relay are supplied through a relay on the main chassis. This relay is energised by the uniselector as soon after the chamber is triggered as possible, breaking the holding voltage and making the triggering voltage supply. The lamps do not flash until they are triggered by the spark coil. The uniselector actuates a relay which discharges a condenser through the primary after a suitable delay (0.1 - 0.2 sec).

When the switch S is in the other position, the primary circuit of the high voltage transformer is broken and the grid bias resistor for V_2 is shorted out. The valve then conducts strongly, discharging the condensers through it.

Power supplies for this chassis are brought in from the main chassis, using 6-core shielded cable and connectors. These supplies consist of A.C. mains, filament voltages and holding and triggering voltage supplies for the relay.

(h) The clearing-expansion cycle.

The method of operation of the clearing-expansion cycle can be seen from figure 10(a) which shows the pin connections on banks 2, 3 and 4 of the selector. The connections on bank 1 have been given in figure 6 for the selector drive circuit.

It can be seen that relay D which opens the recompression valve also triggers the flash tubes. This does not matter as the high voltage relay is returned to its original position (condenser across charging voltage) immediately after the picture has been taken, and so the flash tubes cannot be retriggered. The only reason for the above arrangement is one of convenience.

The delays between recompression and slow expansion (about 15 sec) are obtained by inserting appropriate resistances in the driving circuit, no connections being made to the corresponding pins on the other contact banks.

The slow expansions are obtained by connecting the +120V D.C. supply directly to the slow expansion valve coil, thus opening the valve against the tension of its spring. A suitable delay (about 15 sec) before recompression is made as above. A multi-bank switch (S) enables one, two or three clearing expansions to be done. When a clearing expansion is omitted the long delay corresponding to the wait before recompression is replaced by a short delay, by charging the resistance valve in the selector drive circuit with the switch.

(k) Other circuits.-See figure10(b)

In order to prevent the chamber from being re-triggered by a pulse coming in while a cycle is in progress, a relay is provided

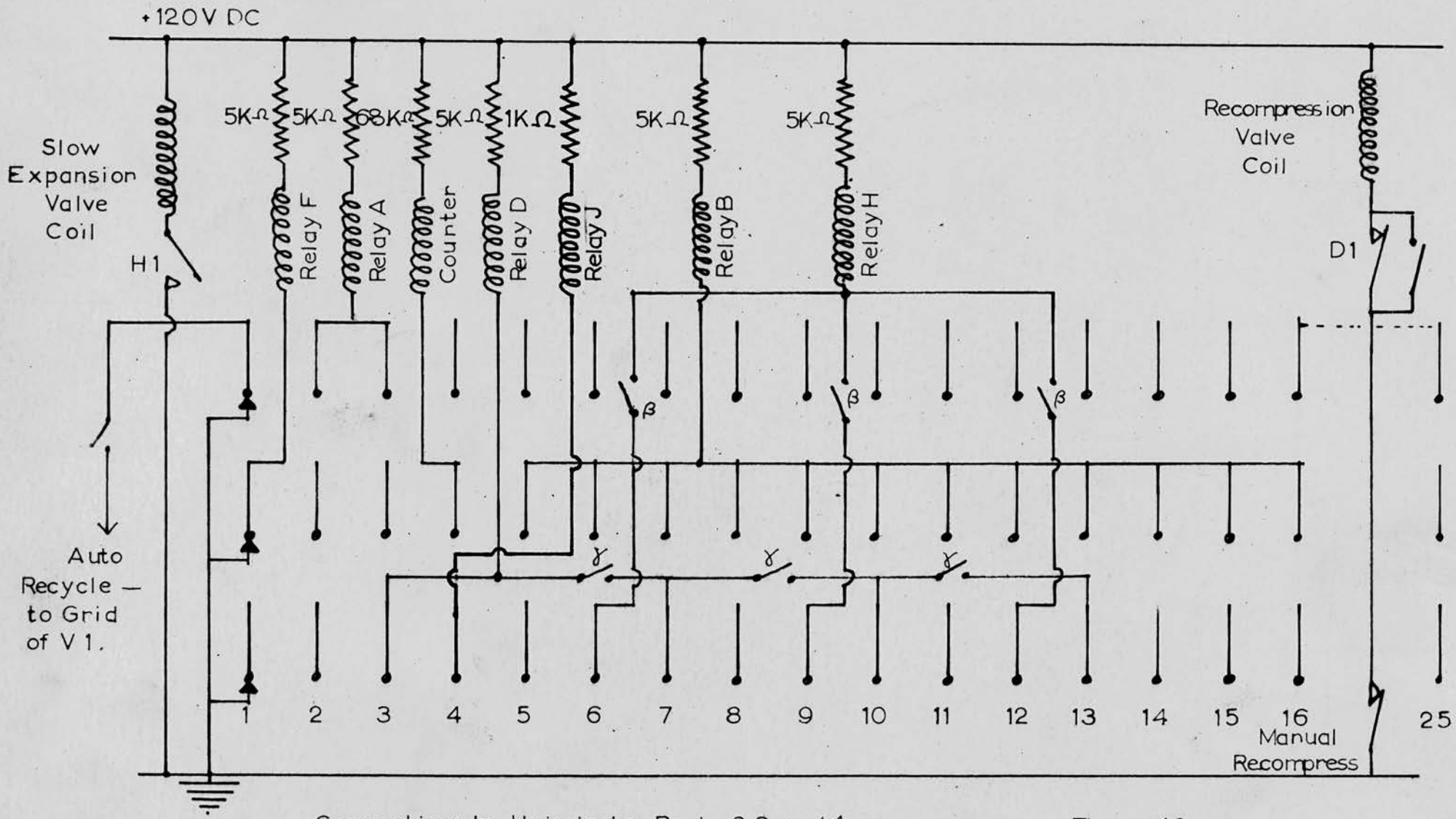

Connections to Uniselector Banks 2, 3 and 4.
(See also text and figures 6, 7 and 8)

Figure 10a

Switches α, β and γ (also figure 6) are operated by a ganged multi-pole switch to set the number of cleaning expansions done

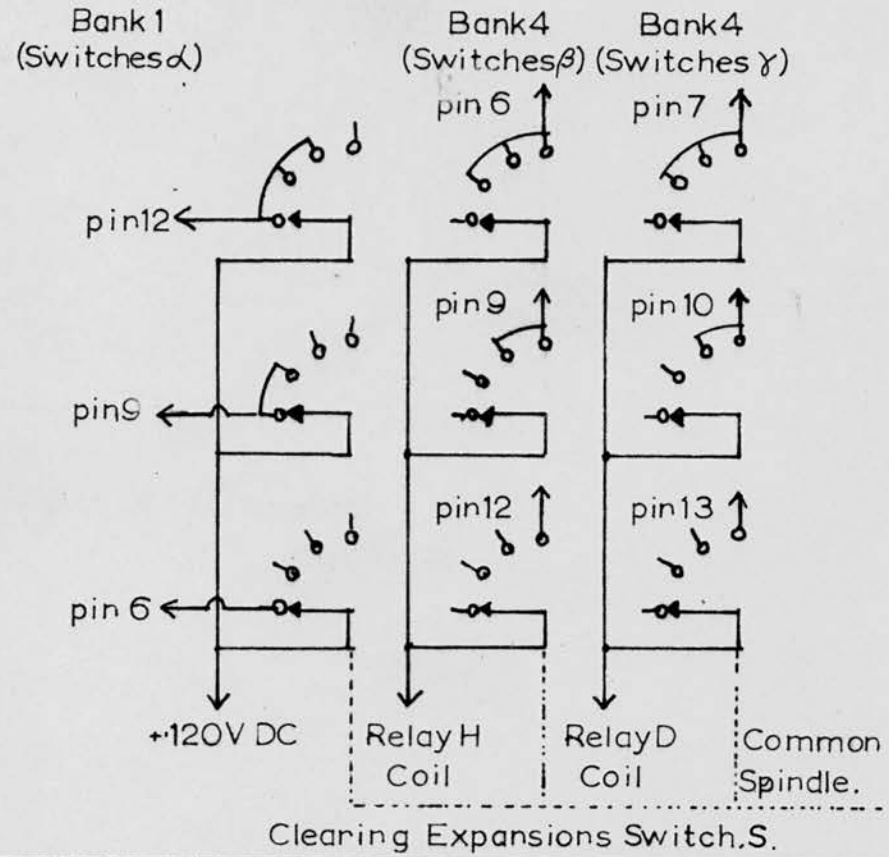

Clearing Expansions Switch. S.

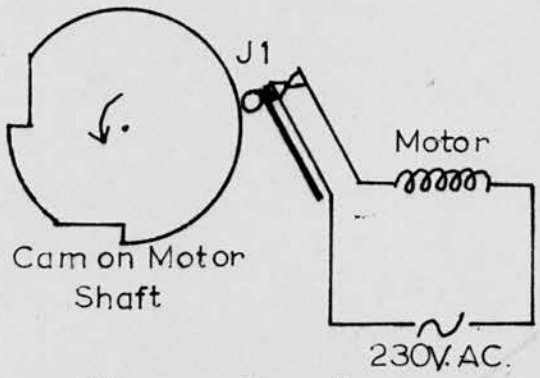

Camera Wind-on Circuit.

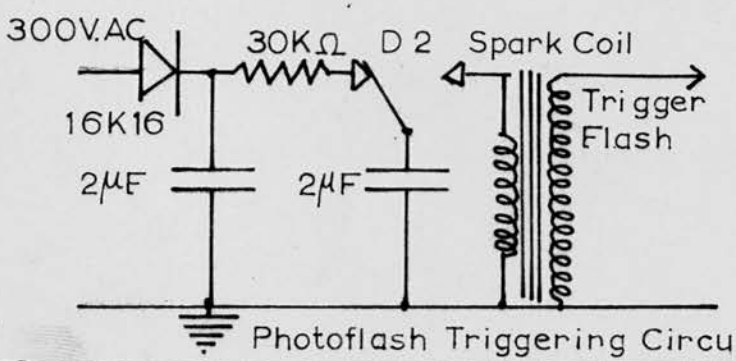

Photoflash Triggering Circuit

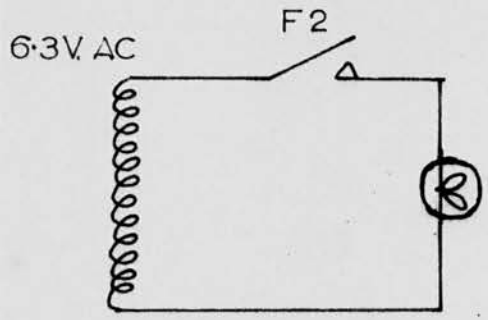

Indicator Lamp Circuit

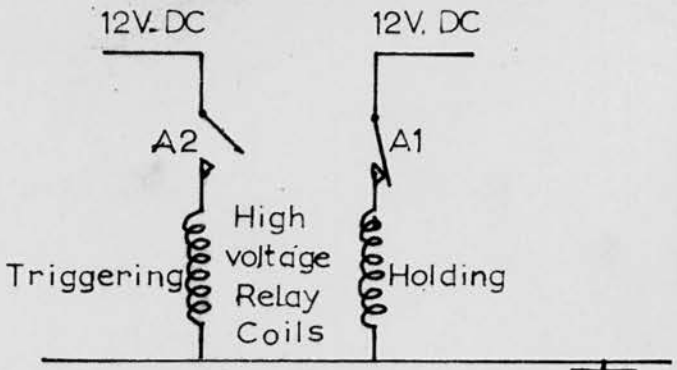

High-voltage Relay Change-over Circuit

Additional Cloud-Chamber Control Circuits

Figure 10b.

which breaks the circuit, between the input socket and the grids of V_1, V_2 and V_3, except when the uniselector wiper arm is in contact with pin 1 of the selector drive contact bank. This relay is held down by passing a current through it from the 120V H.T. supply, through a dropping resistor, the relay coil circuit being made by the uniselector. Another contact on this relay makes the circuit for a 6.3V indicator lamp which shows when the chamber is ready to be re-triggered.

A switch is provided which enables the chamber to be re-triggered again immediately the cycle is completed, the chamber then recycling indefinitely at a preset rate. This is done by arranging that the grids of V_1, V_2 and V_3 are earthed through pin 1 on bank 2 of the uniselector with the switch in one position. With the switch in the other position, this circuit is broken and the selector rotation stops when the wiper arms are in contact with pins 1.

An electromagnetic counter is used to count the number of cycles of the chamber. The counting rate of the counter-control system can thus be ascertained without developing the photographs.

2.8. Summary.

A description has been given of an automatic chamber, together with details of its mechanical valves, optical system and electronic control system. Brief details have also been given of the original, non-automatic, chamber system.

Chapter 3.

EXPERIMENTAL BEHAVIOUR OF CHAMBER.

3.1. Introduction.

3.1.1. Application of fast recompression and overcompression to reduce the recycling time of a chamber.

The minimum recycling time of a cloud chamber is largely determined by three factors:-

(i) The time taken to remove from the sensitive volume any condensation nuclei produced by the previous fast expansion. If this is not done, these nucleii contribute to the background cloud present in the next fast expansion. One method of removing them is to do a number of slow cleaning expansions (see section 3.1.2.).

(ii) The time taken for the chamber gas to reach thermal equilibrium with the walls. During the expansion, the gas is cooled adiabatically (approx.), and during the recompression it is heated. Any cleaning expansions will increase the temperature difference between the gas and the walls.

(iii) The time taken for the sensitive volume to become resaturated with alcohol.

Since 1949, two methods have been described to reduce the recycling period. The first one is the technique of overcompression described by Gaerttner and Yeater (1949); the second, that of fast recompression described by Emigh (1954). Both methods have since been used by other workers, overcompression being generally the more favoured.

In the overcompression cycle, the fast expansion takes place as usual. The chamber is then recompressed, but the diaphragm (or piston) is returned to a position more forward than the original, thus overcompressing the gas in the working volume. The overcompression is normally arranged to take place as soon as possible after the fast expansion.

The chamber is left in the overcompressed state for a short time and the diaphragm (or piston) is then returned slowly to the position before the fast expansion. This final stage acts as a slow cleaning expansion.

The increase in temperature of the gas due to the overcompression has a tendency to reduce the size of the drops formed during the fast expansion. Thus, to a certain degree, it increases their mobility sufficiently for the cleaning field to remove them. During the fast expansion, the temperature of the gas falls below that of the surroundings, receiving heat from them. Conversely, during the recompression, the gas temperature rises above that of the surroundings, losing heat to them. It should therefore, in principle, be possible to make the cycle a reversible one, so that the initial gas temperature is reached when the chamber returns to its original waiting position.

Gaerthner and Yeater used a chamber about 5 inches in diameter and $1\frac{1}{2}$ inches deep. They were able to re-cycle it in 5 secs. with consistently good tracks, and in 2.5 secs. with some deterioration in quality. They used an overcompression ratio about equal to the expansion ratio. The overcompression ratio is the difference between the normal and overcompressed volumes, expressed as a fraction of the normal volume. The chamber gas

consisted of equal parts of helium and argon at atmospheric pressure, the condensant being an ethyl alcohol - water mixture. For very fast recycling periods, pure helium was superior to the mixture. Emigh (see reference) reports that pure helium is unsatisfactory because its high thermal conductivity makes it impossible to form tracks near metal foils, Gaerthner and Yeater showed that over-compression was much superior to conventional operation in the presence of heavily ionizing radiation.

Goldwasser and Nicolai (1955) using overcompression with a chamber 12 inches in diameter and 3 inches deep, have obtained a recycling period of 6 secs. under normal and 15 secs. under heavily ionizing conditions. The chamber gas was helium. Barford and French (1955) reported a recycling period of 30 sec for a cylindrical chamber 28 cm. in diameter and 15 cm. long and the same time for a rectangular chamber 30 x 40 x 20 cm. The chamber gas in these experiments is not stated. More recently, Walker et al (1956) have described a chamber, 9 inches in diameter and 2 inches deep with a recycling time of 10 sec. The chamber gas was argon and the condensant an ethyl alcohol-water mixture. These workers also used the same chamber with fast recompression (see below). They concluded that the build-up of background cloud was very much less for the overcompression case, agreeing with other workers that this was due to the return from overcompression to the waiting position providing a clearing expansion.

The second technique for increasing the recycling rate was first described by Emigh (see reference quoted). This consists of recompressing the chamber rapidly to its original condition as soon as the photograph has been taken. The chamber described by Emigh

was 14 inches in diameter and 2 inches deep. (The chamber described later in this chapter is about 13 inches in diameter and 4 inches deep). Emigh comments on the fog produced by the diaphragm touching the chamber backplate, an effect also found by the writer and mentioned in a paper by Hazen (1942). This latter author also found that if the chamber was worked with a "floating" diaphragm, clean operation was obtainable, in agreement with the writer (see section 3.2.1.) Emigh states that if helium is used, practically no background fog is obtained, whereas argon or air are both unsatisfactory in this respect. The writer has not used helium, as better quality tracks are obtained in argon. The chamber gas used by Emigh was a mixture of argon and helium. He has used a recycling period of 10 sec with this arrangement.

Fast recompression has two disadvantages as compared with overcompression. It is not possible, even in principle, to operate the chamber with a reversible cycle, as the gas gains heat from the surroundings during the first expansion and does not lose an equivalent amount of heat later in the cycle. Thus the gas temperature will always be too high after the recompression. The second disadvantage is that there is no clearing expansion, corresponding to the return from overcompression to waiting conditions. Fast recompression was used with the chamber described here, as it was more convenient to fit and gives an adequate recycling time for the type of experiment done. Triggering rates greater than about 6 per hour are not normally required.

3.1.2. Filling gas and physical operation of chamber.

The sensitive volume of the chamber is filled with argon to a

pressure of about 15 lb. per sq. in. above atmospheric pressure. The condensant is pure ethyl alcohol.

To fill the chamber, argon is let into the sensitive volume through the filling valve, using a high pressure cylinder and a reduction valve. Before commencing to fill, about 10 cc. of alcohol are run into the filling valve, and some is then carried into the chamber with the gas. 10 cc. are sufficient to ensure that the chamber gas will be saturated, and that there will be sufficient liquid in the chamber to make up any losses. The needle valve in the filling valve is shut off after filling is completed. The chamber is then left for a period (usually overnight) to allow temperature equilibrium to be re-established.

If the pressure in the back volume is sufficient to force the diaphragm forward, and the expansion valve circuit is then broken, a rapid expansion of the working volume takes place, tracks being formed if the expansion ratio is correct. (About 1.16 in this case).

After each fast expansion, one or more clearing expansions are required to remove any re-evaporation nuclei remaining in the sensitive volume. A clearing expansion is made by recompressing the chamber, and then letting the gas in the back volume escape slowly to the atmosphere.

3.2. Experimental work to try to discover the reason why clearing expansions are required.

3.2.1. Effects due to the rubber diaphragm.

(a) General

The original type of rubber used for the chamber diaphragm was thin, (3/64 in.) unvulcanized rubber of English origin. This

had a somewhat rough surface and was easily stretched. It was impossible to use the chamber with the diaphragm pushed hard forward, except by performing about a dozen clearing expansions after each fast expansion. If the chamber was operated with the diaphragm "floating", reasonable performance could be obtained using three clearing expansions, which fell to one after the chamber had been operating for a period. This improvement when the diaphragm was not allowed to touch the metal plate was in agreement with the statement by Hazen (loc. cit. section3 .1.1.) A "floating" diaphragm means that it does not touch the front perforated plate when the chamber is pumped ready for expansion, and its position is therefore set by means of the pressure gauges. A chamber worked in this way is very sensitive to the pressures in front and back, as they now determine the expansion ratio.

This disadvantage is not present when the chamber is operated with the diaphragm pumped hard forward, as the expansion ratio is then only determined by the position of the moveable perforated plate H, and is not dependent on the front and back pressures. The number of clearing expansions required was the disadvantage at this stage.

(b) Effect of different types of rubber for diaphragm.

It was now considered established that a large proportion of the background was due to contact between the diaphragm and the perforated metal plate, although no reason for this was known. A high pressure chamber had been successfully operated in Italy, using Italian rubber, with one or two clearing expansions and with the diaphragm pumped hard forward. It was therefore decided to try

diaphragms made from different types of rubber. Two new types were used:-

(a) Vulcanized rubber of British origin with smooth surfaces and a thickness of 1/16 inch.

(b) Vulcanized rubber of Italian origin with a smooth surface and a thickness of 3/64 inch.

With both of these rubbers, good operation could be obtained with a maximum of three clearing expansions, even when the diaphragm was pumped hard forward. This fell to one or two after the chamber had settled down. A recycling period of about five minutes could be used. The need for some clearing expansions was still present.

(c) Effect of rubber coming in contact with the perforated brass plate.

Various experiments have been done to try to discover the reason for the cloud produced by the diaphragm touching the perforated plate. They will be described below.

(i) It was thought that the cloud might be due to the front plate being metal, rather than an insulator. A Tufnol plate of the same size as the perforated plate and drilled out in the same way was made, and fitted between the diaphragm and the metal plate. No noticeable improvement was obtained.

(ii) When the original diaphragm was still in use a piece of copper gauze was stitched to the perforated plate between the plate and the diaphragm to see whether the type of metal had any influence on the effect. No improvement was obtained.

(iii) Samples of the original rubber and of other rubbers were put in contact with a brass plate and weights placed on them. The

original rubber stuck to the brass, whereas the other (vulcanized) rubbers did not. This was probably part of the reason why the vulcanized rubbers are superior.

(iv) It was thought that the cause of the background might be of an electrical nature. If the fast separation of the rubber and the metal generated static charge, ions might be produced which would be pushed into the front of the chamber when it was recompressed. These should, however, be rapidly removed by the clearing field, unless their mass was very great, or large drops had formed on them.

Using the leakage method, the electrical resistances of samples of the three kinds of rubber which have been mentioned were found. Circular samples were placed between two brass plates of the same diameter and a 0.1 μ F condenser, charged from a 2 volt accumulator, allowed to leak through them. The throws on a ballistic galvanometer, produced by the residual charge after a known time, were compared in each case to the throw when the condenser was discharged immediately. The leakage resistance of the condenser could be allowed for by letting it leak through its own resistance, and calculating this in the same way as above. The resistances of the samples were of the same order of magnitude in each case, so that no conclusions could be drawn.

It was found that whenever a large sheet of rubber of any of the types used was lifted from the table in the neighbourhood of the galvanometer wiring a large throw was produced on the galvanometer. This indicated that considerable static charge was present, but no particular conclusions could be reached.

(v) The surface of the diaphragm in contact with the metal plate

was painted with a coating of "Aquadag" colloidal graphite to make it electrically conducting. No improvement in chamber performance was produced, and the coating was removed.

3.2.2. Temperature effects.

There was a possibility that some of the background was due to an uneven temperature distribution at the foot of the chamber due to alcohol condensing out there. The original clearing field electrodes, which consisted of copper gauze, were replaced by the present ones. These consist of pieces of thin copper sheet 12 inches x 4 inches in contact with the chamber walls and held in place by vacuum grease. This provides a layer at the foot of the chamber which is a good conductor of heat, so that temperature changes due to alcohol condensing on it should be rapidly spread over the whole sheet. Some improvement in chamber operation was produced, but one clearing expansion was still required. The new electrode arrangement is also more efficient as a clearing field, there being no spaces between the electrodes and the walls where the field strength is small.

3.2.3. Other effects possibly present.

(a) Electrical.

The electrodes were temporarily connected to equal positive and negative supplies instead of both positive. No effect on performance was observed. The replacement of the original electrodes mentioned in section 3.2.2. ensured good clearing field operation.

(b) Mechanical.

It was possible that the movement of the centre of the diaphragm was too rapid, possibly producing cloud between the

diaphragm and the brass plate. This expansion rate was slowed down by sticking a disc of rubber of about 6 inches diameter over the centre part of the perforated plate to cover the holes in this region. The effect, if anything, was to make the chamber operation worse.

Blumenfeld and Lederman (1954) have reported that improved operation of a cloud chamber was obtained when a clearing electrode was placed between the diaphragm and the perforated plate. They attributed this improvement to the removal of cloud formed by overexpansion behind the plate due to resistance to gas motion through the holes. The holes in the plate of the present chamber were enlarged from $\frac{1}{8}$ inch diameter to $\frac{1}{4}$ inch diameter at an early stage, but no effect was observed. A clearing field electrode has not been tried in this position in the chamber described here owing to the considerable alterations to the chamber which would be required.

(c) Effect of amount of alcohol in sensitive volume.

It was thought by the writer at one time that clearing expansions could be omitted if the chamber was worked in a very unsaturated condition, with little alcohol in the sensitive volume. The chamber worked in this way for one period, but this operation was found to be non-reproducible. The tracks produced in unsaturated conditions are not as good as those under saturated conditions.

3.3. Chamber recycling time.

3.3.1. Original recycling time.

The original recycling time without recompression was about three to five minutes. This was reduced by the recompression.

3.3.2. Recycling time with fast recompression.

It had been hoped that the recompression would dispense with the need for clearing expansions. Though there was some improvement, it was insufficient to allow the chamber to be operated for long periods without cleaning. The cleanest operation was obtained when the sensitive volume was in an unsaturated condition, but frequent adjustment of the expansion ratio was then required and the tracks were inferior in quality to those obtained under saturated conditions. A recycling time of $\frac{1}{2}$ to 1 minute could be used in this condition, but deterioration of quality occurred after the first few expansions, due to the development of background cloud.

If the diaphragm had been used in the "floating" position, clearing expansions would not have been needed. The additional complication of the control system to ensure sufficiently accurate pressures decided against this. Also, small leakages of pressure which do not matter for "hard forward" working would be serious in this case.

The chamber was automatically recycled in a saturated condition for fairly long periods, with a recycling time of about two minutes, no clearing expansions being used at this stage. The growth of background cloud was not particularly rapid, but it did not take very long to become too serious for photographic purposes. When the chamber was used to take counter-controlled pictures at a rate of about 5 per hour, the background still become steadily worse, although the waiting period between expansions was longer.

Clearing expansions were introduced into the cycle at this stage, and pictures could now be taken at the rate of 5 or 6 an hour, with no deterioration in quality.

3.4. Optical problems.

Considerable trouble was experienced from scattered light, and steps were taken to prevent this. All metal or other parts which could scatter light into the camera lenses were painted black. A plywood baffle, with a circular hole in the centre the size of the chamber window was placed between the chamber and the camera, so that only light from the window could enter the camera.

In addition to the plastic lenses on the flash lamps (section 2.5.2 (b)) strips of black paper were attached to the outside of the pyrex cylinder B in order to restrict the width of the light beam and prevent light falling on the velveteen at the back of the chamber, or the inside of the front window. This system worked satisfactorily with the plate camera.

When the 35 mm. film camera was installed, bad optical background was at first present. This was cured by removing the plastic lenses and substituting a new system consisting of four biconvex lenses of 5 cm. focal length for each lamp. The arrangement is shown in the diagram.

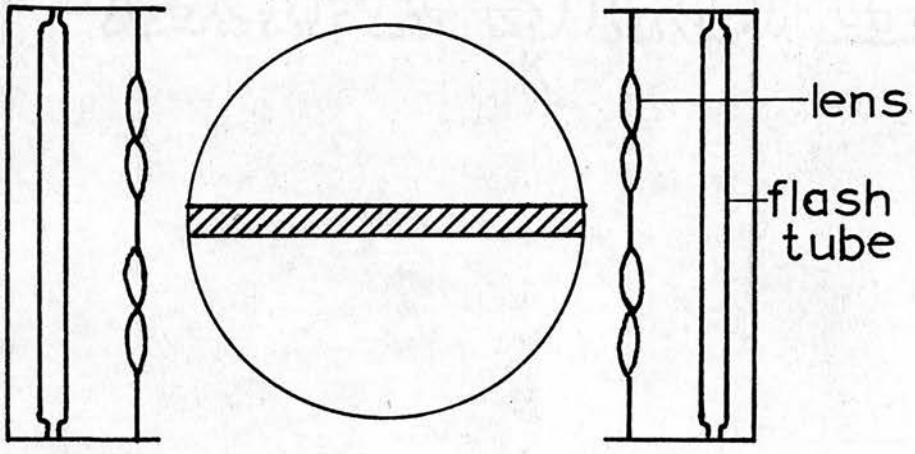

The lenses were placed somewhat farther than 5 cm. from the flash tubes so as to give a convergent beam. Very good background was then obtained.

Chapter 4.

DESCRIPTION OF SCINTILLATION COUNTERS AND ORIGINAL COINCIDENCE SYSTEM

4.1. General.

The components and arrangement of the original slow coincidence system are described in the following sections. Coincidences were obtained either between two scintillation counters, or, between a scintillation counter and a tray of Geiger counters. A block diagram of the arrangement used is shown in figure 11.

4.2. The scintillation counter.

4.2.1. Theoretical.

A scintillation counter consists of a phosphor (organic or inorganic) and a photomultiplier tube with its associated circuitry. Some details of the processes occurring in the phosphor and a description of the photomultiplier will be given in the following sections.

(a) Types of phosphors used in scintillation counters

The classical phosphor was Zn S, which was used as scintillator in the early visual scintillation counters. These were used, among others, by Rutherford (1919) in his discovery of the artificial disintegration of nitrogen nucleii bombarded by α-particles and by Cockcroft and Walton (1932) in their studies of the $Li_3(p, 2\alpha)$ reaction. This latter experiment is also of interest because a coincidence technique was used to count the two α-particles, using two counters and two observers. Zn S has a very high conversion efficiency for the energy expended in it by incident particles by collision loss of $\sim 20\%$, but its

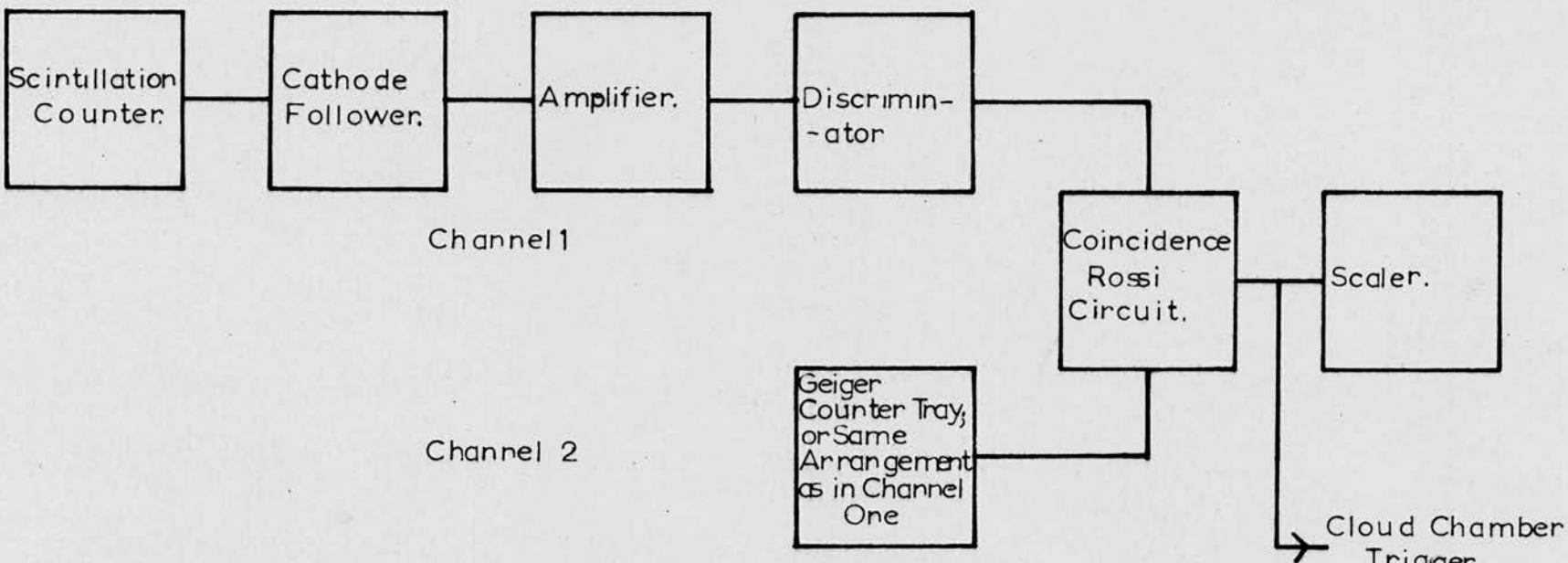

Block Diagram of the Original Coincidence System

Figure 11

very long decay time of $\sim 10\,\mu s$ renders it unsuitable for modern coincidence applications.

The most widely used of the inorganic phosphors is Na I, activated with Tℓ. Its large cross sections for the photo-electric, Compton and pair production processes, due to the presence of the iodine atoms of high atomic number (Z = 53), make it especially valuable for the detection of γ-rays, and for use in scintillation spectrometers. It also has a large density (3.67 gm per cc), so that the rate of loss of energy of an incident particle is large, and it can be obtained in large single crystals. Its emission spectrum consists of a band in the violet, with a mean wavelength of 4100 Å, while the absorption spectrum is in the far ultraviolet, with peaks at 2930 Å and 2340 Å. Hence it is highly transparent to its emitted radiation. The energy conversion efficiency is about 8%.

After the passage of an ionizing particle, the photons are not all emitted instantaneously, but the number emitted decays exponentially with time. The time constant of this decay is called the emission decay time constant of the phosphor. For fast coincidence work, the decay times of the inorganic phosphors are too long, and organic crystal and plastic phosphors are used instead. Some of these have decay times of only a few $m\mu s$; compared with 250 $m\mu s$ for Na I (Tℓ), which has the shortest decay time of the inorganic phosphors.

One of the most used of the organic crystal phosphors is anthracene, which has a decay time constant $\sim$ 32 $m\mu s$ and an

energy conversion efficiency of $\sim 4\%$ for fast electrons. Another one, stilbene, has a decay time constant ~ 6 mμs and an energy conversion efficiency about 60% of that for anthracene. The plastic phosphors have decay time constants ~ 4 mμs, and their energy conversion efficiencies are all less than that for anthracene. The majority of these phosphors are highly transparent to their emitted radiation. The plastic phosphor used here (NE 101) has an efficiency of 55% of that for anthracene and a decay time of 4 mμs.

For work where very large phosphor volumes are required, for example in experiments on the detection of extensive air showers, an organic solution phosphor may be used. These generally have decay times $\sim$ 3 mμs.

(b) Energy loss by charged particles in the phosphor and emission of photons.

When a charged particle passes through a medium, it dissipates energy in the ionization, excitation, and possible dissociation of the molecules of the medium. In a non-luminescent solid or liquid, the whole of this molecular energy is eventually converted into thermal energy, the molecules returning to the ground state by radiationless transitions. In a phosphor, part of the excitation energy is re-emitted as photons, corresponding to direct energy transitions from an excited electronic level to the ground state. The emission spectrum is not, in general, monochromatic, but is spread over a definite emission band. The efficiency of conversion of the incident particle energy into emitted photons depends upon the phosphor, and varies from

about 8% (Na I (Tℓ)) to about 3% (plastic phosphor) for useful phosphors. For particles of low specific ionization (e.g. fast electrons) the conversion efficiency is independent of energy loss in the phosphor, so that the number of photons produced is proportional to the energy loss by collision. For particles of high specific ionization, this efficiency decreases rapidly with increase of specific ionization, so that the number of photons produced depends on the nature of the particle as well as on the energy loss. This problem is further considered in section 9.2.1. This effect is more marked for organic than for inorganic phosphors. For example, the number of photons produced by a 5-MeV α-particle completely absorbed in an anthracene crystal is only about 10% of the number produced by an electron of the same energy. On the other hand, for an α-particle travelling at such a velocity that its specific ionization has its minimum value, the number of photons produced by it per cm path length is about four times the number produced by an electron travelling at its minimum ionization velocity.

As has been mentioned in the previous section, the emission of photons is not instantaneous, but is given by

$$I = I_o e^{-t/t_o}$$

where t_o is the time constant of the decay.

We must distinguish here between fluorescence and phosphorescence. In fluorescence, the transition from the excited state of the phosphor molecule to the ground state is an "allowed"

transition. In phosphorescence, the excited state is meta-stable; the direct transition to the ground state being "forbidden". Emission can only occur from a higher level after the molecule has received sufficient thermal energy to make the transition.

The decay period for a fluorescence process is usually much less than that for a phosphorescence process, and the former is therefore the major one in materials suitable for scintillation counting. Nevertheless, these materials are still generally referred to as "phosphors".

As has already been mentioned, the generally used phosphors are highly transparent to their own emitted radiation, and very little of it is re-absorbed. It is desirable that the maximum amount of this light should reach the photocathode. Gillette (1950) has calculated the amount of emitted light which escapes from each face of a rectangular prism assuming that it is generated uniformly throughout the volume, and gives $\sim 11\%$ for anthracene of refractive index 1.59. The NE101 plastic phosphor used here has a refractive index of 1.54, so that the percentage will be somewhat higher.

Several methods can be used to increase the light emitted from the face adjacent to the photocathode of the multiplier tube. The opposite face can be covered with aluminium foil, so that light is reflected back into the phosphor. For an E.M.I. tube, where the photocathode is deposited on the inside of a flat window, the best method is to cement the phosphor to the window with a thin layer of liquid paraffin or glycerine. The critical angle

at this surface is then increased, being determined by the refractive index of the phosphor relative to the tube envelope. Hence if the other faces of the phosphor are silvered, practically all the emitted light can be collected. Instead of silvering, a diffuse coating of magnesium oxide is often used.

(c) Operation and limitations of the photomultiplier.

Two main types of photomultiplier tube have been used for scintillation counting. These are the circular electrostatically-focussed type developed by R.C.A., and the longditudinal, unfocussed type developed by E.M.I. It is not proposed to consider the former type here as they have not been used in the present experiments. Full details of both types can be found in the literature (for example - Birks - Scintillation Counter - Pergamon; Curran - Luminescence and the Scintillation Counter - Butterworth; Rodda - Photoelectric Multipliers - Macdonald).

The E.M.I. type tube has a semi-transparent Sb-Cs photocathode deposited on the inside of a flat window. The dynodes are arranged longditudinally, and each one consists of a number of narrow solid activated strips arranged in a Venetian blind fashion. The coating consists of an Sb Cs mixture. The electrons from the last dynode are collected by a flat disc anode. Successive dynodes are maintained at increasingly positive potentials, using a potential divider.

Photons incident on the photocathode are converted into photoelectrons with an efficiency of about 5% to 10% for this type of cathode. The response of the cathode depends on the

frequency of the photons, and has a wide peak at about 4100 Å for E.M.I. tubes. The maximum of the emission spectron of Na I (Tl) occurs at 4100 Å, of anthracene at 4450 Å and of the NE101 plastic phosphor at 4400 Å. Hence the response of the cathode to all these phosphors is good.

Electrons leaving the photocathode will then produce secondary electrons at the first dynode. These electrons are then multiplied by the succeeding dynodes, so that for every one photoelectron leaving the cathode, 10^6 - 10^8 electrons arrive at the anode, the actual number depending on the particular tube.

Limitations. A number of factors limit the linearity of the photomultiplier. If the sensitivity of the photocathode is not uniform over the whole area, the output pulse height for a given energy loss in the phosphor will depend upon the part of the cathode upon which the photons are incident. Modern photocathodes are good in this respect. Also, the presence of magnetic fields may interfere with the collection of photoelectrons by the first dynode. This effect is much more serious for the R.C.A.-type tubes than for the E.M.I.-type, and the latter can be used in small magnetic fields (e.g. earth's field) without magnetic shielding. An increased voltage between the cathode and the first dynode is an advantage.

If the output current at the anode is too large, fatigue effects in the last few dynodes may occur, resulting in a permanent loss of sensitivity. The E.M.I. tubes are superior to R.C.A. ones in this respect.

The following limitations are in general more serious than those mentioned above, which can be reduced greatly by suitable operating conditions. These are:-

(1) Photomultiplier noise.

(2) Statistical fluctuations in electron. emission in the tube, giving rise to a decrease in energy resolution.

(3) Transit time spread in the tube, increasing the possible resolving time obtainable.

(4) Non-linear response of the tube when the output current pulses are too large.

(1) The main cause of the noise current, or dark current, is the random thermal emission of electrons from the photocathode and from the following dynodes. The electrons emitted by the cathode will make the largest contribution, as they are amplified by the succeeding stages. The effect of this noise may be reduced by cooling the photocathode, or by using two photomultipliers in coincidence to view the same phosphor. As the noise is random, coincidences will only be obtained for genuine signals, if the resolving time of the system is sufficiently small. Except for the measurement of very small energy losses, the signal to noise ratio is large, and the noise pulses may be biassed out. For the experiments described here, noise could therefore be neglected.

(2) The statistical nature of photoelectron and secondary electron emission gives rise to a distribution of output pulse heights for a given number of photons incident on the photocathode, instead

of the same pulse height on each occasion. Also, for the same number of photons emitted, the collection efficiency by the photocathode may not always be the same, owing to the geometry of the system. The spread in pulse height due to these factors has been analysed by Garlick and Wright (1952) who give an expression for the half-width of the pulse height-frequency distribution produced by particles which lose equal amounts of energy in the phosphor. Using a neon lamp connected in a "sawtooth" generator, they showed that the experimental results were in accord with theory.

(3) The effects of transit time spread on the multiplier output pulse shape are dealt with in chapter 7 section 7.2.2., where the effect of this in limiting the time resolution is considered.

(4) The non-linear response of the E.M.I. type of photomultiplier (Venetian-blind type of dynode structure) has been investigated by Raffle and Robbins (1952). They found that the linearity decreased with increase of output pulse height. They attributed this effect to the build-up of instantaneous space charge in the comparatively field-free spaces between the dynode strips of the last few dynodes, when a pulse of large current density reaches the final stages of amplification. The effect can be reduced by increasing the voltages on the last few stages. Also, for good linearity it is desirable to use the tube at lower overall voltages than those mentioned by the makers, in order to decrease the output pulse height. Additional gain can then be provided by an amplifier. Owing to the type of dynode construction, space-charge limitation does not occur in the R.C.A.-type tubes until much higher current densities.

This effect is worse for counters using organic phosphors than for those using inorganic phosphors. The reason for this is that, owing to the much shorter fluorescence decay time of the organic phosphors compared to the inorganic ones; the charge densities on the pulses produced by them are much greater. Raffle and Robbins (loc. cit.) showed that, with a given tube, space charge effects with anthracene occurred with pulses about 100 times smaller than for sodium iodide.

4.2.2. The large counter.

The counter consists of a block of NE101 plastic phosphor 5 inches in diameter and 2 inches thick, together with a photomultiplier having an effective photocathode diameter of at least 4.5 inches. This is an 11-stage E.M.I. type 6099B, and has the cathode deposited on the inside of a plane glass window.

Figure 12 shows the main features of the counter. The scintillator fits onto a recess in the circular ebonite base A. Three ebonite pillars B are fixed to this base and support the Tufnol disc C which carries the photomultiplier base D. The photomultiplier rests on the top of the phosphor, optical contact between them being made by means of a film of glycerine. Vaseline had been tried for this purpose but glycerine was found to be superior. Firm contact between the phosphor and the multiplier is ensured by the springs E.

The dropping resistors for the dynode E.H.T. voltage supply are soldered directly to the pins of the photomultiplier base D. Decoupling condensers are connected to the last two dynodes before

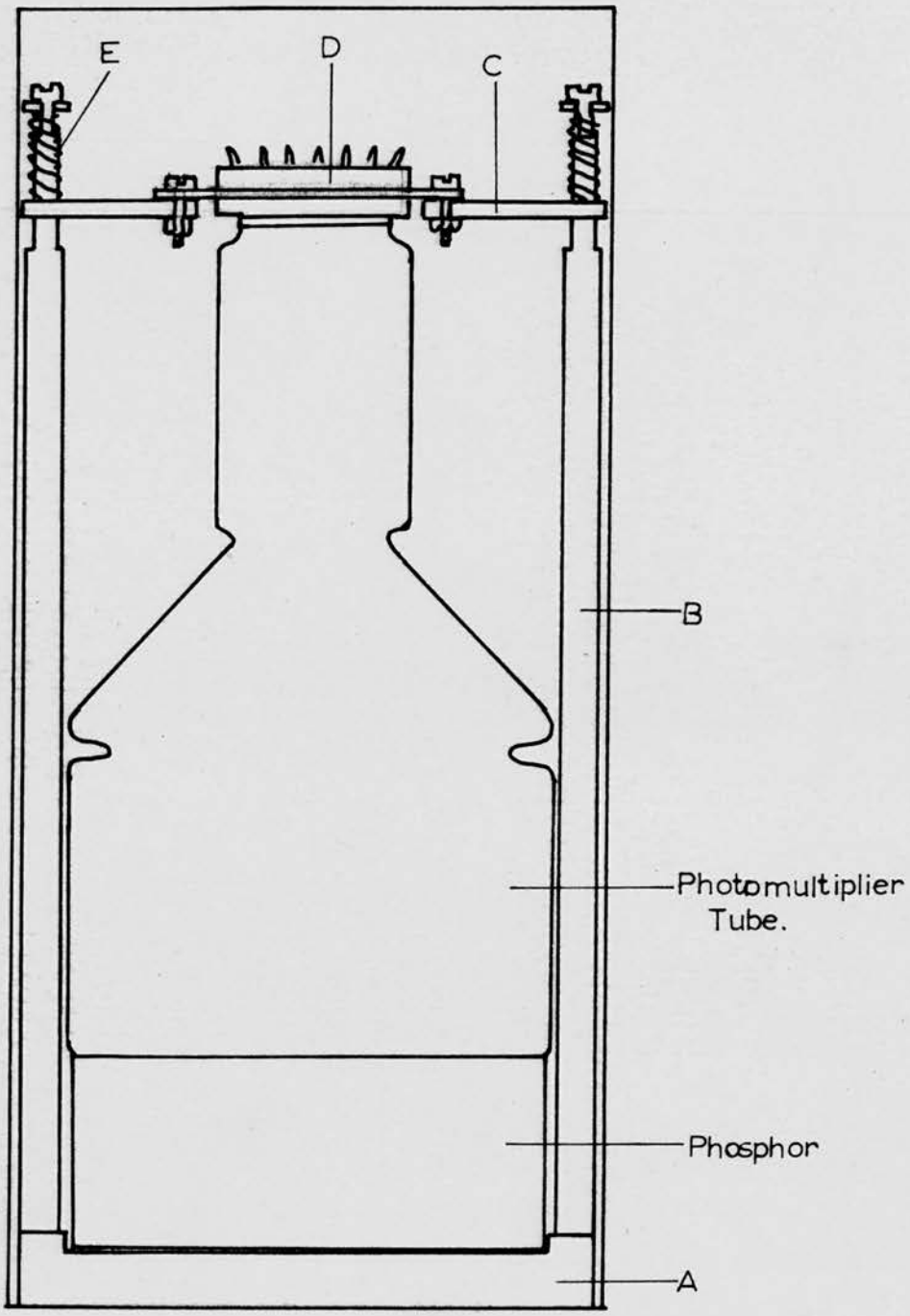

The Large Scintillation Counter
(See section 4.2.2.)

Figure 12

the output to bypass any pulses produced on them. The negative end of the E.H.T. supply is connected to the photocathode, so that the output is at about earth potential. A separate H.T. positive supply of about 120 volts is connected to the collecting anode. Output pulses are taken from the last dynode.

The counter is enclosed in a thin, light-tight, metal box, electrical connections being brought out to sockets in the lid. The counter base A is secured to the bottom of the box by three screws.

Output pulses are taken from the last dynode, as positive pulses are then obtained, because of the net loss of electrons from the dynode. The final anode collects the electrons, so that negative pulses are obtained from it.

4.2.3. The small counter.

This counter employs a 2 inch cube of NE101 phosphor, together with a 14-stage E.M.I. type 6262 photomultiplier, with a cathode diameter of about 2 inches. Ths counter is shown in figure 13.

The counter system is assembled on two 0 B.A. threaded rods A and B which project from each end of the metal box containing it. The phosphor is held at one end by the brass support C (see small diagram). The photomultiplier base is supported by the Tufnol ring D. A second ring E supports the centre of the tube. The distance between C and D is adjusted so that the photocathode and the phosphor are in optical contact, with a film of glycerine between them.

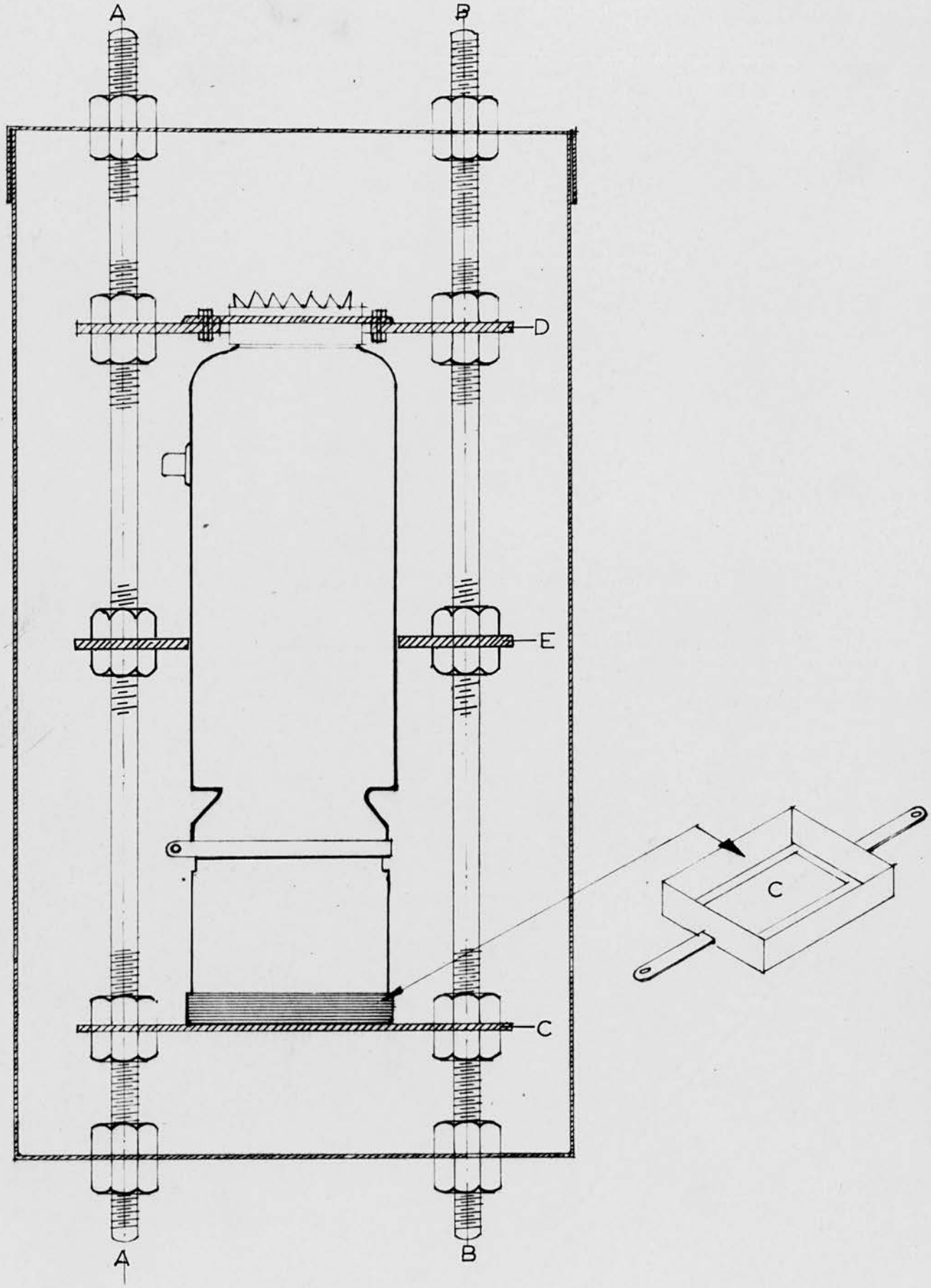

Small Counter

Figure 13

The threaded rods project through the bottom and lid of the containing box and hold the whole assembly rigidly in position. The counter can be used with the multiplier either vertical or horizontal.

Negative E.H.T. for the dynodes and positive H.T. for the anode is supplied in the same manner as for the large counter.

4.3. The cathode follower

The output pulses from each photomultiplier were fed to a cathode follower. This was mounted on a separate chassis. The circuit of the large photomultiplier and cathode follower is given in figure 14. The theory of the cathode follower is considered in section 7.2.3. The circuit of the small multiplier and cathode follower is identical, except for the larger number of dynodes.

4.4. The pulse amplifiers.

The output from each cathode follower went to a pulse amplifier type 1008A. This consists of two separate stages containing three valves each. Each stage is stabilized in gain by the use of negative feedback, the ratio "feedback gain" to "unfedback gain" being about 1 : 15. The "fedback gain" of the first stage is 100, and of the second stage 200.

Input pulses first enter a network containing a variable differentiating time constant T_1 and a variable integrating time constant T_2, the input impedance being about 100 Ω. The differentiating time constant determines the cut-off frequency at the lower end of the amplifier pass band and the integrating

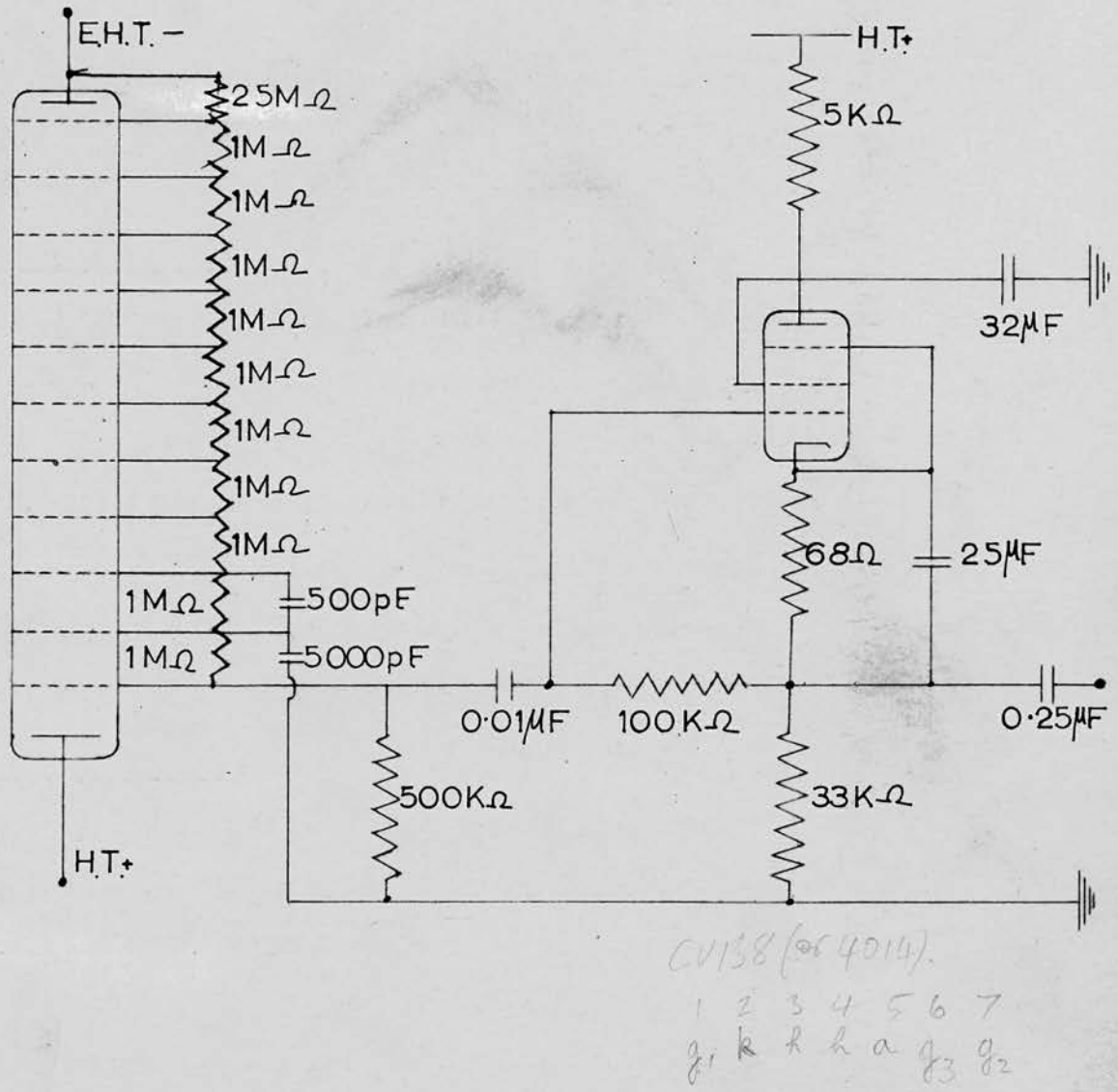

CV138 (or 4014).

1 2 3 4 5 6 7

g_1 k h h a g_3 g_2

Figure 14 Circuit of photomultiplier tube Type E.M.I. 6099 and cathode follower employing valve Type C.V. 138

time constant that at the copper end. Maximum bandwidth is obtained when T_2 is a minimum and T_1 a maximum. The amplifier was used in this way with $T_1 = 1500\,\mu s$ and $T_2 = 0.15\,\mu s$. To obtain the optimum signal to noise ratio, the time constants should be equal. (See Gillespie - Signal, Noise and Resolution in Nuclear Counter Amplifiers - Pergamon Press, p. 63). In the present case, the gain required is not high (never $>$ 400), and the time constants chosen give the least distortion of the original pulse shape. Also, as we are not interested in any pulses which are not considerably larger than the noise level, corresponding to fairly large energy losses in the phosphor, any noise pulses can be biassed out by the discriminator.

An attenuator system, calibrated in decibels, enables the amplifier gain to be varied from 200 to about 20,000 in steps of 2 db. A gain of ~ 300 was normally used. The quoted accuracy of the attenuator is $\sim 5\%$, so that the gain could be conveniently varied by a factor known to this accuracy, which was sufficient for the applications to be described. These included calibration of the photomultiplier system for energy loss. (See section 9.3.).

4.5. <u>The discrimination system</u>.

Output pulses from the amplifier went to a discriminator. This consisted of either

(a) A Dynatron scaler type 1009B, which incorporates a discriminator with a bias level variable from 5 volts to 50 volts.

(b) A single channel pulse height analyser which is described in Chapter 5.

The discriminators enabled pulse heights corresponding to

various amounts of energy loss in the phosphors to be selected.

4.6. The coincidence circuit.

Coincidences between the two counters were recorded by a standard Rossi coincidence circuit, using two E.F. 50 pentodes as the coincidence valves. Input pulses to these valves were supplied by flip-flop circuits triggered by the discriminator outputs in order to provide large, standard size pulses for each valve.

The operation of this circuit is as follows. The two pentodes, which have a common anode load resistor, are normally conducting, with the common anode voltage at a low value. If one valve is cut off by a negative pulse on the grid, the other continues to conduct and the anode voltage rises slightly. If both valves are cut off by coincident pulses, the anode voltage rises to the full H.T. potential and a large positive pulse is obtained. If one valve is switched out of circuit, large output pulses are obtained for single input pulses to the other valve.

Output pulses from the coincidence unit were used to operate a scaler (for counting purposes) or to trigger the cloud chamber.

4.7. Summary of coincidence arrangements used.

Experiments were done using

(a) The large scintillation counter (Section 4.2.2.) in coincidence with a tray of geiger counters - see Section 10.2.1.

(b) The large counter only - see Section 10.2.2.

(c) The large and small scintillation counters in coincidence - see Section 10.2.3.

The two scintillation counters were also used with the fast

coincidence system (see Chapter 7).

Chapter 5.

CONSTRUCTION AND CALIBRATION OF A SINGLE-CHANNEL PULSE HEIGHT ANALYSER

5.1. Theory of operation.

The analyser was constructed from a circuit designed by Park (1956). The circuit diagram is given in figure 15. The lower level of the discriminator can be varied from 0 - 60 volts and the channel width from 0 - 20 volts. Both bias voltages are nominally read directly on a 0 - 200 μA meter, although calibration was found to be necessary in practice. The discriminator employs germanium diodes instead of thermionic valves, eliminating the necessity for zero or threshold adjustments. Only three thermionic valves are used in the circuit; two double triodes in trigger circuits (upper and lower channel limits) and a third in an anticoincidence arrangement.

Input pulses first enter the discriminator section. The arrangement of the diodes in this section is shown in figure 16. The bias voltage across D_1 can be set to any value between 0 and 60, thus determining the lower level. The bias across D_3 can be varied from 0 to 20V, determining the channel width.

Pulses from the upper and lower channel limits are fed to flip-flop trigger circuits (see figure 17). In the quiescent state, the current values are as marked on the diagram. The pulses are differentiated by the C R circuit before reaching the grid g_1. Calculation shows that the rising edge of the input pulse produces a positive pulse at the grid while the trailing edge produces a negative pulse. The positive pulse is bypassed

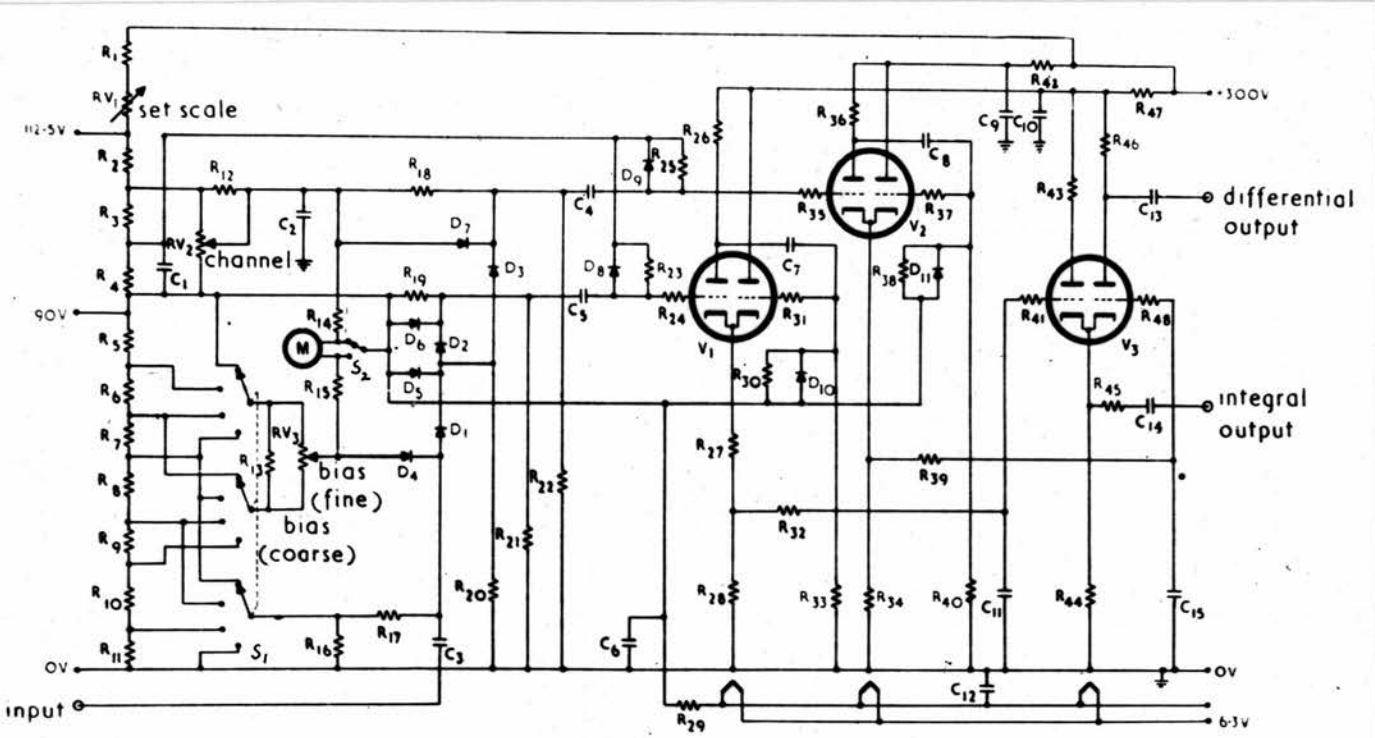

Circuit diagram of single-channel, pulse height analyser

R_1 = 10 kΩ, 3 W, w.w.
R_2 = 170 Ω
R_3 = 2·7 kΩ, h.s.
R_4 = 330 Ω, h.s.
R_5–R_9 = 1 kΩ, h.s.
R_{10} = 1·2 kΩ, h.s.
R_{11} = 1 kΩ, h.s.
R_{12} = 100 kΩ
R_{13} = 22 kΩ
R_{14} = 100 kΩ, w.w. (selected)
R_{15} = 300 kΩ, w.w. (selected)
R_{16} = 330 kΩ
R_{17} = 220 kΩ
R_{18}, R_{19} = 47 kΩ
R_{20}–R_{22} = 820 kΩ
R_{23} = 12 kΩ
R_{24} = 470 Ω
R_{25} = 12 kΩ
R_{26} = 4·7 kΩ, 1 W, h.s.
R_{27} = 330 Ω
R_{28} = 6 kΩ, 2 W, h.s.
R_{29} = 470 kΩ
R_{30} = 15 kΩ, h.s. (selected)
R_{31} = 470 Ω
R_{32} = 15 kΩ
R_{33} = 820 kΩ, h.s.
R_{34} = 6 kΩ, 2 W, h.s.
R_{35} = 470 Ω
R_{36} = 4·7 kΩ, 1 W, h.s.
R_{37} = 470 Ω
R_{38} = 15 kΩ, h.s. (selected)
R_{39} = 15 kΩ
R_{40} = 820 kΩ, h.s.
R_{41} = 470 Ω
R_{42} = 3 kΩ, 2 W
R_{43} = 2·7 kΩ
R_{44} = 10 kΩ, 2 W
R_{45} = 680 Ω
R_{46} = 2·7 kΩ
R_{47} = 2 kΩ, 3 W
R_{48} = 470 Ω

RV_1 = 5 kΩ, 2 W, w.w.
RV_2 = 2·5 kΩ, w.w.
RV_3 = 5 kΩ, w.w.

C_1–C_3 = 0·01 μF
C_4, C_5 = 17 pF
C_6 = 0·25 μF
C_7, C_8 = 100 pF (selected)
C_9, C_{10} = 0·25 μF
C_{11} = 22 pF
C_{12}–C_{14} = 0·01 μF
C_{15} = 22 pF

V_1–V_3 = ECC91

D_1 = CG4
D_2 = CG1
D_3, D_4 = CG4
D_5–D_{11} = CG1

M = 200 μA

Figure 15

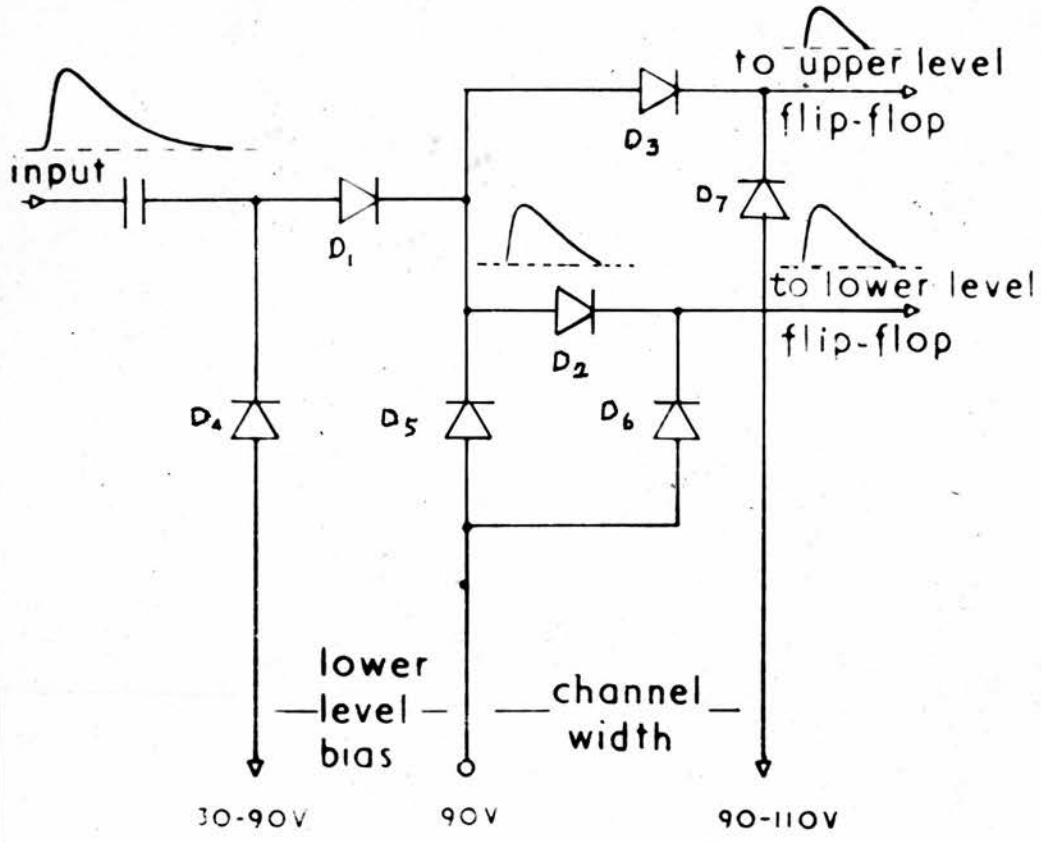

Arrangement of germanium diodes in the discriminator circuit

Figure 16

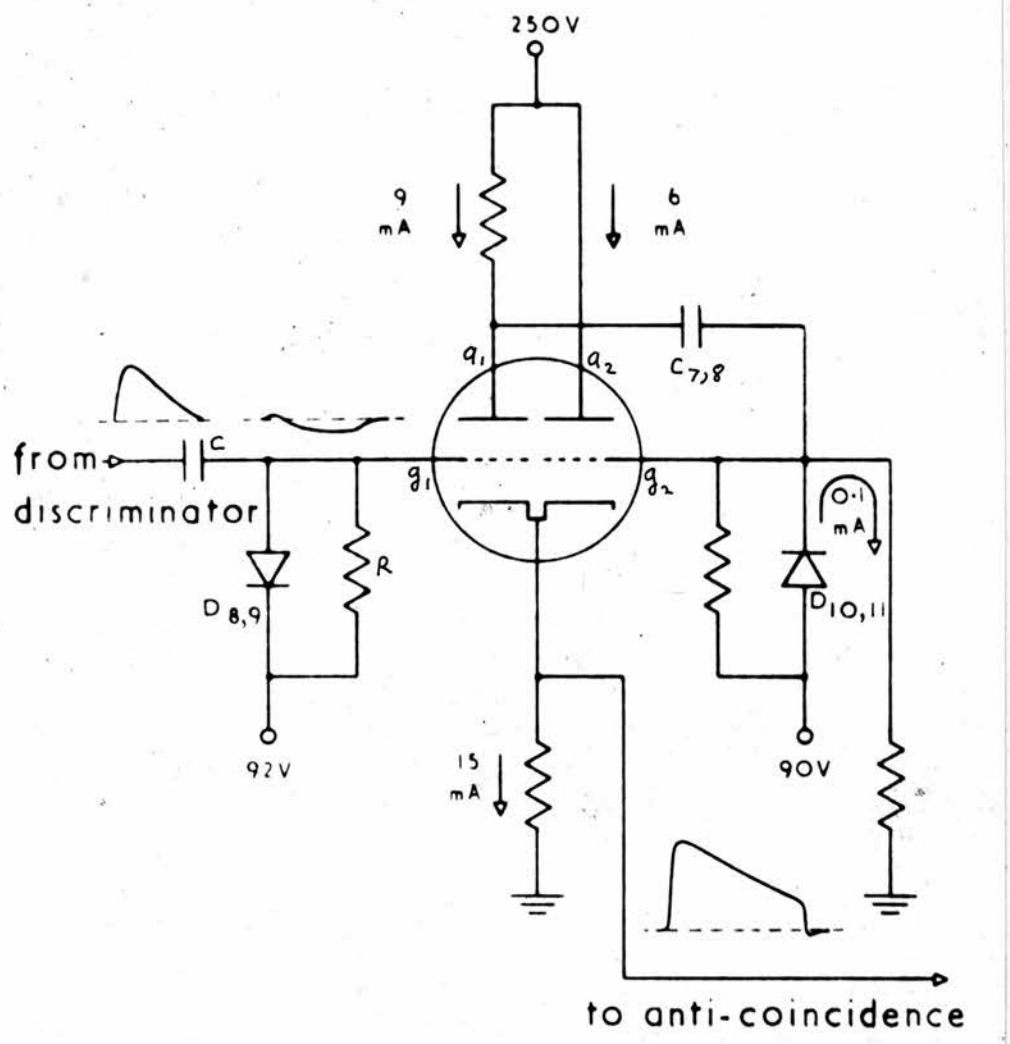

Flip-flop circuit, including input differentiating network. (Currents shown are for quiescent conditions)

Figure 17

by the diode (D_8 or D_9). The amplitude of the negative pulse is equal to k . RC where RC is the differentiating time constant and k is the rate of fall of the trailing edge of the input pulse. The value of RC is 0.2 μs and the minimum negative pulse at the grid for triggering is $\sim$ 10 mV. Hence, k $\sim$ 0.05 Volts/μ s. This method of triggering ensures that the trigger circuits only respond to pulses with a fast initial rate of fall.

This negative pulse on the grid g_1 produces a positive pulse on the corresponding anode a_1 which is fed to the opposite grid g_2 through the CR coupling circuit. This pulse tends to cut off the diode (D_{10} or D_{11}) and the potential of g_2 rises. As the circuit is of the long-tailed pair type (See Farley - Elements of Pulse Circuits - Methuen, pp. 29-31), the potential of anode a_1 also rises, so that the action is cumulative and the grid g_2 is driven hard positive, until all the available current is flowing in this side of the valve, and the other side is cut off. The cathode potential follows the potential of g_2 as in the cathode follower (see section 7.2.3.), and a positive output pulse can be obtained from it. This condition persists until the potential of g_2 has fallen sufficiently, by the charging of C_7 or C_8, for the other side to start drawing current again, when the circuit returns to its original condition. The pulse length is thus determined by the time constant of the anode-grid coupling circuit. In the absence of the conducting diode D_{10} or D_{11}, the grid g_2 would now be driven negative and continuous oscillations would be obtained. The negative pulses are bypassed by the diode so that the quiescent condition is stable.

Pulses from the cathodes of the trigger circuits are fed to the anticoincidence valve V_3 which is arranged as a long tailed pair (see Farley - reference cited). In the quiescent condition, the side connected to the lower level flip-flop is cut off.

A pulse from the lower level flip-flop only will give positive output pulses at both the integral and differential outputs. If it occurs in coincidence with a pulse from the upper level flip-flop the cathode potential will rise, but the anode potentials will remain almost constant, although falling slightly. Thus a positive output pulse is obtained at the integral output and a small negative pulse at the differential output. Hence, positive output pulses are obtained at integral output for all input pulses larger than the lower level of the discriminator, while they are obtained at the differential output only for pulses lying within the channel.

5.2. Constructional details.

The analyser is constructed on a standard chassis 17 in x 12 in x 3 in with a front panel 19 in x 9 in on which the 200μA meter is mounted. The lower level bias can be set by means of a four position switch (coarse control) and a potentiometer (fine control). The channel width is varied by means of a potentiometer. A switch connected in the meter circuit enables it to be used to read the lower level bias or the channel width as required. Full scale deflection is nominally equal to a bias of 60 V or a channel width of 20 V, but calibration was necessary in practice.

Electrostatic screening is provided between the three valves and their circuits, in order to prevent spurious triggering of one by another.

5.3. Calibration of analyser.

5.3.1. The lower level.

Calibration of the lower level bias was carried out by means of pulses from a pulse generator type 1074A which gives pulses of length $\sim 10\mu s$, and of suitable shape. Before commencing, the "Set Scale" potentiometer (figure 15) on the analyser was adjusted so that a full-scale reading on the meter was obtained with switch S_2 at "set bias". This provided a reproducible voltage distribution on the potentiometer. Pulses of various known pulse heights were now injected, and the lower level bias adjusted so that counting at the integral output was just prevented. A graph of Meter Reading in scale divisions (full scale = 200) and Bias Voltage was plotted. This is a straight line with a fixed threshold at zero meter reading (see figure 18). The pulses at the output were counted on a scaler.

5.3.2. Channel width.

The channel width was calibrated in the following manner. The "Channel Width" potentiometer was adjusted to give a known reading on the meter. Using a fixed pulse height from the same pulse generator as above, the lower level bias was adjusted so that counting of pulses at both the integral and differential outputs was just prevented. The lower level bias was then equal to the pulse height. This bias was now reduced until counting in the channel was again stopped, this time because the pulse height was greater than the upper bias level. The difference between the lower level biases in the first and second case was then equal to the channel width, the lower level calibration curve being used.

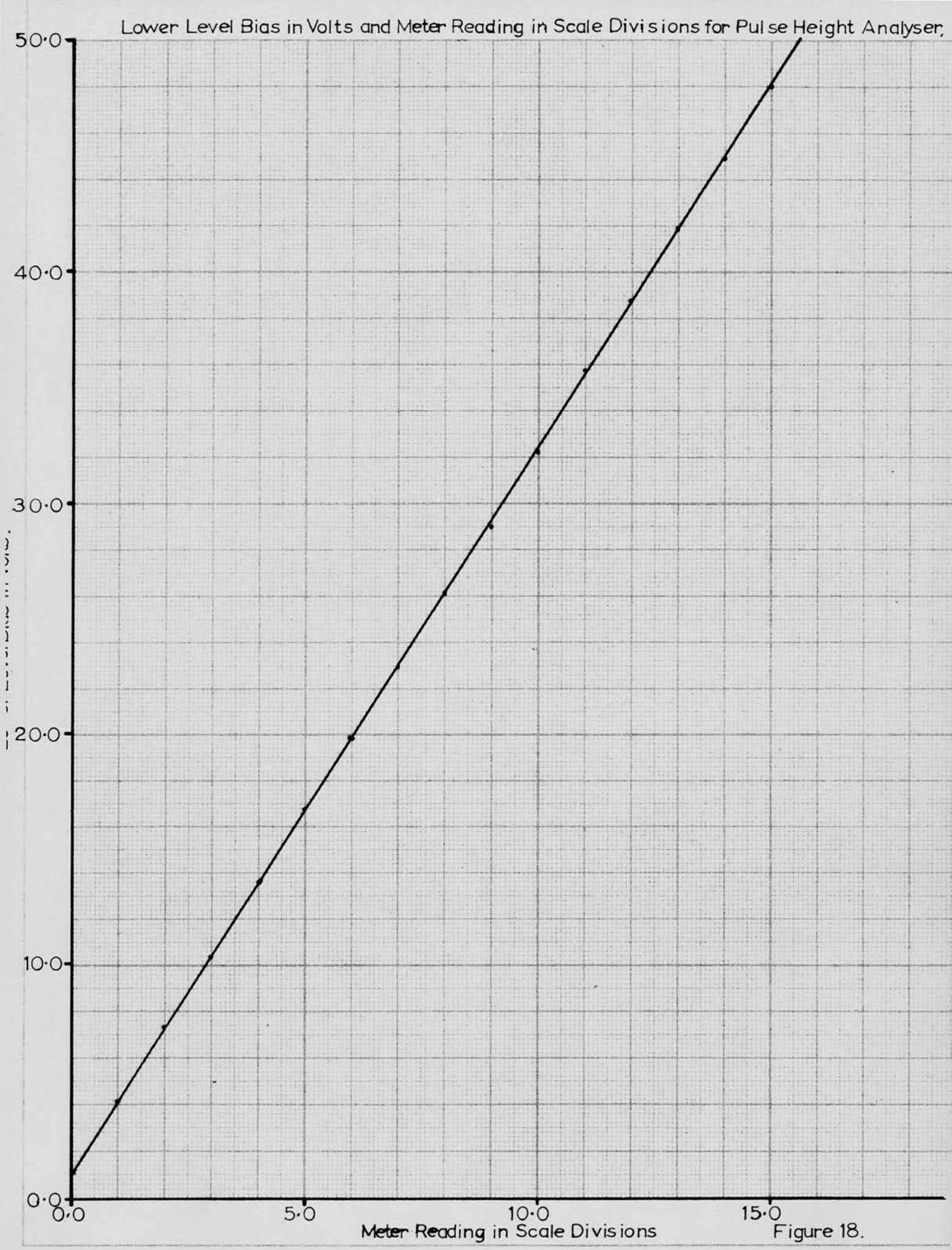
Lower Level Bias in Volts and Meter Reading in Scale Divisions for Pulse Height Analyser.
50·0
40·0
30·0
20·0
10·0
0·0
0·0
5·0
10·0
15·0
Meter Reading in Scale Divisions

Figure 18.

The channel width was altered and the above repeated. A graph of meter reading in scale divisions and channel width in volts was then plotted, which was a straight line. A small variation in channel width occurred when the lower level bias was altered, but this was not appreciable compared to the errors in setting. The results are shown in figure 19.

5.4. Uses of analyser.

The analyser was used to obtain the Rossi curve for the counting rate due to cosmic ray showers under a variable thickness of lead (see section 9.4.2.)

It was also used to trigger the cloud chamber by using output pulses from the channel, in an attempt to select events in which a predetermined energy loss by the primary particle had occurred.

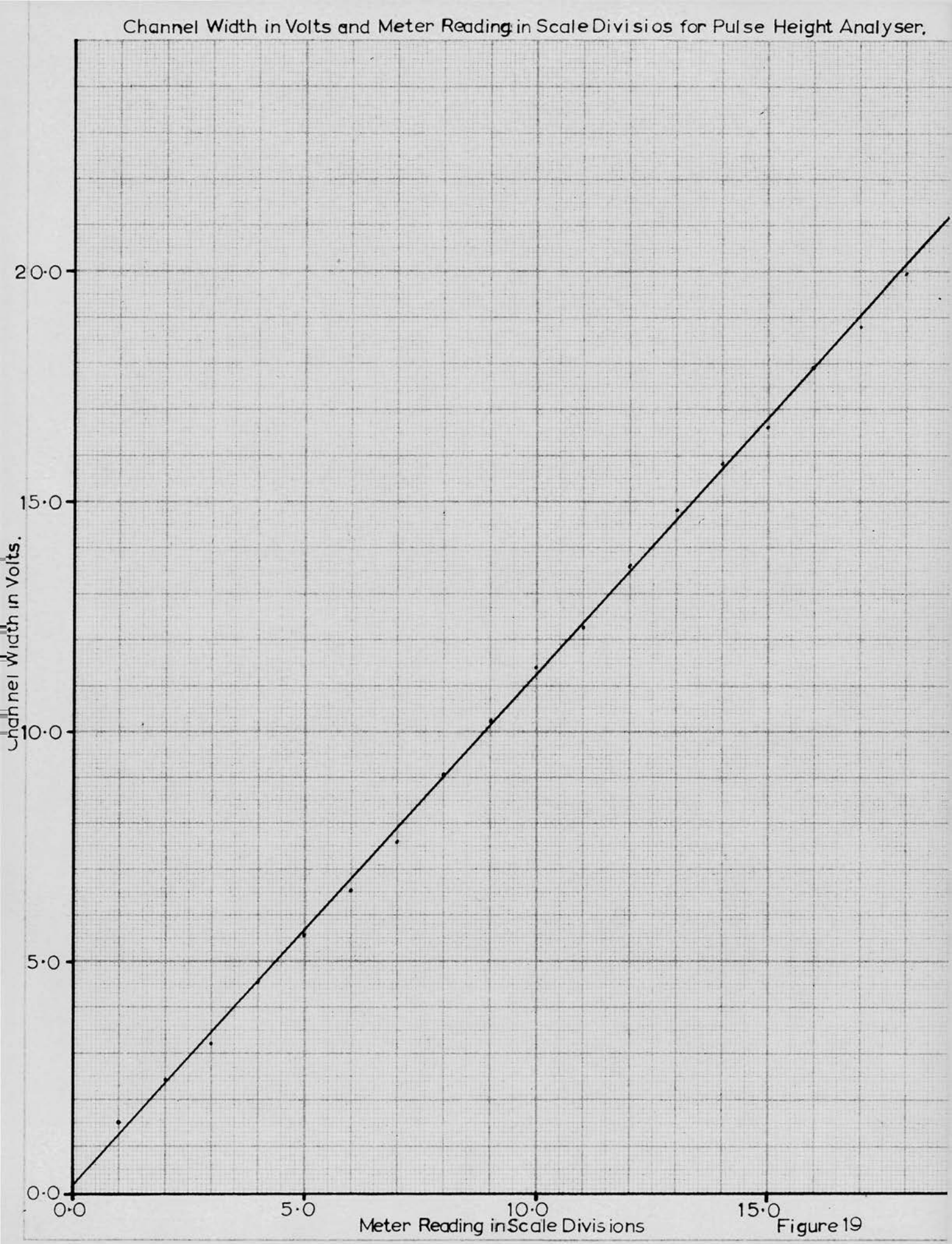
Channel Width in Volts and Meter Reading in Scale Divisios for Pulse Height Analyser.
20·0
15·0
10·0
5·0
0·0
Channel Width in Volts.
0·0
5·0
10·0
15·0
Meter Reading in Scale Divisions
Figure 19

Chapter 6.

INTRODUCTION TO MILLIMICROSECOND PULSE TECHNIQUES

6.1. General.

Before about 1947, a coincidence system with a resolving time (see below) of 100 mμs (10^{-7} sec) would have been considered fast. With the advent of the photomultiplier tube in its present form, the limit of resolution has fallen to a few times 10^{-10} sec. The coincidence system to be described in the next chapter is not as fast as this, having a resolving time of 20 mμs (2×10^{-8} sec.)

6.2. Definition of resolving time of coincidence circuits.

A coincidence circuit may be defined as a nonlinear circuit, having two (or more) inputs and one output, such that a pulse is obtained at the output only when the inputs have received pulses within a short time of each other. This short time is the resolving time of the coincidence circuit.

If the two input pulses to the coincidence circuit are both rectangular, and of the same length τ mμs, then an output pulse will be obtained whenever the two input pulses overlap in time, i.e. whenever one pulse arrives at a time $\pm \tau$ mμs with respect to the other. The time τ can be defined as the resolving time of the system, and is then equal to the length of time after the arrival of one pulse during which the arrival of a second pulse will record a coincidence. It is therefore obvious that the shorter the pulses with which one can work, the better.

If the two input pulses to the unit are initially coincident in time, but a variable delay is then put in series with one of them,

we should expect the curve of counting rate versus delay time to resemble the full line curve in the diagram, of width 2τ.

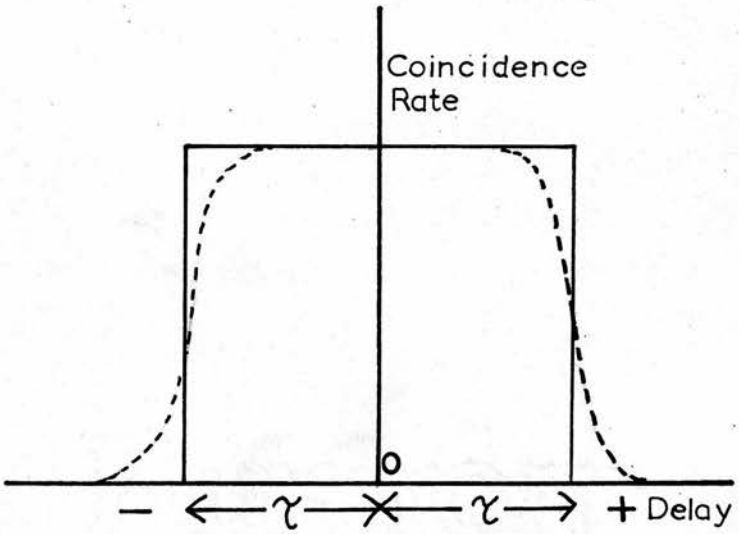

In practice, for reasons to be fully discussed in the next chapter, such a curve is never obtained. We can then define the resolving time as the half width at half maximum height of the curve that is obtained in this way. There is some confusion in the literature concerning the definition of resolving time, which, according to Bell (1954) is often taken as the **full** width at half height of the prompt coincidence curve. We shall use the first definition in the work which follows.

6.3. Applications of fast coincidence circuits.

There are three main types of measurement in which the shortest possible resolving time is required. These are:-

(1) Measurement of velocities by the "Time of Flight" Method.

(2) Reduction of the chance coincidence rate for coincidence measurements with high individual counting rates.

(3) The measurement of the half life of very short-lived radioactive elements.

6.3.1. Time of flight measurements.

The fast coincidence technique can be used to measure the velocity of a beam of particles. If the beam passes through the two counters which are separated by a suitable distance, a delayed coincidence curve can be obtained. If the measurement is now repeated with an increased counter separation, a second curve is obtained. The two curves are normalized to the same maximum ordinate, and the separation of the curves in time is then equal to the time taken for the particles to travel the additional distance between the counters. This method was applied to measure the velocity of γ-rays from Co^{60} as a test of the fast coincidence unit constructed (see Chapter 8.) It will be seen that at a given counter separation and with a given delay in one channel with respect to the other one, particles with different velocities will be counted with different efficiencies owing to the transit time of the particle between the counters. For example, if the delay in the channel containing the first counter is greater than that in the second channel, slow particles will be preferentially selected, the velocity range depending on the delay and upon the counter separation. It will also depend, of course, on the resolving time, the range being narrower as the resolving time is decreased.

To select particles of relatively high velocity ($\beta \gtrsim 0.7$), Čerenkov counters can be used, but these cannot be used for velocities less than the velocity of light in the detection medium. A fast coincidence system can be used to select slow particles from an accelerating machine, as the short resolving time ensures

that the background chance coincidence rate is small. If we select particles of the same momentum by means of an electromagnet, the fast coincidence unit can then be used to select velocity, and hence the type of particle counted. This method can be used to select, for example, heavy mesons.

6.3.2. Reduction of chance coincidence rate.

The chance coincidence rate N_c for two counters having singlefold counting rates N_1 and N_2 is given by:-

$$N_c = 2 N_1 N_2 \tau$$

where τ is the resolving time of the coincidence circuit. In a given case, N_1 and N_2 will be determined by the experimental conditions, so that it is essential to make τ as small as possible, in order that the ratio of genuine coincidences to chance coincidences shall be large.

6.3.3. Measurement of very short half-lives.

The fast coincidence method can be used for the measurement of the half-life of a short lived radioactive element, and has been much employed for this purpose.

Two separate coincidence curves are needed to use this method with a given coincidence apparatus. Using an element which emits two particles or γ-rays with a time separation much less than the resolving time of the apparatus, a prompt coincidence curve is obtained which will be symmetrical about zero relative delay. Co^{60} can be used for this purpose, as it emits two γ-rays within $\sim 10^{-12}$ sec. This source is then replaced by the one under investigation and a second coincidence curve obtained, which will

be unsymmetric by an amount depending on the half life being measured. An analysis of the two curves, due to Newton (1950) and other workers, is then used to calculate the half life. By this method, half-lives much shorter than the resolving time of the apparatus can be found, the present limit being ~ 0.1 mμs.

6.4. Components of a fast coincidence system.

6.4.1. General.

The different circuits comprising a fast coincidence system will now be considered in outline. As a full description of the operation of a typical system is given in the next chapter, the details are given there.

The following units are contained in any fast coincidence system:-

(a) Counters
(b) Amplifiers
(c) Pulse-shaping circuits
(d) Discriminator and trigger circuits
(e) Coincidence circuits

Some brief details of each of these will now be given.

6.4.2. Counters.

The primary requirement for a counter to be used with a fast coincidence system is that the rise-time of the pulses produced by it shall be as short as possible. This requirement precludes the use of the conventional gas counters; such as the Geiger or proportional counters; which have rise-times in the microsecond region.

Two types of counter are suitable, those using photomultipliers to detect scintillations in phosphors, or Čerenkov radiation;

and spark counters.

The scintillation counter has been used for most of the fast coincidence work which has been done. The Čerenkov counter has been used for certain specialized applications, such as velocity measurement for charged particles, or precise timing experiments. It has the advantage that the decay time constant for the Čerenkov radiation is at least an order of magnitude less than that for the fastest phosphors. The disadvantage is the much smaller light output for a given collision energy loss.

The operation of the spark counter depends on the primary particle producing ionization between two plates with a large potential difference between them. They have been described by Chang and Rosenblum (1945) and used for the detection of cosmic rays by Robinson (1953), but have been very little used for fast coincidence work owing to the greater convenience of the scintillation counter.

The factors affecting the performance of a scintillation counter are discussed in Chapter 7 (section 7.2.2.) and in Chapter 4 (section 4.2.1.)

6.4.3. Amplifiers.

Amplifiers used for this work must have the maximum possible bandwidth in order to amplify the short pulses involved with the minimum of distortion. This problem is considered in section 7.2.5., where the main methods of increasing the bandwidth of an amplifier are discussed.

Wide-band amplifiers have been designed by a large number

of workers. They are of the distributed type, and of the type using secondary emission pentodes, to which class the circuit described in the next chapter belongs. References to many designs are given in Lewis and Wells (Millimicrosecond Pulse Techniques - Pergamon, pp. 141 and 160).

6.4.4. Pulse-shaping circuits.

As the counter pulses have a long exponential decay they must be shaped to give short rectangular pulses. This is commonly done by a delay line pulse-shaping circuit of a type described by Wells (1952) and employed in the circuit described in section 7.2.4.

6.4.5. Discriminator and trigger circuits.

In order to make use of the relationship between energy loss in the phosphor and output pulse height from the photomultiplier, a discriminator circuit is used. This ensures that only pulses greater than a predetermined height can reach the coincidence circuit. Hence, pulses due to noise in various parts of the circuit, and to background radiation of low energy can be biassed out. The pulses getting through the discriminator operate a trigger circuit which gives an output pulse of standard size and shape suitable for operating the next stage of the circuit, normally the coincidence mixer. The circuit described in section 7.2.6. is typical, and employs a secondary emission pentode. It is a modification of a circuit described by Moody (1952).

6.4.6. Coincidence mixers.

Many types of coincidence mixer have been employed by different

workers. The main types are:-

(a) Series coincidence circuits
(b) Parallel coincidence circuits
(c) Bridge coincidence circuits.

A brief description of these types will now be given.

(a) Series coincidence circuits

This type of circuit can be described as consisting of two switches in series connected to a power source through a common load resistor. When the two switches are closed simultaneously, a current will flow through the resistor. If either one is closed separately, no current flows. The double switch consists of a multi-grid vacuum tube.

The tube normally used is the 6EN6 gated-beam tube. This has two control grids, which are normally biassed negative so that no anode current flows. Simultaneous positive pulses on the two grids will allow a short burst of current to pass to the anode. The possibilities of this tube have been investigated by Fischer and Marshall (1952). They claim a possible resolving time $\sim$ 0.3 mμs.

(b) Parallel coincidence circuits

A parallel coincidence circuit may be described as a device consisting of two switches in parallel which have a common load. When one switch is opened, the voltage drop across the load does not change appreciably, but when both are opened simultaneously there is a large change of potential in the load circuit.

The original circuit of this type was due to Rossi, using

triode or pentode vacuum tubes as the switching devices. The use of germanium diodes for this purpose was first suggested by Howland et al. (1947). The circuit described in section 7.3. is of this latter type. Variations of the parallel coincidence circuit have been described by Garwin (1953) and numerous other workers.

(c) Bridge coincidence circuits

In a bridge coincidence circuit, a number of ohmic and non-linear elements are arranged in the form of a balanced bridge, A single pulse applied to one end of the bridge results in no output pulse, while the simultaneous application of a second pulse to a different point of the bridge produces an unbalance, and therefore an output pulse. Circuits of this type have been described by many workers, among them Bay (1951) and Strauch (1953). Such circuits respond to small signals and have a fast recovery time.

6.5. The complete coincidence system.

In a complete system, the operations of fast coincidence and pulse height selection are often performed by separate channels, in order to obtain the minimum resolving time. The pulse height analysis circuits can be relatively slow. The outputs of these channels and of the fast coincidence circuit can then be fed to a three-fold coincidence circuit to give a final output pulse.

In the unit described in the next chapter, separate channels are not used as this simplifies the circuitry. A resolving time of about 20 mμs is obtained, which is about the limit for the type of circuits described.

Chapter 7.

CONSTRUCTION AND THEORETICAL OPERATION OF A FAST COINCIDENCE UNIT.

7.1. General Introduction to the Apparatus.

The coincidence unit described below was constructed to a design by Collinge et al (1956) and has a resolving time of about twenty millimicroseconds. The original design was intended for use as a fourfold coincidence unit, but only twofold has so far been used in the experiments described here. A fourfold coincidence unit is one which requires simultaneous pulses at four separate inputs in order to give an output pulse. Similarly, a twofold coincidence unit requires only two pulses. A larger number of channels may be used later as some experiments require anticoincidence or Čerenkov counters in addition to coincidence scintillation counters.

A block diagram of the two channels and the coincidence mixer unit is shown in figure 20. Each channel consists of a scintillation counter feeding into a cathode follower, a pulse shaping circuit, an amplifying stage, a discriminator and a trigger circuit. In addition, one channel also includes a preamplifier which is connected between the counter output and the cathode follower. This provides additional gain for the large photomultiplier (see below). The output pulses from the two channels are fed into a coincidence mixer, which gives an output pulse when the two input pulses are coincident in time. The block diagram also shows the shapes of the pulses occurring at various stages of the circuit.

Block Diagram of Fast Coincidence Unit, Showing the Ideal Pulse Shapes at Each Stage of the Circuit.

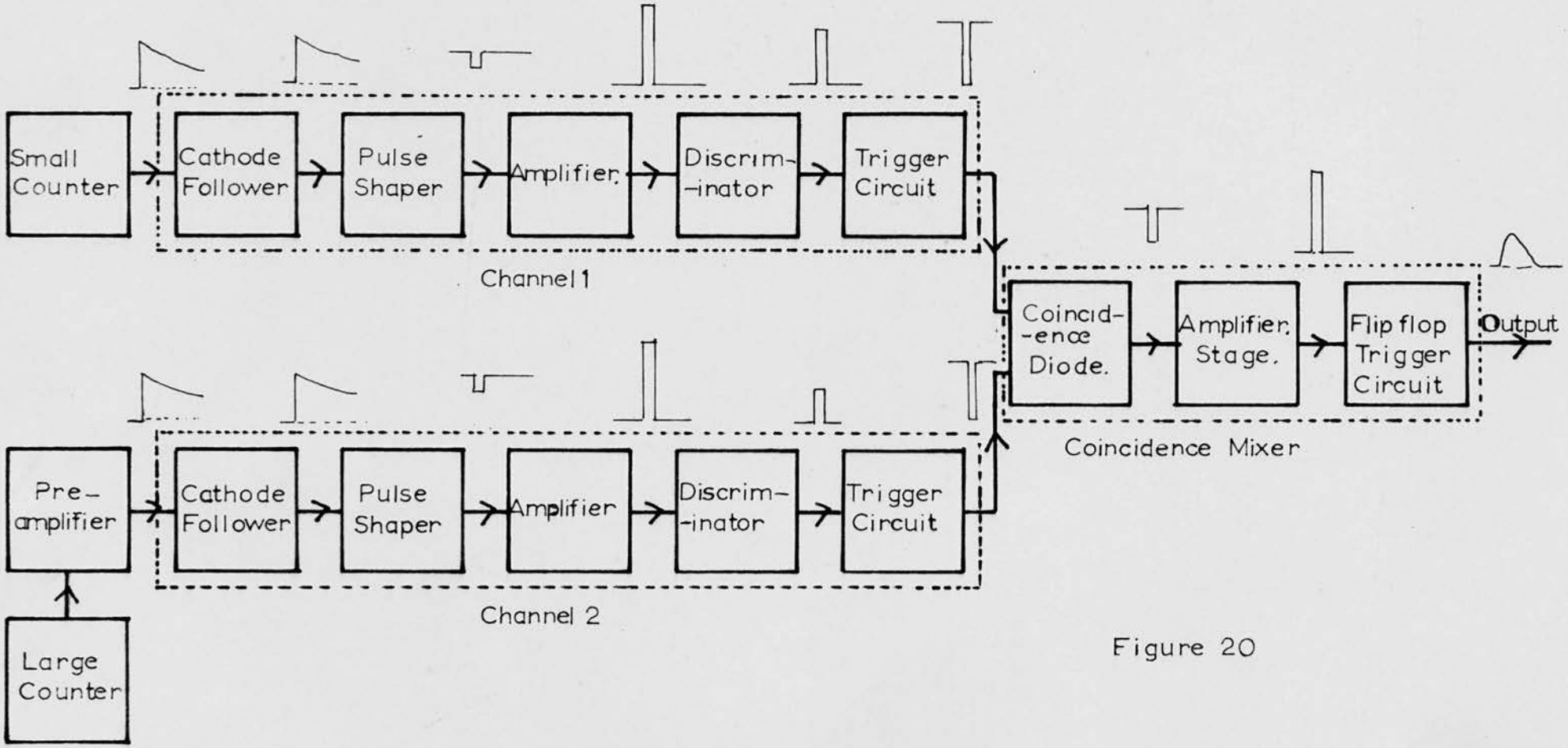

Figure 20

7.2. Theoretical description of operation of each channel.

7.2.1. General.

A circuit diagram of one channel is given in figure 21. The two channels are identical except that the photomultiplier in channel one is an E.M.I. 14 stage type 6262 with a photocathode diameter of two inches while that in channel two is an E.M.I. 11 stage type 6099B, with a photocathode diameter of five inches. This second tube requires additional gain, which is provided by the preamplifier. Both counters have already been described in an earlier chapter. The operation of one channel will now be considered in detail.

7.2.2. The photomultiplier.

The general principles of the photomultiplier have already been discussed in Section 4.2.1(c). At this point the shape of the output current and voltage pulses produced by it are of interest.

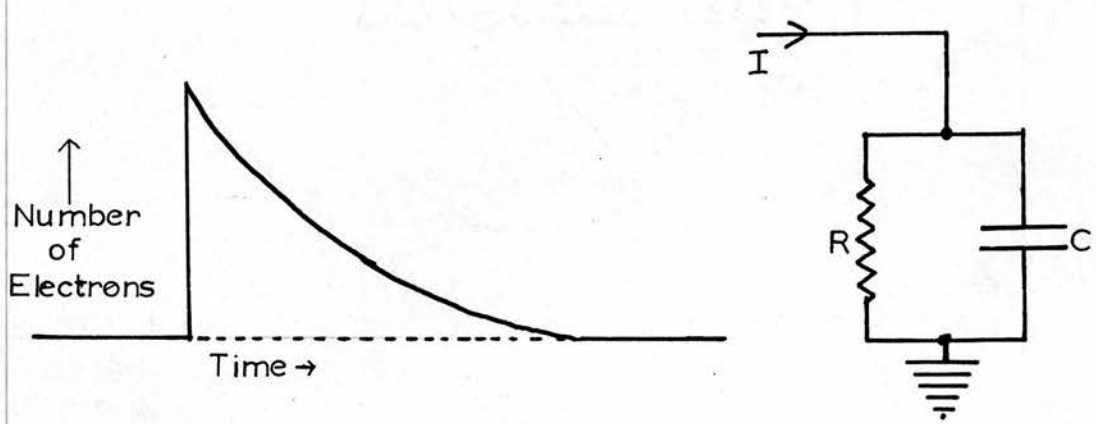

The diagram above shows the equivalent output circuit of the photomultiplier, and also the shape of the current pulse produced

A fast multiple coincidence circuit

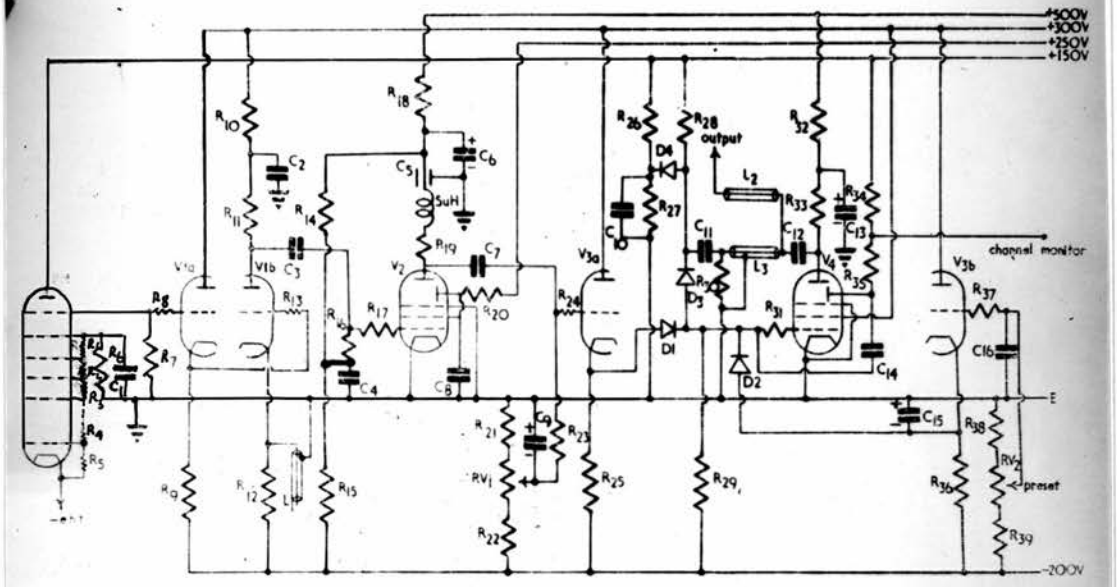

Amplifier, discriminator and trigger circuit

R_1–R_6 = 1 MΩ
R_7 = 22 kΩ
R_8 = 22 Ω
R_9 = 41 kΩ
R_{10} = 6·8 kΩ
R_{11} = 270 Ω
R_{12} = 41 kΩ
R_{13} = 22 Ω
R_{14} = 1 MΩ (high stability carbon)
R_{15} = 560 kΩ (high stability carbon)
R_{16} = 10 kΩ
R_{17} = 22 Ω
R_{18} = 10 kΩ w.w.
R_{19}, R_{20} = 1 kΩ
R_{21} = 1 kΩ
R_{22} = 68 kΩ
R_{23} = 10 kΩ
R_{24} = 22 Ω
R_{25} = 41 kΩ
R_{26} = 150 kΩ
R_{27} = 1·8 kΩ
R_{28} = 330 kΩ
R_{29} = 100 kΩ
R_{30} = 120 Ω
R_{31} = 22 Ω
R_{32} = 12 Ω
R_{33} = 1·8 kΩ
R_{34} = 120 Ω
R_{35} = 1 kΩ
R_{36} = 47 kΩ
R_{37} = 1 kΩ
R_{38} = 1·8 kΩ
R_{39} = 56 kΩ

RV_1 = 10 kΩ
RV_2 = 2·5 kΩ

C_1 = 0·001 μF
C_2 = 0·1 μF
C_3 = 1000 pF
C_4 = 5 μF
C_5 = 200 pF
C_6 = 8 μF
C_7 = 100 pF
C_8 = 0·5 μF
C_9 = 5 μF
C_{10} = 0·25 μF
C_{11} = 0·01 μF
C_{12} = 1000 pF
C_{13} = 8 μF
C_{14} = 50 pF
C_{15} = 5 μF
C_{16} = 0·02 μF

$V_{1a, b}$ = CV455
V_2 = CVX2276
$V_{3a, b}$ = CV455
V_4 = EFP60

PM = photomultiplier

L_1 = 120 Ω line, open end
L_2, L_3 = 120 Ω line

Figure 21

by it when an ionizing particle passes through the phosphor. The effect on the pulse shape of the transit time spread (see later) through the photomultiplier has been neglected. The pulse then has a sharp rise time, followed by an exponential decay, the decay time constant depending on the phosphor used for the counter.

The photons produced by the passage of the ionizing particle through the phosphor are emitted with a distribution similar to that shown in the diagram for the current pulse shape at the multiplier output. These photons travel to the multiplier photocathode where they are converted into photoelectrons.

In an actual photomultiplier, the different electrons formed by electron multiplication from the same initial photoelectron do not all reach the collecting electrode at the same time, as their path lengths are not all identical. This effect is called the transit time spread, and its magnitude depends on the type of photomultiplier in use. In general, the circular electrostatically focussed construction used in the R.C.A. type tubes is better in this respect than the longitudinal construction used in the E.M.I. tubes.

The joint effect of phosphor decay time and transit time spread on the shape of the output current pulse is complicated, and has been discussed by Lewis and Wells (Millimicrosecond Pulse Techniques - Pergamon Press - pages 220-223). For a given phosphor, an increase in the transit time spread leads to a decrease in the steepness of the current pulse rise time and its maximum amplitude. For a given photomultiplier, an increase in the phosphor decay time has a similar effect. Graphical results are given in the reference quoted.

It follows, therefore, that in order to obtain the minimum pulse rise time, the two effects should both have the minimum possible values. For this reason organic crystal and plastic phosphors are used where short resolving times are required, as the inorganic phosphors all have much longer decay times. For NaI(Tl) the decay time constant is 0.25μs, which is shorter than that for the other inorganic phosphors.

The following values are typical of organic phosphors. For napthalene, the time constant is 0.06μs; for anthracene 0.032μs and for stilbene 0.006μs. These values are given by Sharpe (Nuclear Radiation Detectors - Methuen - p. 41). For the NE101 plastic phosphor used in the present apparatus, the time constant is given by the makers as 4 mμs. As the emission of photons by the phosphor is a statistical process dependent upon the decay time, the time between the passage of the nuclear particle through the phosphor and the emission of the first few photons, and hence photoelectrons, decreases with the decay time. For the R.C.A. type 1P21 photomultiplier the transit time spread is about 1.5 mμs. For the E.M.I. 14 stage type 6262, it is about 15 mμs, giving a rise time to full amplitude of about 20 mμs. Figures for the 11-stage type 6099B are not available, but it can be expected to have a transit time spread of at least 10 mμs. Thus for these tubes, the effect of the photomultiplier itself is larger than that of the phosphor.

The voltage output pulse is produced by the above current pulse flowing into the stray capacity of the multiplier output C, shunted by a high resistance R (see earlier diagram). If there

were no transit time spread in the multiplier, this voltage pulse would rise with a time constant equal to that of the phosphor, and decay with a time constant R.C. A calculation for this case has been given by Swank (1954). If $RC \gg \tau$, (phosphor decay time) the amplitude is independent of τ. Transit time spread in the multiplier will increase the rise time of the voltage pulse. If this spread is greater than τ, the former will have the main effect on the rise time.

The calculation by Swank shows that the amplitude of the photomultiplier output voltage pulse is not much dependent on the phosphor decay time for the apparatus described here. Swank gives the maximum pulse amplitude, V_{max} as:-

$$V_{max} = \text{constant} \times \gamma^{\frac{1}{1-\gamma}}$$

where $\gamma = RC/\tau$ If $\gamma \gg 1$, $\gamma^{\frac{1}{1-\gamma}} \to 1$

In this case, R = 22 KΩ; C≈10 μμF and τ = 4 mμs.

$$\therefore \gamma = \frac{22 \times 10^{3} \times 10 \times 10^{-12}}{4 \times 10^{-9}} \approx 55$$

This gives $\gamma^{\frac{1}{1-\gamma}} = 0.93$, which is reasonable.

If the amplitude of the voltage pulse is of importance, as well as the initial rate of rise of the leading edge, it can be seen that the minimum order of magnitude of the pulse length that can be obtained by shaping is about 20 mμs, if full amplitude is to be obtained. By shaping is meant the removal of the long tail of the voltage pulse, to yield a short pulse. Once maximum amplitude has been reached, the rest of the pulse is not wanted, as short pulses are required to obtain minimum resolving time. From the

figures given above, it will be seen that the minimum resolving time of a coincidence system using E.M.I. multipliers and including amplitude discrimination, so that the full amplitude of the voltage pulse is used, is about 20 mμs. The system used has a nominal resolving time of this amount.

It is possible to obtain resolving times much less than the rise time of the output voltage pulse, by using only the first part of the rising edge. In this case, of course, amplitude discrimination cannot be used. The statistical spread in time between the passage of the particle through the phosphor and the emission of the first photoelectron from the multiplier cathode is now one of the limiting factors. Post and Schiff(1950) have investigated this problem and conclude that resolving times of less than 1 mμs can be obtained by this method. The transit time spread introduced by the multiplier will increase the possible resolving time, and Morton(1952) has given the minimum value as about 0.25 mμs for typical organic phosphors and R.C.A. tubes. Pulse height discrimination can be obtained in this type of circuit by using separate channels for it, fed by the same input pulses as the fast coincidence circuit. A final output pulse then requires coincident pulses from the discriminator channels as well as from the fast coincidence circuit. The discriminator channels need not be nearly as fast as the coincidence circuit. A system of this type is described by Bell(1948) following an idea by Bell and Petch.

In the unit described in this thesis, simplicity of circuitry was considered desirable for first experiments in this field, at some sacrifice of resolving time. The unit described is much

simpler than the system mentioned in the previous paragraph, but the resolving time is greater for the reasons discussed. E.M.I. tubes were used because counters employing them were already available, and a change to R.C.A. tubes would not have made a very great difference with the type of circuit used.

7.2.3. The cathode follower.

The output impedance of the photomultiplier is high, and a step type of output voltage pulse is obtained, the rise time being determined by the factors already discussed. In order to match this output impedance to the input impedance of the pulse shaping valve, a cathode follower circuit is used. This is effectively a feedback amplifier with a feedback factor of unity. The operation is discussed in the reference below. Referring to the circuit diagram, figure 21, the value V_{1a} used is an ECC81, which has a mutual conductance of 4.8 mA per Volt. The cathode resistor R has a value of 41 kΩ. According to theory (see, for example Parker - Electronics p. 272-3), the output resistance of the cathode follower is given by

$$R_o = \frac{R_a}{1 + \mu}$$

where R_o is the output resistance, R_a is the dynamic plate resistance of the valve and μ is its amplification factor. This assumes that the cathode resistor is much larger than the effective internal resistance of the valve, as the output impedance is equivalent to the value given above, in parallel with the cathode resistor. If $\mu \gg 1$ (57 in this case), $R_o \approx 1/g_m$

As g_m = 4.8 mA/volt, $R_o \approx 210\,\Omega$.

The reference quoted above gives the voltage amplification of the cathode follower as

$$A' = \frac{A}{1 + A}$$

where A' is the amplification and A is the amplification that would be obtained without feedback, given by

$$A = \frac{\mu R_k}{R_k + R_a}$$

In this case, $\mu = 57$, $R_k = 41\ k\Omega$, $R_a = 12\ k\Omega$. Hence $A = 44$. The actual amplification obtained is therefore 44/45, which is very nearly unity.

The other quantity of importance is the input impedance of the device. The same reference (Parker, p. 330) gives this as

$$R_i = \frac{R_g}{1 - A'}$$

where R_i is the input resistance and R_g is the grid leak resistance. In this case, $R_g = 22\ k\Omega$ and $A' = 44/45$

$$\therefore \quad R_i \approx 1\ M\Omega.$$

This will be sufficiently high to match the photomultiplier output impedance satisfactorily, as this impedance is equal to the same resistance as the grid leak, in parallel with the dynode stray capacity and a large resistance due to the rest of the multiplier. The resistive part is therefore $22\ k\Omega$.

A few remarks on impedance matching are relevant here. It will be evident that a small impedance feeding into a large one will effect a satisfactory match. If R_1 is the output resistance of the first circuit and R_2 the input resistance of the second, then the amplitude of the voltage signal developed

across the second resistance will be $\frac{R_2}{R_1 + R_2}$ times that at the output of the first. If $R_2 \gg R_1$, this approaches unity. If $R_1 \gg R_2$ on the other hand, the match is bad and a very great loss of amplitude occurs. Stray capacities etc. have been neglected above.

If the cathode follower were not present, distortion would occur, and also loss of pulse amplitude. The main function of the cathode follower is thus to act as an impedance transformer, giving an output of the same shape as the input, but at a much lower impedance. Cathode followers are used in several other parts of the circuit the action being, of course, the same as that described above.

7.2.4. <u>The Pulse Shaping Circuit</u>.

As can be seen from the circuit diagram, the pulse shaping circuit consists of the valve V_{1b} and associated components. The anode load resistor is 270 Ω and the cathode resistor 41 kΩ. If a positive pulse was applied to the grid in the absence of the coaxial cable L_1 in the cathode circuit, the cathode voltage would follow the grid voltage in a manner similar to that of the cathode follower. Owing to the presence of the cable, this action is somewhat modified.

The input step function from the cathode follower is fed to the grid of the valve. The potential at the junction of the valve cathode and the shaping cable rises by about half this amount, assuming that the input impedance at the cathode is equal to the characteristic impedance of the cable. If this is not the case, the action will be similar but the potential changes will be

different. At the same time, a voltage step of about half the input amplitude travels down the cable and is reflected without change of polarity at the open circuited end. It then returns along the cable to the cathode, raising the potential of the cathode so that the grid-cathode potential becomes the same as it was before the pulse was applied.

The output pulse from the anode is therefore a negative pulse of length equal to the time taken for the step function to travel down the cathode cable and be reflected back to the cathode. If the cathode input impedance of the valve is equal to the characteristic impedance of the cable, there will be no reflection at the cathode.

A discussion of the reflection of pulses by transmission lines and the variation of potential at the input end is given in Lewis and Wells (loc. cit., pages 33-38). The case above is that of a line having a terminating impedance of infinity. The diagram shows the changes in potential which occur in the different parts of the circuit. Two input pulses are shown.

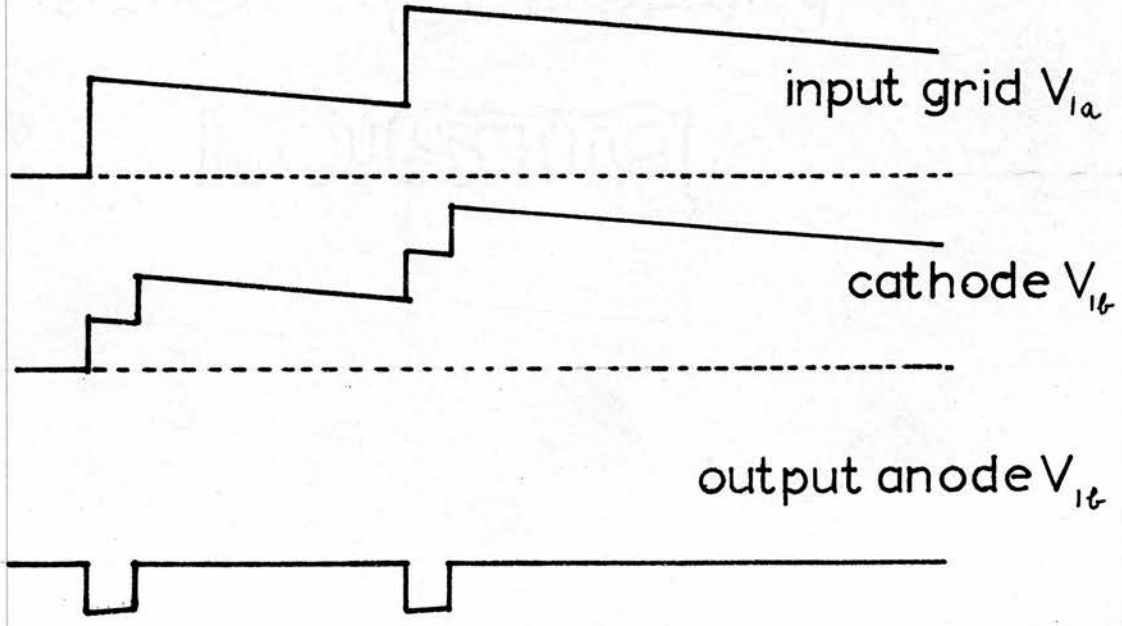

For the cable used in this apparatus, the delay per metre is about 5 mμs. As a pulse length of about 20 mμs was required, the length of the cable was made about 2 metres. Short pulses are required, as the length of the pulse determines the resolving time of the system. Also the long tail of the pulse would tend to paralyse the circuit at high counting rates.

7.2.5. The amplifier stage.

The negative output pulses from the anode of V_{1b} are amplified by the circuit containing the secondary emission valve V_2 which is a Mullard type EFP60.

Pulse amplifiers employing conventional pentodes suffer from the fact that the input and output capacities of the valves limit the minimum pulse rise time which can be handled by the amplifier. Consider a pentode with anode load R and mutual conductance g. The gain at moderate frequencies is then given by the usual formula for the pentode, $G = gR$. At high frequencies, the anode load impedance is reduced by the stray capacity C which shunts the load R and causes a reduction is gain. This stray capacity consists of the anode to earth capacity of the valve, plus the input capacity of the following valve. When the impedances of R and C are equal, the response is reduced to $1/\sqrt{2}$ of that at moderate frequencies, defining the cut off frequency which is taken as the bandwidth. When this happens,

$$R = \frac{1}{\omega C}$$

$$B = f_c = \frac{1}{2\pi RC} \quad , \quad \text{as the lower cut-off}$$

frequency is very small.

The product of gain and bandwidth is thus

$$G.B = gR \frac{1}{2\pi RC} = \frac{g}{2\pi C}$$

and is thus dependent only on the valve and not on the load resistance. The value of C will also include any capacity introduced by the wiring.

For a typical pentode used in amplifier circuits, type EF91 (CV138); g = 7.5 mA/V and $(C_{in} + C_{out}) = 9\mu\mu F$, giving a gain bandwidth product of 130 Mc/s. From the equation for this quantity, it is obvious that its value increases if C decreases or if g increases. It is not possible to decrease C below certain limits, but there are two methods by which g can be increased without a corresponding increase in C.

The first method is to connect a number of valves in parallel in such a way that their mutual conductances are added without adding their stray capacitances. Such an arrangement is known as a distributed amplifier, and details of this can be found in numerous references (see, for example, Farley - Elements of Pulse Circuits, p. 95, or Bell - Annual Review of Nuclear Science, Volume 4, p. 95).

The second method is to employ a secondary emission pentode in the amplifier stage. This type of tube consists of a normal pentode with a secondary emitting dynode in place of the usual anode. The grid of the pentode controls the electron flow to the dynode in the usual way, and an anode collects the secondary electrons emitted from the dynode. If the secondary emission ratio is four, this means that the current to the anode is four times that to the dynode, the net dynode current being a reverse current of three

times the incident current. Thus if the original pentode had a mutual conductance g_m, the secondary emission pentode has a mutual conductance of $4\ g_m$ for the anode and $-3g_m$ for the dynode, with no appreciable change in stray capacities. Thus a considerable improvement in the gain-bandwidth product has been achieved.

For the EFP60, g is given as 25 mA/V and $(C_{in} + C_{out}) = 15 \mu\mu F$. This gives a gain-bandwidth product of 260 Mc/s, which is about twice as good as that for the conventional pentode. In the amplifier described, the anode load resistor is 1 kΩ, giving a gain of 25 for the amplifier, so that the bandwidth is about 10.5 Mc/s.

For an amplifier transmitting frequencies up to f the approximate minimum rise time, t_r is given by Farley (loc. cit. p. 87) as

$$t_r = \frac{1}{3f}$$

In this case $f = 10.5$ Mc/s

$$\therefore \quad t_r \approx \frac{1}{32} \times 10^{-6} \text{ sec.}$$

$$\approx 30 \text{ m}\mu\text{s.}$$

This time is thus of the same order of magnitude as the limitation in rise time imposed by the transit time spread of the photomultipliers.

It is, of course, also true that the greater the bandwidth of an amplifier, the less the distortion of any pulse amplified by it. Hence the circuit above will transmit short rectangular pulses with small distortion. This is necessary in the apparatus described here. To obtain bandwidths greatly in excess of those used here, in order to amplify pulses 1 mμs long, requires considerably

more complicated circuits than that described above.

As the mutual conductance of the dynode is negative, this implies that amplified output pulses can be taken from it which are in phase with the input pulses. This fact is used in the preamplifier described later.

7.2.6. The discriminator and trigger circuit.

It will be convenient to consider this section as one unit. The whole circuit is similar in several respects to one which has been described by Moody, and which is discussed in Lewis and Wells (loc. cit. p. 232-4).

In the circuit described here, positive pulses from the anode of the amplifying valve V_2 are fed at low impedance to the cathode of the germanium diode D_1, via the cathode follower V_{3a}. The cathode follower V_{3b} applies a negative bias to the grid of the trigger circuit valve V_4, to ensure that it is non-conducting in the quiescent state. As soon as the grid potential of V_4 rises positively, above the value set by V_{3b}, the diode D_2 ceases to conduct and the grid potential can continue to rise rapidly. The potentiometer RV_2 which controls this bias is preset at a suitable value.

The potential difference across the diode D_1, which determines the height of output pulse from the amplifier which is needed to operate the trigger circuit, is varied by means of the potentiometer RV_1, if RV_2 is preset. A pulse which is large enough to overcome this bias, and the grid bias on the trigger valve, will cause the latter to start conducting. An amplified pulse in phase with the input pulse at the grid is then fed back from the dynode via the

condenser C_{14}. This drives the grid potential still more positive so that the circuit is regenerative due to this positive feedback. The current through the valve therefore continues to rise, a large proportion of the dynode current being taken by the grid, dependent on the circuit parameters. In the absence of the delay cable L_3, the anode potential would rapidly reach a value determined by the circuit parameters, and then gradually rise as the condenser C_{14} connecting dynode and grid charged up owing to the grid current. When the grid current had fallen to a small value, the dynode current would begin to fall so that its potential dropped. This charge being fed to the grid, the valve would be regeneratively turned off again. The pulse length would be $\sim 1\,\mu s$.

The presence of the delay cable L_3 modifies this action. The anode potential rapidly falls to its minimum value, dependent on the anode load resistor and other circuit parameters; also on space charge effects in the valve. A negative pulse from the anode is transmitted via the cable L_3 and the diode D_3 to the control grid. When this pulse reaches the grid, it initiates the regenerative cutting off of the valve as mentioned above. In this case, however, the pulse length is equal to the delay time of the cable L_3. L_3 is about 4 metres long, so that negative pulses about 20 $m\mu s$ long are obtained from the anode of V_4. The pulse height with the circuit as used is about 30-35 volts. These pulses are then fed via the cable L_2 to the coincidence mixer.

The diode D_4 and its associated circuit bypasses any positive components of pulses appearing at the function of D_3 and D_4. These would otherwise tend to cut off D_3 and prevent it operating with the negative pulses.

7.2.7. Summary of channel description.

The operation of a single channel of the coincidence system has been explained. A theoretical discussion of some of the physical problems associated with such a system has also been given, where relevant.

The original designers gave the gain of the combination of pulse-shaper, amplifier and discriminator as seven. They used a CVX2276 valve instead of an EFP60 for the amplifier stage, which had a gain-bandwidth product of 280 Mc/s and a mutual conductance of 19 ma/volt. Thus with the same anode load (1 kΩ) as used here the gain of the amplifier stage was 19. In the absence of the cable L_1, the gain of the shaping circuit valve V_{1b} would be about unity, with the anode load used. Owing to the shaping action of the circuit (see earlier) this gain is effectively reduced to ~ 0.5, giving a value of 9 for the total amplification of the stage. The rest of the loss of gain occurred by attenuation in the cathode followers and other coupling components. The total gain of the circuit described here is about 10.

7.3. Theoretical Description of Operation of Coincidence Mixer.

The circuit diagram of the coincidence mixer is given in figure 22 . The coincidence circuit used consists of an arrangement of biassed diodes. Switches are inserted between the diodes D_1, D_2, D_3, D_4 and the cable matching resistors R_1, R_2, R_3, R_4; in order to select the number of coincident input needed to give an output pulse large enough to operate the succeeding circuits. If the switches connected to any inputs are open, these inputs are not operative.

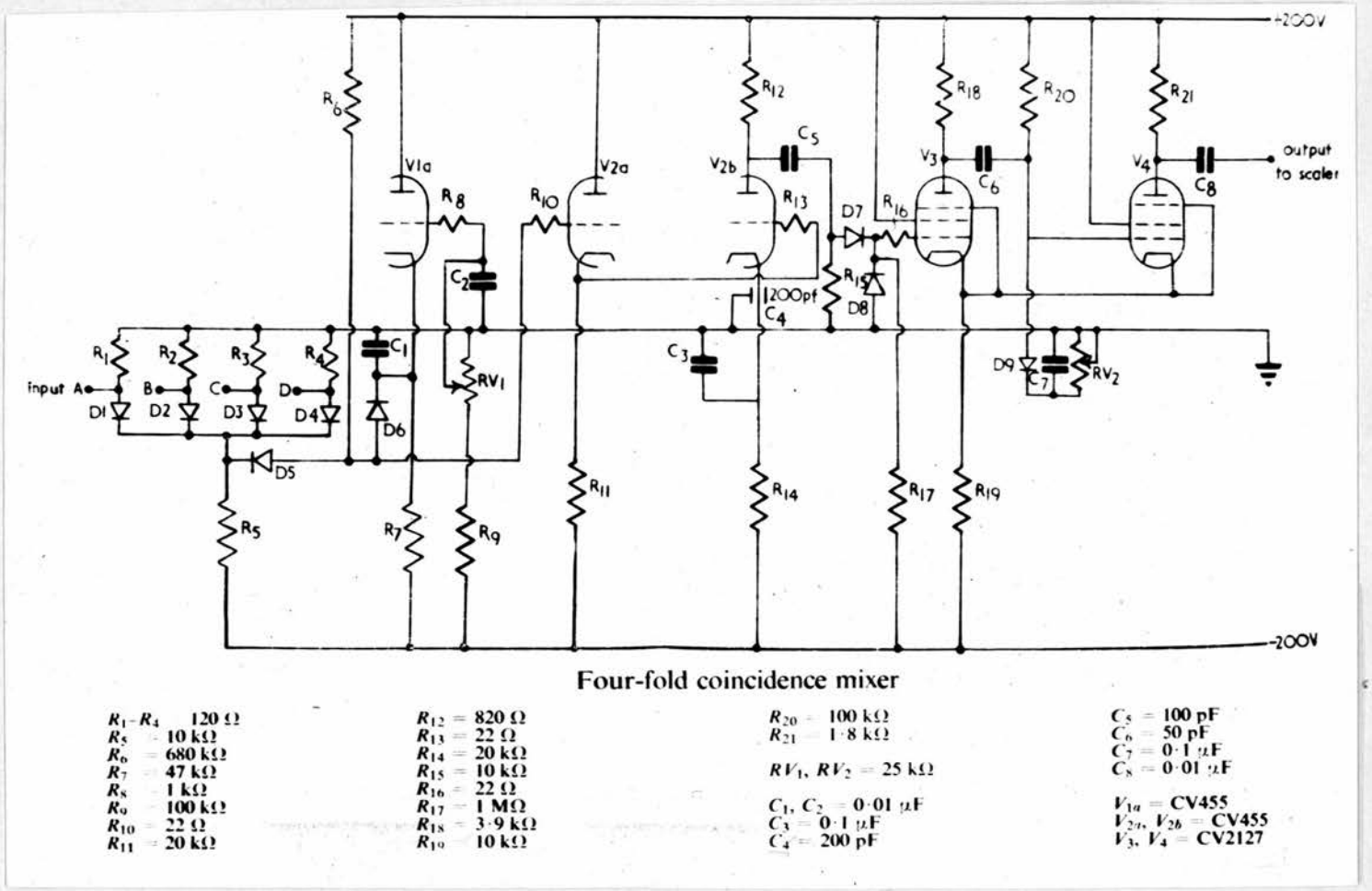

Four-fold coincidence mixer

R_1–R_4 = 120 Ω
R_5 = 10 kΩ
R_6 = 680 kΩ
R_7 = 47 kΩ
R_8 = 1 kΩ
R_9 = 100 kΩ
R_{10} = 22 Ω
R_{11} = 20 kΩ

R_{12} = 820 Ω
R_{13} = 22 Ω
R_{14} = 20 kΩ
R_{15} = 10 kΩ
R_{16} = 22 Ω
R_{17} = 1 MΩ
R_{18} = 3·9 kΩ
R_{19} = 10 kΩ

R_{20} = 100 kΩ
R_{21} = 1·8 kΩ

RV_1, RV_2 = 25 kΩ

C_1, C_2 = 0·01 μF
C_3 = 0·1 μF
C_4 = 200 pF

C_5 = 100 pF
C_6 = 50 pF
C_7 = 0·1 μF
C_8 = 0·01 μF

V_{1a} = CV455
V_{2a}, V_{2b} = CV455
V_3, V_4 = CV2127

Figure 22

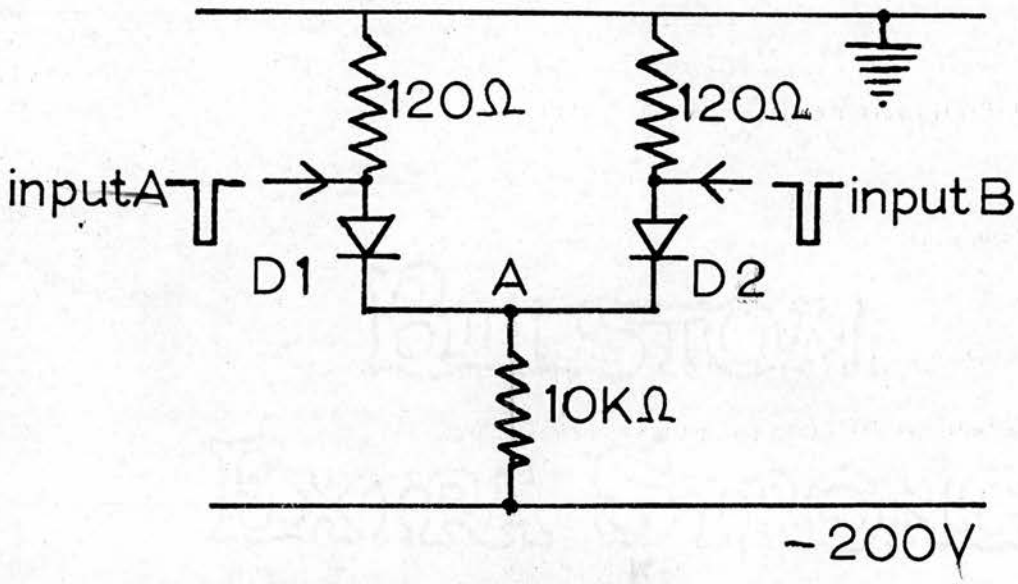

Consider the arrangement in the diagram above. In the quiescent state, current flows through the 10 kΩ resistor and the parallel arrangement of diodes. If the forward resistance of a diode is taken as about 330 Ω (Maker's Data), the potential at point A will be $-\frac{225}{10,225} \times 200 = -4.5$ volts.

If a negative pulse of sufficient amplitude is supplied to only one input, the diode on that side is cut off, so that the potential at the point A changes by about 4.5 V to −9 volts.

If simultaneous negative pulses of the same amplitude (in this case 35 volts) are applied to the two inputs, the potential at the point A goes down by 35 volts, the pulse height. A similar result is obtained if an input pulse is applied to a single diode D_1, the switches S_2, S_3, S_4 being open.

The cathode of the diode D_5 has a variable negative bias applied to it via the cathode follower V_{1a}. This bias is varied by the potentiometer RV_1. Using the calculations in the previous

paragraphs, if the system is set to record doublefold coincidences, singlefold pulses will fail to get through the diode D_5 if the cathode potential of this diode is more than 9 volts negative. Doublefold events will be rejected by a bias of more than about -35 volts at this point. The bias is normally set at -25 to -30 volts.

Valve V_{2b} is an amplifying stage which amplifies pulses fed to it by the cathode follower V_{2a}. The positive output pulses are fed to V_3, via the condenser C_5 and the diode D_7.

The valves V_3 and V_4 are arranged as a long tailed pair (see Farley - loc. cit. p. 29-31). In the quiescent state, each valve is conducting 9 or 10 mA (measured with meter), RV_2 being adjusted so that the grid potentials are approximately equal. Referring to the reference (p.30) a positive (or negative) signal on one grid in the long tailed pair circuit produces a positive (or negative) signal respectively on the opposite anode. If a positive signal is applied to the grid of V_3, the anode potential falls and a negative pulse is fed to the grid of V_4 via the condenser C_6. This produces a further negative signal on the anode of V_3 which is also fed to the grid of V_4 by the condenser. Thus the action is cumulative and continues until V_4 is cut off. The change of potential at the anode of V_4 is equivalent to a current change of about 9 mA through a resistance of 1.8 kΩ. This gives a positive output pulse of about 16 V at the anode of V_4, which can be used to operate the subsequent circuits. The pulse length (about 1μsec. in this case) is determined by the time taken for the grid potential of V_4 to rise sufficiently to start the valve conducting again, when the circuit will return to its initial state. The

diode D_9 prevents the grid of V_4 going further positive than originally, and starting continuous oscillation of the circuit, by shorting positive pulses to earth, via the diode and the 0.1μF condenser C_7. The circuit therefore returns to its original current condition, as determined by the setting of RV_2, after one output pulse.

7.4. Concluding Remarks.

As no oscilloscope was available which could show pulses as short as 20 mμs at anything like their true shape or amplitude, the action of the circuits described above had largely to be inferred from the results obtained. As will be seen in the later chapters correct operation was confirmed.

7.5. Constructional Details and Auxiliary Apparatus.

7.5.1. General.

Each channel, and the coincidence mixer unit, is mounted on a separate welded steel chassis 12 in. x 17 in. x 3 in., with a front panel 19 in. x 9 in. The input and output leads for the power supplies consist of three and six-core screened cable, connected to appropriate coaxial sockets and fitting appropriate coaxial plugs on the chassis. The pulse input and output leads are single core coaxial cable. In addition to the above units, there are also a voltage distribution chassis and a preamplifier chassis.

7.5.2. Voltage distribution chassis.

This chassis supplies the following voltages to the coincidence

unit channels viz. +500V, +300V, +200V, +150V and -200V with respect to earth. The positive voltages are all obtained from a 500V supply by means of voltage stabilizers and current limiting resistors.

A stabilized power pack (Solartron type SRS151A) supplies +500V at a rated peak current of 300 mA. This is fed to the voltage distribution chassis, the circuit of which is shown in figure 23. As the voltage drop across a stabilizer remains almost constant while the current through it varies within certain limits, this provides a method of obtaining a constant voltage supply, the value of which does not vary with the current drawn from it. If dropping resistors were used, the voltage obtained would, of course, vary with the current. A typical voltage stabilizer, the CV216, has a voltage drop across it of about 150V while the current through it varies in the range 5 mA to 40 mA. If a suitable resistance is placed in series with it to limit the maximum current to 40 mA, up to 35 mA can then be obtained at a potential of 150V. Combinations of different stabilizers can be used to give different voltages. All the positive voltages are obtained from the 500V supply by this means. The negative supply (-200V) is obtained from a stabilized power pack (Solartron type AS517) which gives -300V at a maximum current of 100 mA. This supplies current to two Mullard 4687 stabilizers in series, together with a current limiting resistor. The burning voltage of each stabilizer is about 100V, giving a total across both of 200V. A circuit diagram of the unit is shown in figure 23.

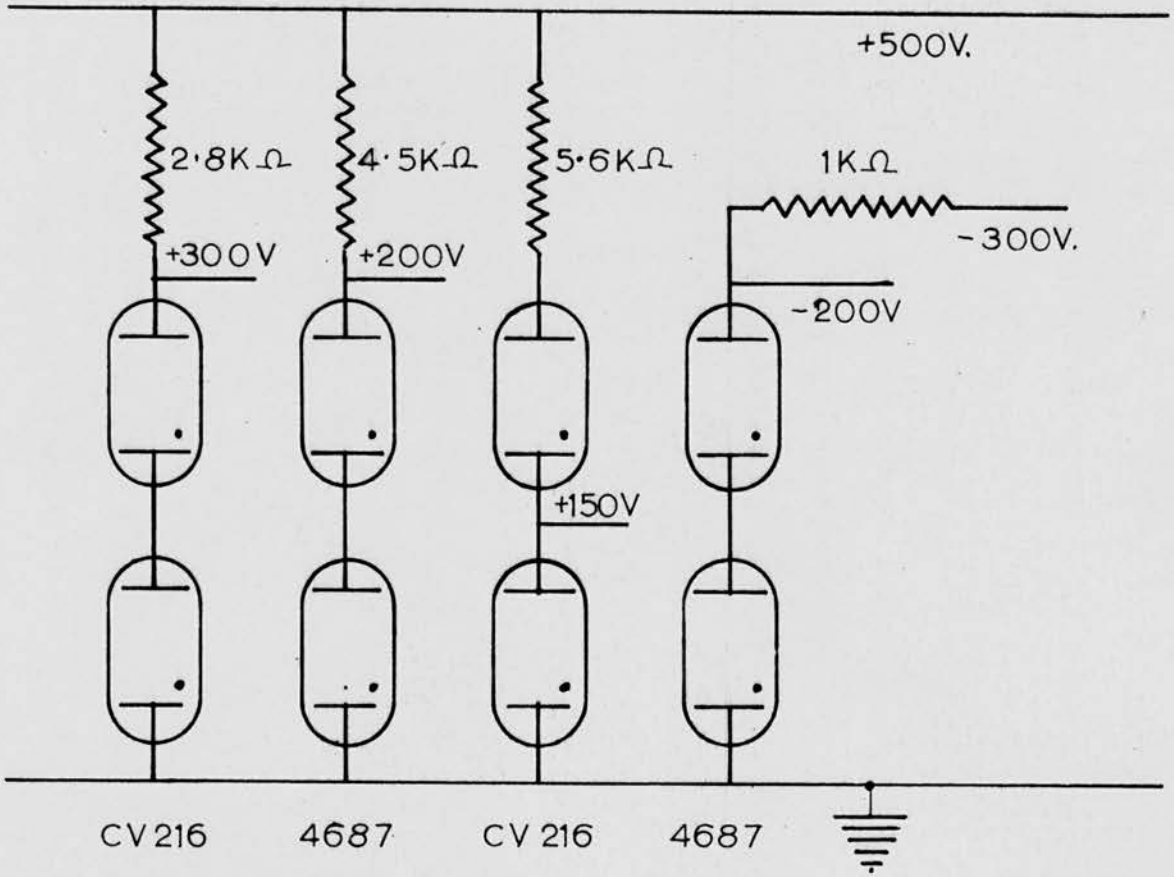

Voltage Distribution Chassis Circuit. Figure 23.

7.5.3. Preamplifier.

The preamplifier was constructed as it was found that output pulses of sufficient height were not available from the 5 in. photomultiplier tube, without running it at a very high E.H.T. voltage. This would lead to non-linearity of operation, due to space-charge effects in the tube, and would be detrimental to its performance.

An amplifier stage using a single EFP60 secondary emission pentode gives sufficient gain ($\sim$20). The circuit for this is identical to that used in each channel of the coincidences unit, except that the output pulses are taken from the dynode instead of the anode. This gives amplification without phase inversion, as has already been mentioned in the earlier description of the channel amplifier stage. Pulses are fed to the amplifier valve by a cathode follower, the circuit of which is the same as that used in the early experiments with photomultipliers (chapter 4). A circuit diagram is given in figure 24.

7.5.4. Delay-line box.

For most of the experimental work to be described, a variable time delay in one or other channel was necessary. This consisted of a variable length of coaxial cable, of characteristic impedance 122 Ω (B.I.C. cable type T3042) and having a solid polythene dielectric. For such a cable, the velocity of propagation of a pulse is independent of the frequency, and is equal to that of a plane wave in an infinite volume of the dielectric which fills the space between the conductors. The time delay per unit length, T, is therefore given by:-

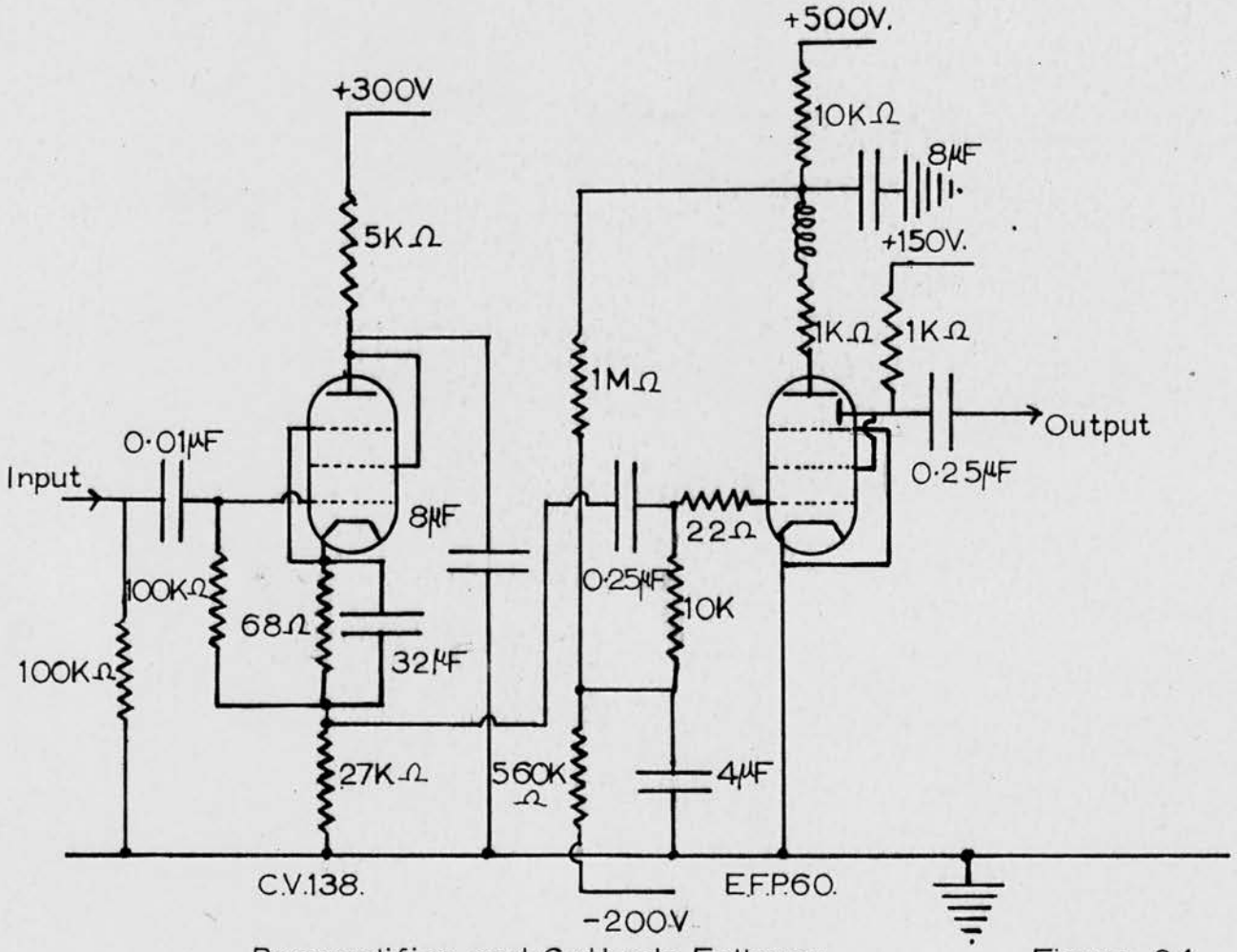

Preamplifier and Cathode Follower

Figure 24.

$$T = \sqrt{\varepsilon\mu} = \frac{10}{3}\sqrt{K_e K_m} \text{ m}\mu\text{sec/metre}$$

where $K_e = \varepsilon/\varepsilon_o$ is the relative permittivity of the medium and $K_m = \mu/\mu_o$ is the relative permeability of the medium. For polythene, $K_e = 2.30$ (Kaye and Laby, p. 95) and K_m can be taken as 1.00. Hence:-

$$T = \frac{10}{3}\sqrt{2.30} \text{ m}\mu\text{s/metre}$$

$$= 5.05 \text{ m}\mu\text{s/metre.}$$

The cable is stated by the makers to be suitable for use at frequencies up to 500 Mc/s with an attenuation of 0.27 db per 100 feet at a frequency of 1.0 Mc/s.

The characteristic impedance of a cable depends on the ratio of the diameters of the inner and outer conductors, and on the dielectric used. For this cable the inner conductor diameter is 0.0148 in. and the outer conductor diameter is 0.335 in. (approx.) The ratio $r_{outside}/r_{inside}$ is thus equal to 22.6. The characteristic impedance (Z_o) of an air-spaced cable is $138 \times \log_{10} \frac{r_{outside}}{r_{inside}} \Omega$. For a cable with a dielectric, this value is multiplied by $\sqrt{K_m/K_e}$ which is $\sqrt{\frac{1}{2.30}}$ in this case. Hence for the given cable, $Z_o = \frac{138}{\sqrt{2.30}} \log_{10} 22.6$ which gives 123.5 Ω, in good agreement with the value of 122 Ω given by the makers, allowing for the approximate value of the ratio $r_{outside}/r_{inside}$ used.

The delay line box as constructed consists of ten metres of cable, composed of ten separate lengths of one metre which can be

joined together as required. A rotary switch enables the output plug to be connected to any one of the junctions between the lengths. The ends of each separate metre of cable are connected to small sockets which are fixed to the front of the box. The lengths can be joined together by means of short lengths of wire with a plug on each end. This enables the length of cable not in use for a given delay to be disconnected, as otherwise undesirable reflections would take place from the open circuit end. For example, if seven metres of cable are in use, the remaining three are disconnected.

It can be noted at this point that an unknown amount of extra delay is incorporated in one channel with respect to the other, owing to the presence of the preamplifier, and to any assymmetry in the two channels. This is of no importance, as it will be seen later that it is only the difference in the two delays which matters, and this can be adjusted by means of the variable delay.

7 .5.5. Conclusion.

The construction and theoretical operation of the fast coincidence circuit has been given. Descriptions have also been given of the auxiliary apparatus needed in conjunction with it. The calibration of the apparatus, its use to determine the velocity of γ-rays and the experiments done in conjunction with a Wilson Cloud Chamber will be described in the following chapters.

Chapter 8.

EXPERIMENTAL TESTS OF FAST COINCIDENCE UNIT

8.1. Determination of resolving time of unit.

8.1.1. Introduction.

Experiments were performed to find the resolving time of the unit. This was done by two separate methods:

(a) Insertion of a variable delay in one channel, in order to obtain a delayed coincidence curve from which the resolving time was measured.

(b) The use of a double pulse generator.

Values of the resolving time were obtained which were self-consistent, and in accord with the design value.

8.1.2. Theory of delayed coincidence method, and shape of curves obtained.

If the output pulses from both channels of the coincidence unit are rectangular and of length τ, the delayed coincidence curve will be rectangular and of width 2τ. This is fully explained in Chapter 6(section 6.2.) Delay inserted in one channel can be arbitrarily called positive and in the other, negative.

In a practical circuit, a truly rectangular shape is never obtained. The shape of the curves actually obtained is shown below.

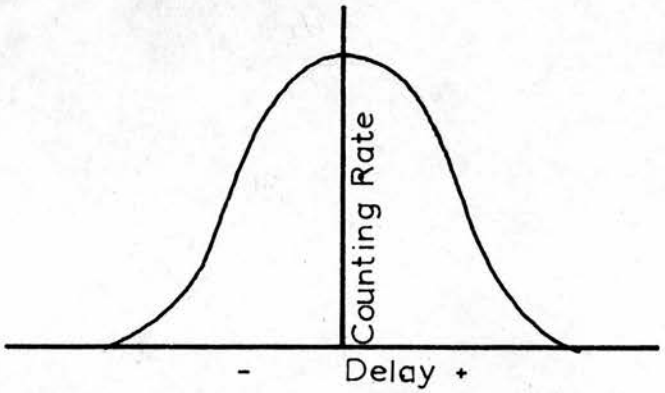

The main reason for this difference is that an output pulse from a channel is not produced at a fixed time after the input pulse, but there is a statistical spread in the time due to the channel itself. Binder (1949) has investigated this problem mathematically, and he concludes that the shape of the distribution should be that of the Gaussian error curve assuming that the resolving time of the circuit can be considered small compared to the statistical spread in channel delays. He compares his theory with some results obtained by MacIntyre (1949) for the decay of Na^{24} by β -emission into Mg^{24}, which then decays by γ -emission with a half life much less than the resolving time of the apparatus. Good agreement is obtained. That the shapes of the curves obtained are reasonable is shown in the following diagram and discussion.

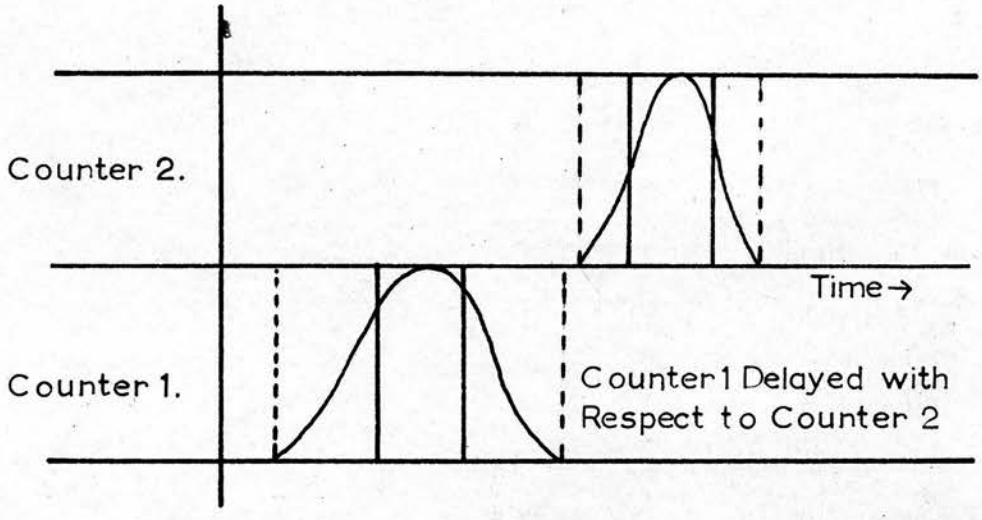

If the statistical spreads in transit time for the channels are indicated approximately by the dotted lines, some coincidences will be obtained whenever the extremes of the dotted regions overlap. In theory, of course, there will still be a chance of a coincidence when there is no overlap, but it will be very small. If the distributions of pulses in time between the dotted limits are

Gaussian, and have maxima at the centres of the full-line pulses, then delayed coincidence curves of the shapes obtained in practice are to be expected. If the statistical delays are much greater than the resolving time, a curve of approximately Gaussian shape will be obtained, corresponding to narrow full-line pulses and wide dotted regions in the diagram above. If the resolving time is greater than the statistical delays or of the same order of magnitude, the curve will have a flat top corresponding to the period when the overlap between the pulses is large. If the statistical fluctuations in the two channels are different, the same general shape of curve will be obtained. Curves of these types have been obtained in the experiments described later.

Deviations in transit time through the channel arise through a number of factors. The time at which a pulse gets through the discriminator after it starts to rise depends on its amplitude, as the smaller the pulse, the greater the time taken to rise above the discriminator bias. This is because the rise time is the same irrespective of amplitude, as shown in the diagram.

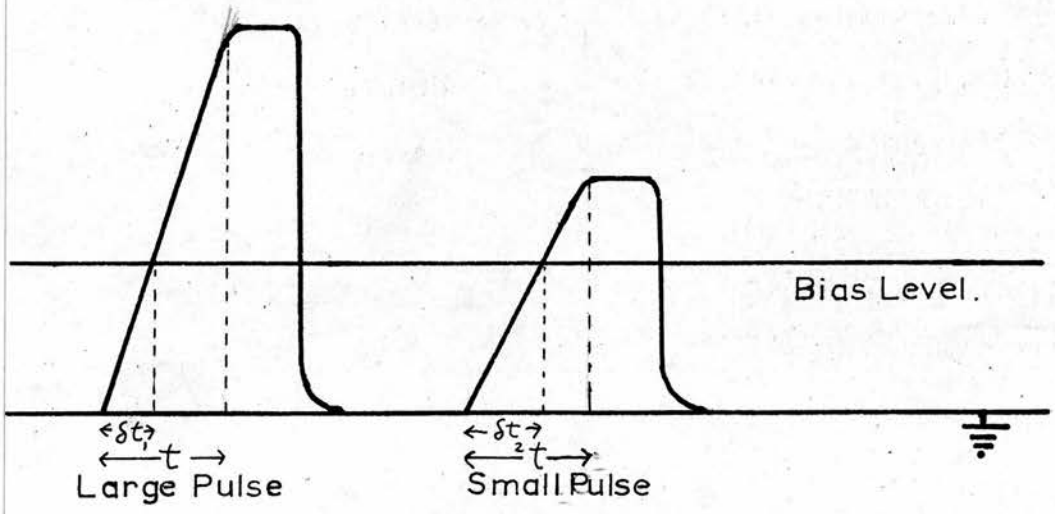

This will tend to give a larger delay for pulses having longer mean rise times. Another cause of statistical delay will be an uncertainty in the triggering time of the channel output trigger circuit, as this will not always trigger on the same size of input pulse. Other statistical delays in transit time through the channel will also be present. A statistical fluctuation in the time of the output pulse from the coincidence mixer due to variations in triggering time of the output flipflop will also contribute to the time spread. The actual value of the r.m.s. deviation from the mean time at which the coincidence is recorded will depend on the apparatus used.

If coincidence counts are performed, using pairs of γ-rays which are emitted with a time separation much less than the resolving time of the apparatus, a curve of the type described above is obtained. Experiments using Co^{60}, which emits two γ-rays within a time $\sim 10^{-12}$ sec of each other, produced curves of this approximate shape.

A γ-ray passing through the scintillator can lose energy by three processes:-

(i) Photo-electric absorption.
(ii) Compton scattering.
(iii) Pair production.

For the γ-rays from Co^{60}, which have energies of approximately 1.2 Mev, the cross-section for Compton scattering is much larger than those for the other two processes. The energy of the Compton electron produced can vary from zero up to a maximum of E_c where E_c is given by:-

$$E_c = \frac{E_1}{1 + m_0c^2/2E_1}$$

Here E_1 is the initial energy of the γ-ray, and $m_o c^2$ (= 0.51 Mev) is the rest energy of the electron. In this case, E_1 = 1.2 Mev. Hence $E_c \approx$ 1.0 Mev.

If the Compton electron has a small energy, the scattered photon may produce a second Compton electron. By this time, the energy of the photon will be small, and as the cross-section for photo-electric absorption increases with decreasing photon energy, a photoelectron will probably be produced. The cross-section for pair production at an energy of 1.2 Mev is very small and can be neglected in comparison with the other processes.

The Compton and photo-electrons now lose energy by ionizing the atoms in the phosphor. If the phosphor is sufficiently large to ensure that all the electrons produced by a given γ-ray are then absorbed in it, the total energy of the γ-ray can be absorbed. The phosphors used here are large enough to satisfy this condition for a large proportion of the incident γ-rays.

If a delayed coincidence curve is obtained using the pairs of γ-rays from the Co^{60} source, the sides of the curve are less steep than for a curve obtained using a single counter, as input to both channels. The reason for this is that the statistical spreads in transit time times through the two channels are now greater; as genuine coincidences can be obtained between pairs of γ-rays which lose all their energy in the phosphors (most likely) between a γ-ray which loses a large amount of energy and one which loses a small amount, and between pairs which both lose a small amount. The photomultiplier output pulse heights are assumed to be proportional to these energy losses. Hence, owing to the non-zero

rise time of these pulses, statistical variations in channel transit time will be produced as explained earlier in this section. The same sort of effect will be present when using cosmic rays, and obtaining coincidences due to single particles passing through both phosphors in turn, as the energy losses will not be constant, but will depend on the path lengths in the phosphors.

8.1.3. Experimental arrangement.

The apparatus was set up as shown in figure 25 , with the variable delay line box in channel one, in the position shown. The pulses from a single scintillation counter (the one with the 2 inch photomultiplier tube) were fed into both channels at the same time. The discriminators ($R\ V_1$) of both channels were adjusted so that reasonable counting rates of approximately equal magnitude were obtained for both when on singlefold count. No source was present at this stage, and the counter counted cosmic rays and background radiation. The singlefold counting rate for each channel was about 1500 per minute. Counting rates at the output of the coincidence chassis were measured on a scaler.

Readings of the coincidence counting rate as measured by the scaler were obtained for various values of the delay time in the delay line box. As the delay was increased, the coincidence rate approached zero, showing that the unit was functioning correctly. Two preliminary curves, taken on succeeding days, are shown in figure 26, each 5.0 mμs corresponding to 1 metre of cable (see earlier discussion of the delay line box). The difference in the maximum counting rates is due to a small difference in the photomultiplier E.H.T. in the two cases. The flat top of the

Block Diagram of Arrangement Used to Determine the Resolving Time of the Fast Coincidence Unit.

Figure 25

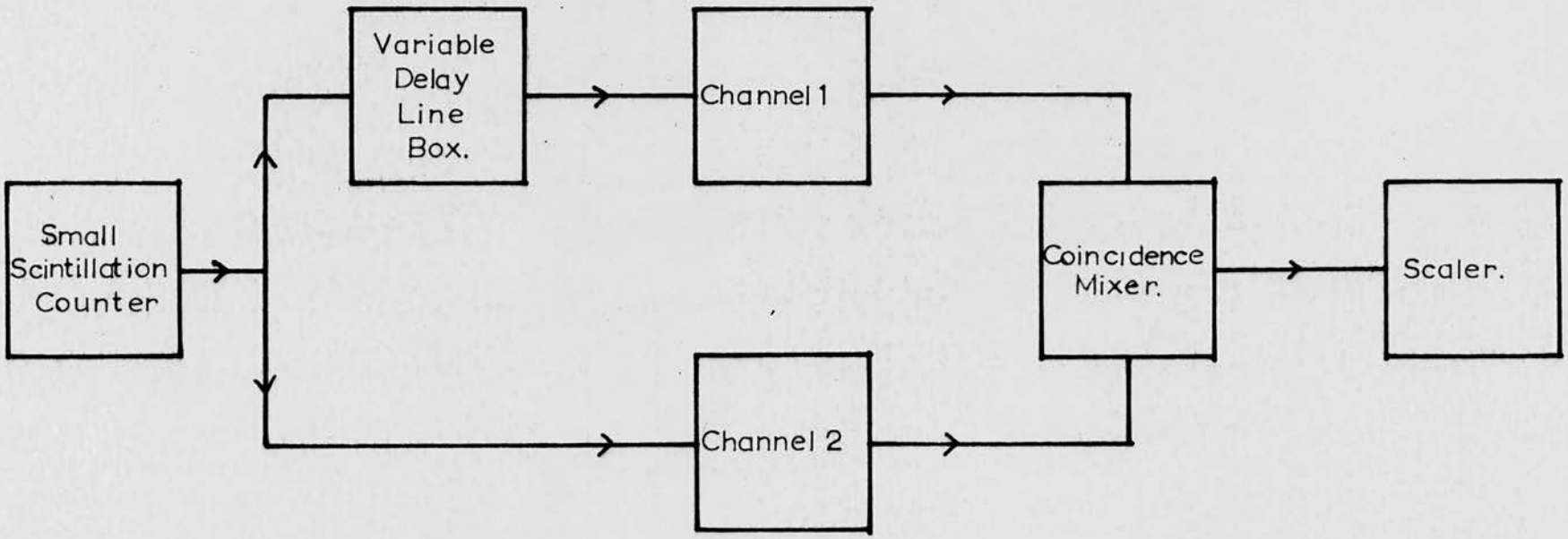

Preliminary Delayed Coincidence Curves for the Fast Coincidence Unit.

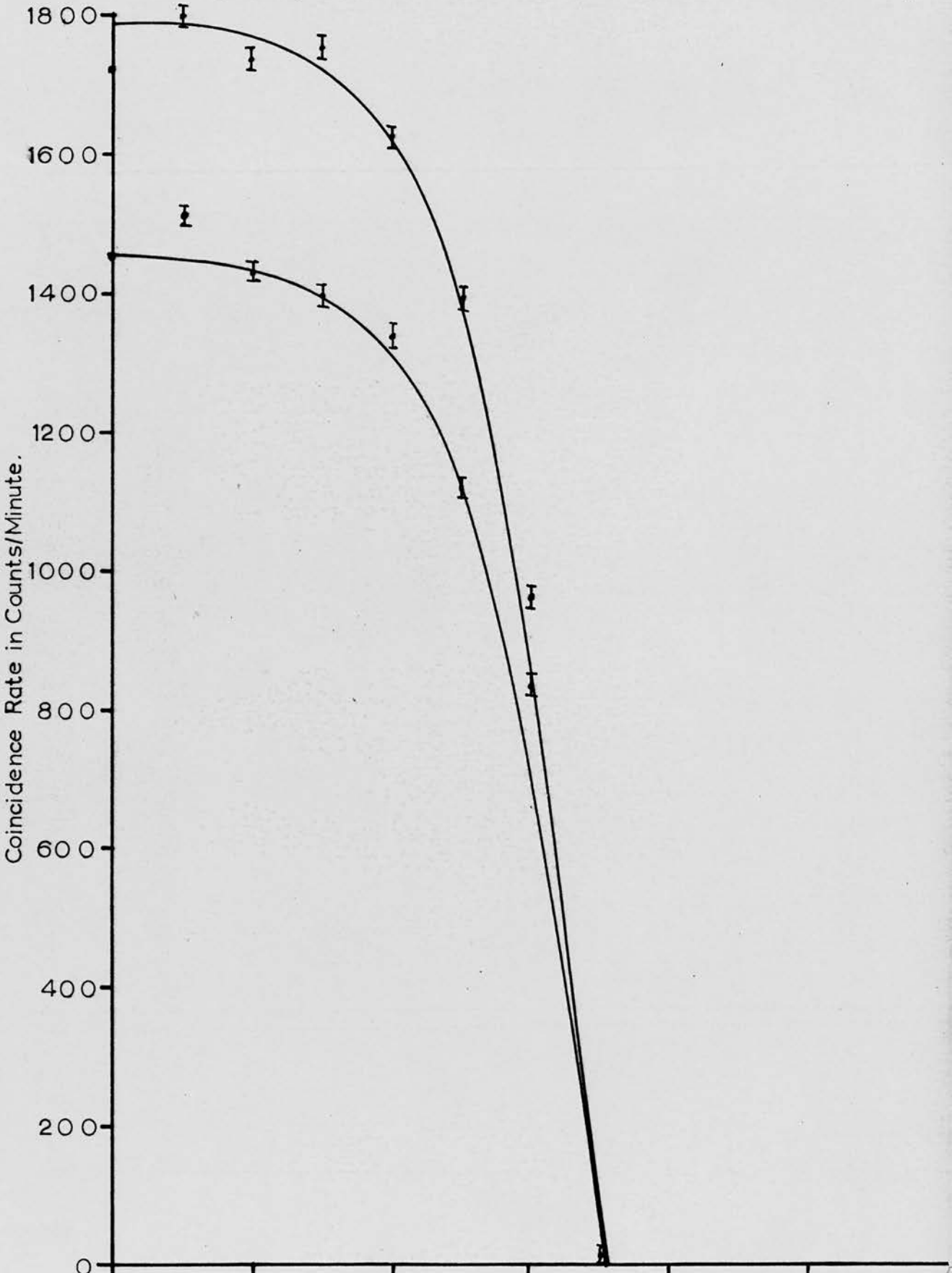

Figure 26

curves shows that the circuit is working efficiently, and that the statistical delays are small compared to the resolving time.

In order to measure the resolving time of the circuit, it was necessary to have the full delayed coincidence curve,, as the centre of the curve was otherwise undefined and the half-width could not be measured. The delay line box was therefore removed from channel one and put in series with channel two instead, in the corresponding position in that channel. The lengths of all other cables on both sides were kept the same. The other part of the coincidence curve was then obtained. Some shift of the centre of the curve with respect to zero delay in the box was present, but this was only due to different mean delay times in the two channels. The experiment was repeated a number of times, in order to esnure that the results were consistent. A typical example of one of the curves obtained is shown in figure 27. The position of the variable bias control, RV_1, in the coincidence chassis remained constant throughout the foregoing measurements.

Owing to the distortion of the circuits and the shape of the original pulses, the channel output pulses are not rectangular and therefore not of constant width, being narrower towards the top. As the pulse heights of this stage are constant, the effective width of a pulse getting through the bias on diode D5 will decrease as this bias is increased. The resolving time depends on the effective widths of the overlapping pulses and this is therefore decreased also. Hence, it is best to use the unit with this bias as large as possible, consistent with all the coincidences being registered when the channel delays are equal.

Complete Delayed Coincidence Curve for the Fast Coincidence Unit.
(Low Bias in Coincidence Mixer)

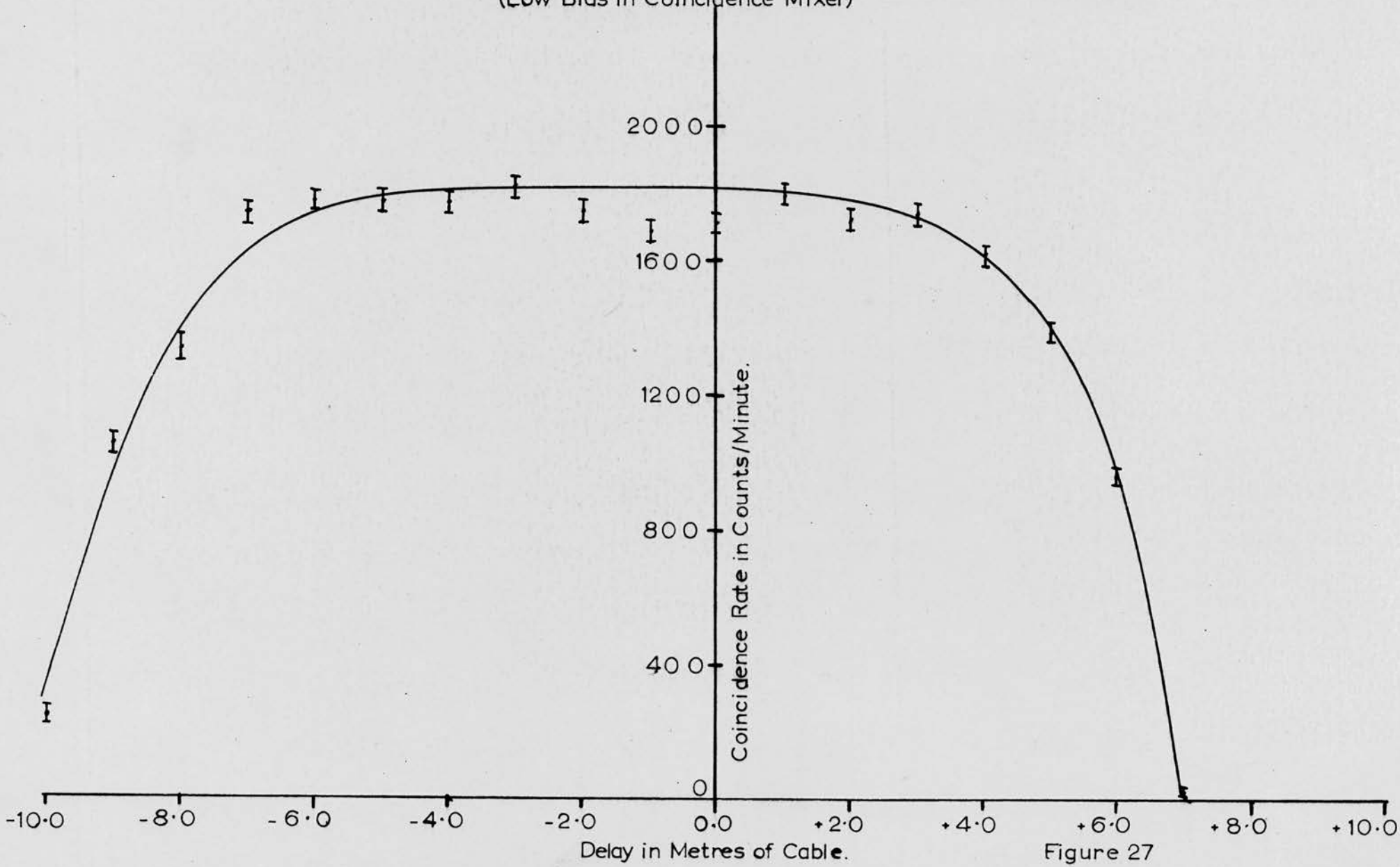

Figure 27

The bias on RV_1 in the coincidence chassis was raised to this maximum value, (about −25 volts) and a new delayed coincidence curve taken (figure 28). This had its centre at approximately the same place as previously, but its width was considerably reduced, as expected. The unit was therefore always used with the bias in this position for the later experiments.

The resolving time was taken as the half-width of the delayed coincidence curve at half the maximum height. The curve in figure 27 gave approximately 35 mμs, and the curve in figure 28, approximately 20 mμs. The difference has already been explained above.

8.1.4. Method of measuring resolving time of unit, using a double pulse generator.

For this method, a double pulse generator type 1147A was used. This provides two rectangular output pulses having quoted rise times of less than 10 mμs. The time separation between the two pulses can be varied, and it was possible to read this to 5 mμs on the generator scale and to about 1 mμs by estimation. A pulse length of 1 μs was used, with a pulse height of about 5 volts. The repetition frequency was 1000 c/s for both pulses.

One output pulse was fed to the input of each coincidence channel. The discriminator bias (RV_1) in one channel was kept constant while that in the other was varied. The bias in the coincidence chassis (RV_1) was also kept constant. The relative delay between the two pulses was then varied, and it was found that an output was obtained from the coincidence mixer when the relative delay was varied over a range of about 35 mμs, corresponding to a resolving time of about 18 mμs. The bias on the coincidence

Complete Delayed Coincidence Curve for the Fast Coincidence Unit
(High Bias in Coincidence Mixer)

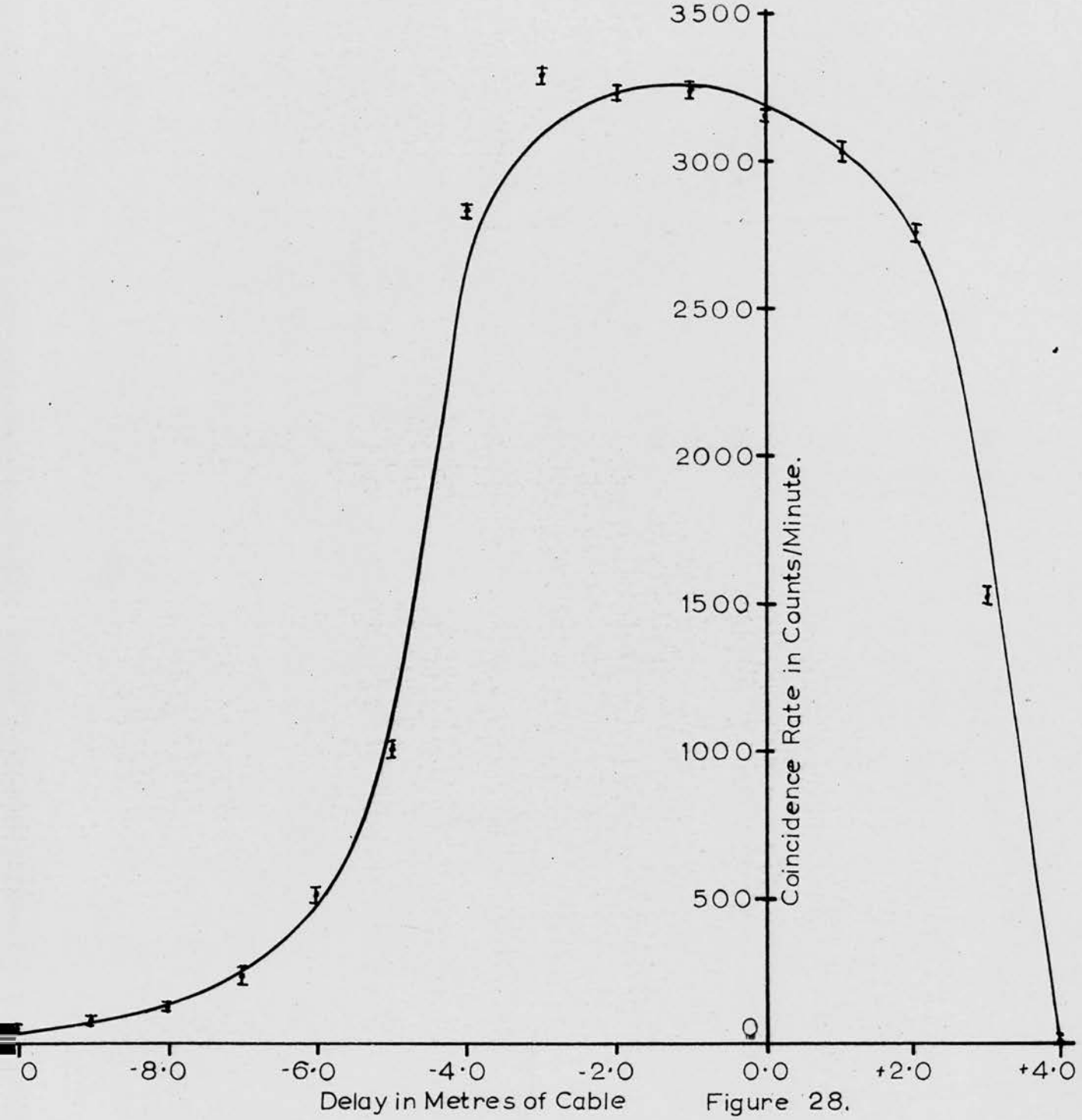

Figure 28.

mixer diode (D5) was −20V, the resolving time varying with this as already explained. The effect of varying the discriminator bias in one channel was to alter the delay time in that channel, owing to the channel triggering at a different time because of the finite rise time of the pulses. This effect has already been explained.

As the bias level in the one channel varied, the resolving time was found to remain nearly constant, but the delay range which gave output pulses (about 35 mμs) occurred in different parts of the pulse generator dial. Hence, for the delayed coincidence curves, the channel biases were not varied during the course of a run. It was also confirmed that the resolving time was altered in the expected manner by altering the bias level in the coincidence mixer.

The pulse generator was also used to obtain an experimental measurement of the delay introduced by the delay line box. With the same conditions as above, the delay line box was connected in series with one channel of the unit. Keeping all biasses constant, the delay ranges for coincidence counts for different lengths of delay cable were found, and the generator scale readings noted. A table of results is given in Table 1 . A graphical representation of the results is given in figure 29. This gives a value of the delay per metre of 6.7 mμs.

8.1.5. Conclusions.

The resolving time of the unit, as determined by two separate methods was about 20 mμs. The values obtained by the two methods were in good agreement.

Table 1.

Table showing variation of position on Pulse Generator dial of delay range for coincidence counts as length of delay cable is varied.

Delay Cable Length in Metres	Delay Range for Counts ($m\mu s$)
0.0	+25 to -25
1.0	+20 to -30
2.0	+12 to -37
3.0	+5 to -45
4.0	0 to -50
5.0	-6 to -55
6.0	-14 to -60
7.0	-22 to -64
8.0	-29 to -68
9.0	-36 to -71
10.0	-42 to -76

Calibration of the Delay-Line Box, Using a Double-Pulse Generator.

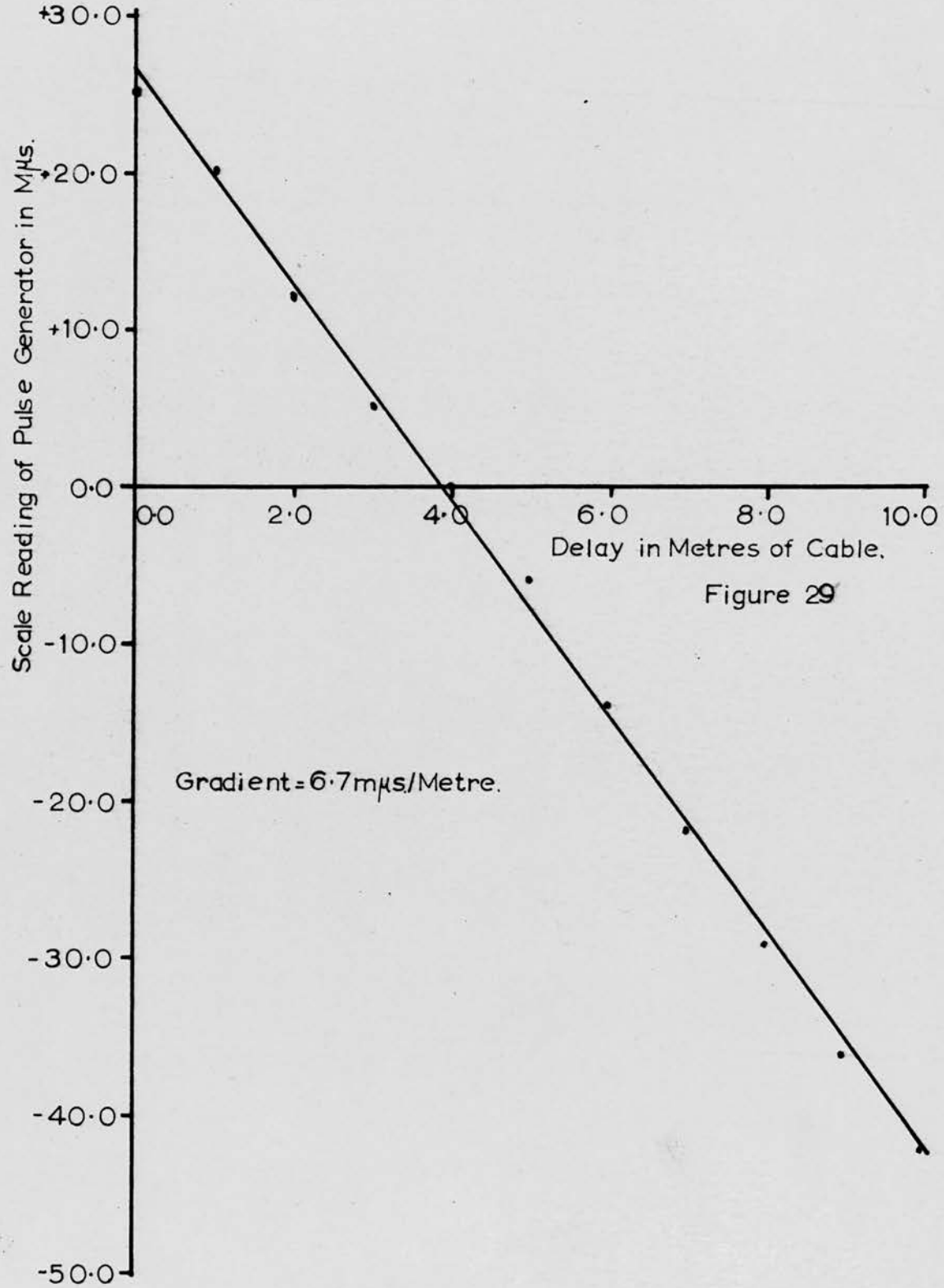

Figure 29

8.2. Time of flight measurements for gamma-rays from Cobalt 60, using Coincidence unit.

8.2.1. Introduction.

One of the important uses of a fast coincidence unit is the determination of the velocity of particles by the time of flight method. A typical example of this is the determination of the velocity, and hence the energy, of neutrons in a neutron beam. The neutrons are detected by means of the recoil protons which they produce in an organic crystal or liquid phosphor. The method can also be used to determine the velocity of a beam of mesons or other particles from a machine.

For testing the coincidence unit, it was convenient to use γ-rays, as their velocity is known and can be compared with the value obtained from the experiment.

Determinations of the velocity of γ-rays have been done by other workers as tests of coincidence equipment. Cleland and Jastram (1951) determined the velocity of the 0.5 Mev coincident γ-rays produced by the annihilation of positrons from Cu^{64}. They used a coincidence apparatus with a resolving time of 5 mμs and obtained a value in accord with the accepted one. Luckey and Weil (1952) measured the velocity of 170 Mev bremsstrahlung γ's by counting them in delayed coincidence with the electrons producing them. The γ's were produced by allowing the circulating beam of 310 Mev electrons in a synchrotron to strike a thin target. The value of velocity was in agreement with the accepted value. Their resolving time was about 5 mμs.

For the experiments described later in this chapter, pairs of coincident γ-rays from a small source of Cobalt 60 were used.

For Cobalt 60, the chief mode of decay is by the emission of a 312 Kev β-particle, followed by two γ-rays in cas cade. The energies of these γ-rays are 1.17 and 1.33 Mev, and according to Allen and Egelstaff, as quoted by Strominger, Hollander and Seaborg in Tables of Isotopes - Review of Modern Physics 30, 630, (1958), the time separation between the γ-rays is about 10^{-12} sec. They can therefore be considered coincident, as compared with the resolving time of the circuit. The β-ray is emitted coincidently with the first γ-ray. As it is of low energy compared to the γ's, and had to pass through the metal boxes containing the counters before reaching the phosphors, any pulses produced it were too small to get through the bias levels used for the γ-counts. A simplified decay scheme is shown in the diagram

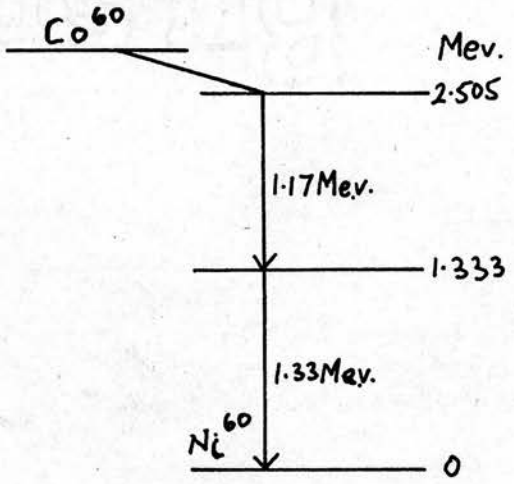

8.2.2. Experimental arrangement.

The apparatus was set up as shown in figure 30. For this experiment, two separate counters were required for the two channels. The small counter, which was used for the resolving time measurements was fed into channel one. The large counter, in series with the preamplifier was fed into channel two. In the absence of the

Block Diagram of Arrangement Used for the Time of Flight Experiments, Using γ Rays from Cobalt 60.

Figure 30

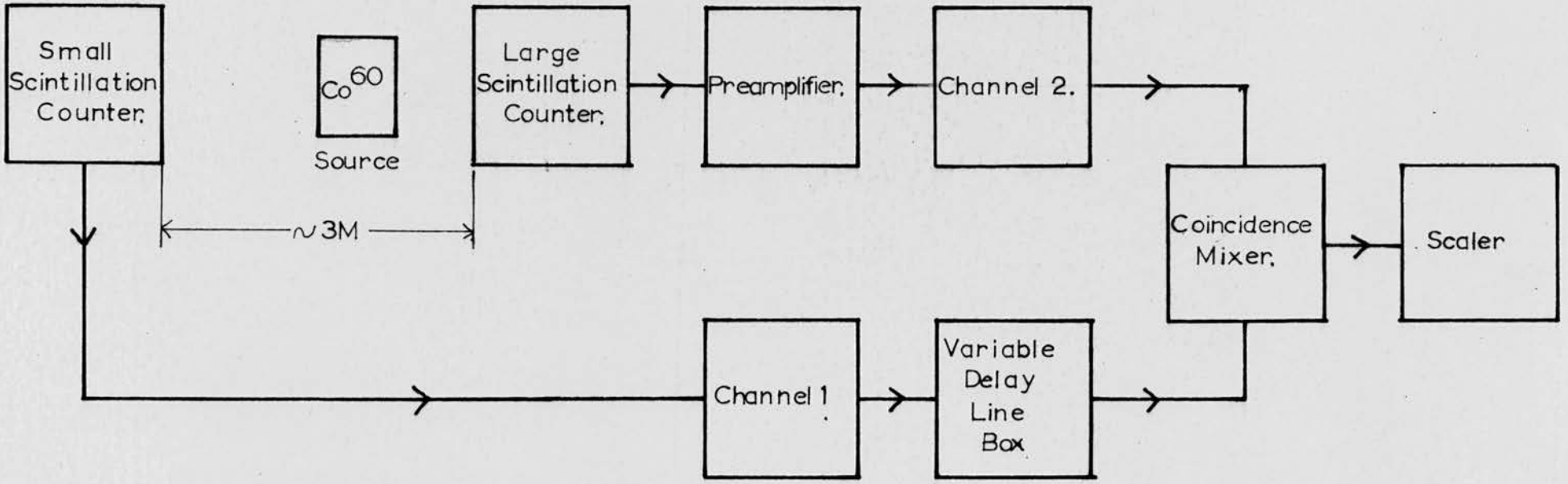

preamplifier, insufficient gain was available from the photomultiplier itself, except by running it at an E.H.T. voltage in excess of the recommended maximum; assuming that the channel bias levels (RV_1) were sufficiently high to cut out any spurious pulses. These spurious pulses were due to pick-up between the two channels, which probably occurred because they share the same power packs for the positive and negative voltage lines. The reason for this is the number of different voltage values required. Pick-up does not occur as long as the channel bias levels are greater than - 5 volts, as measured across RV_1. The preamplifier has a gain of about 25, which enables this condition to be satisfied.

The two counters were placed on the same horizontal level, at a distance apart of three and a half metres. When the Co^{60} was placed at a point equidistant from both counters, coincidence counts could be obtained from pairs of cascade γ-rays, one of which entered one counter and one the other counter. As the time separation between the γ's is so small, they could be considered as entering the two counters at identical times. The coincidence counting rate was, of course, a function of the geometry of the system, increasing when the counter separation was decreased. The γ-rays were counted by means of the processes already described in section 8.1.2.

8.2.3. Preliminary experiments.

If the delay line box setting was varied, with the source equidistant from the counters, a delayed coincidence curve was obtained which was similar to those obtained in the resolving time experiments. The maximum of the curve corresponded to equal delay times in both channels.

If the source was placed adjacent to one of the counters and

the delay setting was again varied, a similar curve was obtained which should have its maximum displaced along the delay time axis by an amount equal to the time taken for the γ-rays to travel 3.5 metres, the counter separation. Placing the source adjacent to the other counter, and repeating the experiment gave a third similar curve, which should be displaced by an equal amount from the central curve, but in the opposite direction. The counters remained fixed in position throughout the experiment. The velocity of the γ-rays could then be obtained from the curves. In order to enable the separation of the curves to be found accurately, they were normalized, so that their maximum ordinates were the same. As the separation of the two extreme curves should be about 23 mμs (4.5 metres of delay cable), it is easily detectable when present.

The first rough results obtained appeared at first sight to verify this, but they turned out to be non-reproducible. This, it was later discovered, was largely due to instability of the large photomultiplier, which was finally replaced. There was some separation obtained between the curves with the source in the two extreme positions, but this was insufficient to be conclusive.

It was at first suspected that an appreciable fraction of the recorded coincidences might be due to pick-up between the two channels, or to some other factor, such as coincidences between a direct γ-ray, and one which had been scattered before reaching the other counter, thus increasing its path length. Such an effect, if present, would tend to spread out the delayed coincidence curve, and make it less sharp.

With the source adjacent to one counter, lead was placed round the source and between it and the other counter, in an attempt to

stop any γ-rays from reaching the counter directly. Any coincidences recorded should then have been due to scattered γ-rays or pick-up, if the screening was effective. The coincidence rate under these conditions was compared with the rate when no shielding was present. This latter rate was between two and four times as great as the former, at different times of measurement. The difference was partly due to differences in the shielding efficiency. These results were inconclusive as to the presence of pick-up, as sufficient γ-rays might have reached the second counter to give the recorded number of genuine coincidences. They did however show that 50% to 80% of the recorded coincidences were genuine.

In order to reduce the possibilities of pick-up between the channels, the two photomultipliers were now given separate H.T. positive supplies (120V). Previously the two anodes had been connected to a common supply. The E.H.T. supplies had always been obtained from separate power packs as it was necessary to have different voltages in each case. Decoupling condensers across the voltage stabilizers in the voltage distribution chassis had already been fitted at an earlier stage, as pulses could otherwise be fed from one channel to the other through the voltage supplies.

It was now decided to test whether the proximity of walls, or other large solid objects which could scatter the γ-rays had any noticeable effects on the shape and position of the delayed coincidence curves. Accordingly, the small counter was moved from its original position near a wall, and placed on top of the enclosure which houses the cloud-chamber. This enclosure being made of fibre-board, should not have had any appreciable scattering effect.

The large counter was supported on a stand at some distance from a wall, and the separation of the counters was about 3.5 metres as before. There did not appear to be any appreciable effect on the positions and shapes of the curves. It was noticed at this stage that the counting rate of the large counter was inclined to vary somewhat, but it was not thought to be serious. It was later necessary to replace the large photomultiplier before reproducible results were obtained.

One fault was, however, definitely found and corrected. The original method of supplying the three chassis with heater current was to feed the supply into the first chassis from the power pack, and then into the other two in series. Owing to the voltage drop in the supply leads, the valves on the coincidence chassis only had a heater voltage of about 4.5 V instead of the measured 7 V at the power pack. The heater supply system was re-wired so that each chassis received its heater voltages directly from a separate supply, the connecting leads being made as short as possible. The effect of the lowered voltage was not noticed until some of the valves, especially those in the last chassis, had aged through use and appeared to cease operating properly. After rectifying the fault it was found that some of these valves which had been removed and replaced were in fact serviceable. One of the effects of the increase in heater voltage was to make the gain in each channel greater, showing that the circuits had not been operating properly before. A large part of the original voltage drop had taken place in the cable between the power pack and the first chassis. The output pulse heights from each channel into the coincidence chassis were also increased and it was possible to work with a

measured bias in the coincidence chassis of up to - 31.0 volts. It was necessary also to work with higher biases in each channel to avoid pick-up, but the increased gain available more than compensated for this. The expected differential shift of the two delayed coincidence curves was still not present. It was checked that the resolving time of the circuit was still the same as before this charge. Also that the width and shape of the delayed coincidence curves were the same, except for the increase in counting rate due to the increase in channel gain.

It was now decided that it would be a better arrangement if the beams of γ-rays incident on the two counters were collimated. For this purpose, a collimating device was built up from lead blocks. This consisted of a pile of lead blocks so arranged that there was a channel six inches long and about three-quarters of an inch square, entirely surrounded by lead at least two inches thick. The collimator was placed adjacent to one or other of the counters, with the channel pointing in the direction of the line joining the counters. The source of Co^{60}, which consisted of an irradiated wire embedded in plasticine, was placed inside it, at the end nearest the adjacent counter. The arrangement is shown in figure 31. It was now possible to shield one or other counter from the source fairly effectively by placing a sufficient thickness (2 or 3 inches) of lead at one end of the collimator channel.

With the source in the channel and adjacent to the small counter, a singlefold counting rate of 2350 counts per min. was obtained for the other counter, in the absence of any lead at the end of the collimator channel. When three inches of lead were placed in position, this rate fell to 1580 per min., showing that

Diagram of Arrangement of Source in Collimator for Time of Flight Experiment, Showing Source by Small Counter.

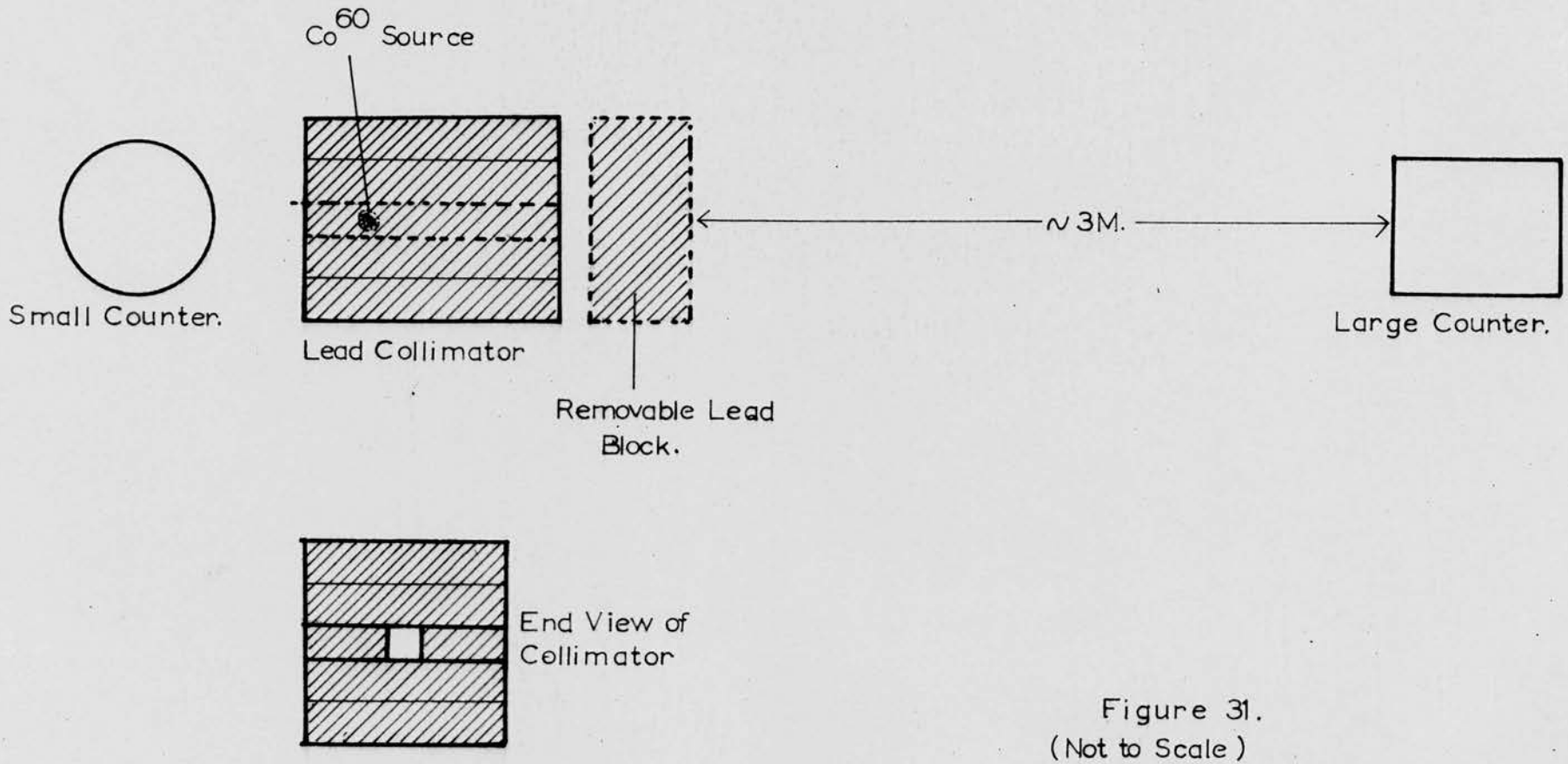

Figure 31.
(Not to Scale)

about 800 counts per min. were due to the source with the given channel bias levels. Of these, a percentage, dependent on the geometry of the system, would give rise to coincidence counts. The counter separation was still 3.5 metres. Before trying any further experiments to obtain delayed coincidence curves, some measurements were made to find out how the calculated and observed chance coincidence rates agreed.

8.2.4. Measurements on the chance coincidence rates for the coincidence unit.

Measurements were now made to discover whether or not the true chance coincidence rate as measured was in accord with that as calculated theoretically. For the first measurements, the small counter was left in channel 1 and counting the Cobalt 60 source; and single pulses from the 1147A pulse generator were fed into channel 2. The chance coincidence counting rate is given by

$$N = 2 N_1 N_2 \tau$$

where N = chance coincidence rate

N_1 = average no. of pulses from channel 1 per unit time

N_2 = average no. of pulses from channel 2 per unit time

τ = coincidence resolving time of system

The formula is quoted by Lewis and Wells - (loc. cit. page 245).

In the first instance, N_1 was 16,300/minute and N_2 was 10,000/sec ± 130 (pulse generator).

Taking $\tau = 30 \times 10^{-9}$ sec (upper limit)

$$N_{(Theor)} = 2 \times 10{,}000 \times \frac{(16{,}300 \pm 130)}{60} \times 30 \times 10^{-9}/\text{sec.}$$

$$\approx (10 \pm 0.1)/\text{minute.}$$

The actual measured rate was $(81 \pm 9)/5\text{mins}$ or $(16 \pm 2)/\text{min.}$

The measurement was repeated with $N_1 = 17{,}000 \pm 130$/min and $N_2 = 1{,}000$/sec (pulse generator). In this case

$$N_{(Theor)} = 2 \times 1{,}000 \times (17{,}000 \pm 130) \times 30 \times 10^{-9}/\text{min}$$

$$\approx (1.0 \pm 0.01)/\text{min.}$$

The measured rate was $(17 \pm 4)/10\text{mins} = (1.7 \pm 0.4)/\text{min.}$

[redacted]

The delay line box was removed from its original position between the output of channel 1 and the coincidence chassis and replaced between the small counter and the input to channel 1. One reason for this was that a certain amount of attenuation takes place in the delay line, so that the pulse height into the coincidence chassis was variable, resulting in a slight variation of the resolving time. This was due to the non-rectangular pulse shapes as previously mentioned. The new arrangement is shown in figure 32 . The attenuation was, of course, still present when the delay cable was in the new position, but it could be arranged (by ensuring that the pulse heights were sufficient) that the attenuation only cut out small pulses which were not of interest. This was possible because only the pulses corresponding to the

Block Diagram of Time of Flight Arrangement, Showing New Position for Delay-Line Box.

Figure 32

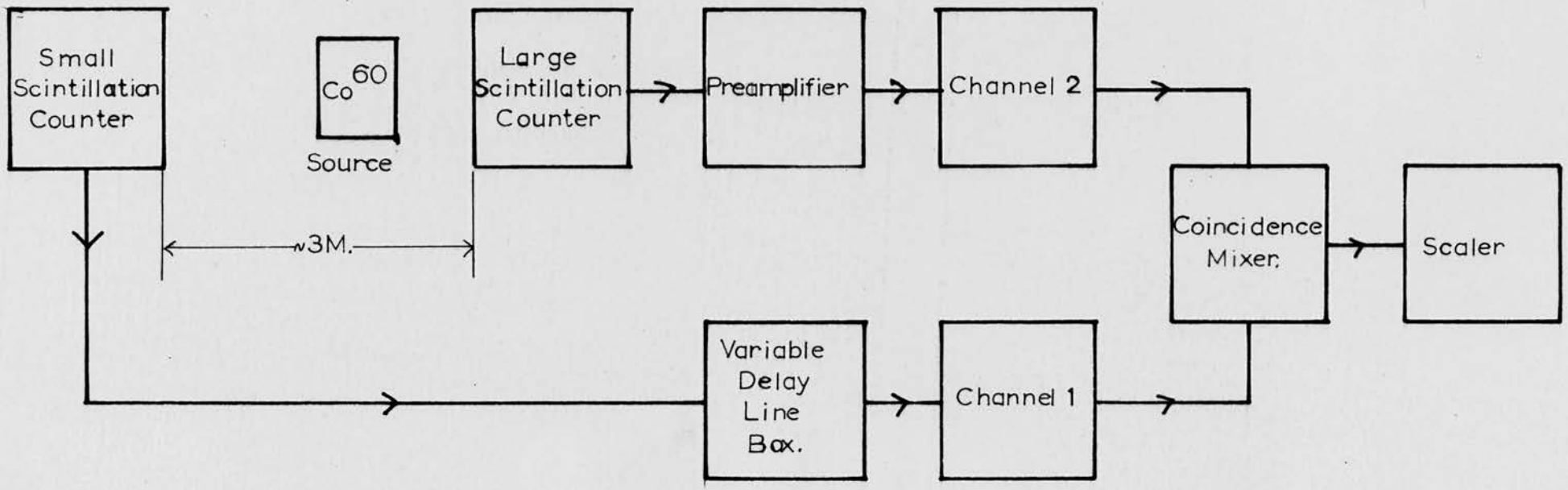

larger energy losses were of importance. The effect of the delay cable is shown by the figures given below corresponding to two different singlefold counting rates.

Length of cable in box	Counting Rates	
	1	2
1 metre	40,000/min. ±200	78,000/min. ±280
10 metres	34,000/min. ±185	71,000/min. ±267

The pulse generator was now removed and the two counters put back into coincidence with the small counter counting a source of RdTh and the large counter a source of Iridium 192. The length of cable in the delay line box was varied, and values of the chance coincidence counting rate were taken in each case and compared with the theoretical value. Good agreement was obtained as shown in Table 2. The two singlefold rates were 83,000/min and 1200/min; whence the theoretical coincidence rate should be given by (using formula already given)

$$N_{(Theor)} = 2 \times 30 \times 10^{-9} \times \frac{83000}{60} \times \frac{1200}{60} \times 60/\text{min.}$$

$$\approx (0{\cdot}1 \pm 0{\cdot}003)/\text{m} \approx (1 \pm 0{\cdot}03)/10\ \text{mins.}$$

This was in good agreement with the experimental values, which varied from 0/10 mins to 3/10 mins

8.2.5. Successful time of flight measurements.

At this stage, it was decided to replace the large photo-multiplier tube by a new tube of the same type, as it had become unreliable for long counts. It was decided to fit a μ-metal

shield to this tube as it is stated by the manufacturers to be rather sensitive to magnetic fields. A suitable shield is manufactured by E.M.I. for this purpose. The small counter is much less sensitive, partly because the separation between the photocathode and the first dynode is much less than in the case of the large tube.

After re-assembly, some singlefold counting rates for the large counter were taken over a period of time in order to check the stability of the new arrangement. Shortly after re-assembly, the counting rate with the given bias was about 4,500/minute, all measurements lying within the statistical limits. On the following morning, the rate was about 4,300/minute, which was quite satisfactory, allowing for a small change owing to the photomultiplier settling down after being fitted.

A repeat measurement of the chance coincidence rate was now made, using the RdTh and Iridium 192 sources as before. The singlefold counting rates in the two channels were arranged so that they were both approximately 40,000 counts/min. A set of readings of the chance rate for different lengths of delay cable in the delay line box were now made. The results are shown in Table 3. The singlefold rates for the large and small counters were approximately 50,000/min (Ir_{192}) and 40,000/min RdTh) as measured on the scaler.

It can be shown that the true counting rate when measured on a scaler which has a paralysis time of τ sec is given by

$$n_t = \frac{n_m}{1 - n_m \tau}$$

Table 3.

Table showing the agreement between the measured and calculated chance coincidence rates as the delay box was varied. This is a repeat of Table 2 after the large photomultiplier had been changed.

Delay (metres)	Coincidence Rate /10 mins.	
	Experimental	Theoretical
1.0	25 ± 5	27.0
2.0	-	-
3.0	-	-
4.0	28 ± 4.6	27.0
5.0	28 ± 5.4	27.0
6.0	26 ± 5	27.0
7.0	-	-
8.0	20 ± 4.5	27.0
9.0	-	-
10.0	22 ± 4	27.0

The large counter counted an Ir^{192} source and the small counter an Rd Th source. The singlefold rates were:-

Large = 50,000/min

small = 30,000/min

where

n_t = true counting rate

n_m = measured counting rate

τ = paralysis time

In this case, $\tau = 400\ \mu s$. Hence the true singlefold counting rates are greater than the measured ones. Substitution in the formula above gives rates of 75,000/min (measured as 50,000/min) and 54,550 (measured as 40,000/min). Using the formula already stated, taking the resolving time of the coincidence unit as 20 $m\mu s$, the chance coincidence rate is given by

$$N = \frac{2 \times 75{,}000 \times 54{,}550 \times 20 \times 10^{-9}}{60 \times 60} / \text{sec.}$$

$$= 2.7/\text{minute}$$

$$= 27/10 \text{ minutes.}$$

This value is in good agreement with the experimental values (Table 3) which are equal to it within statistical limits, and have an average value of 26.5/10 mins, for different lengths of delay cable.

As the large counter now appeared to be much more stable than before, some delayed coincidence curves were taken. The Co^{60} source in the lead collimator as described earlier, was placed adjacent to the small scintillator and a delayed coincidence curve taken. The source and collimator was then placed next to the large scintillator and the process repeated. It was found on plotting the results on a graph (after normalization) that one curve was displaced with respect to the other by the correct sort of amount. The results are shown in figure 33.

Delayed Coincidence Curves for Time of Flight Experiment, Using γ-Rays from Co^{60}

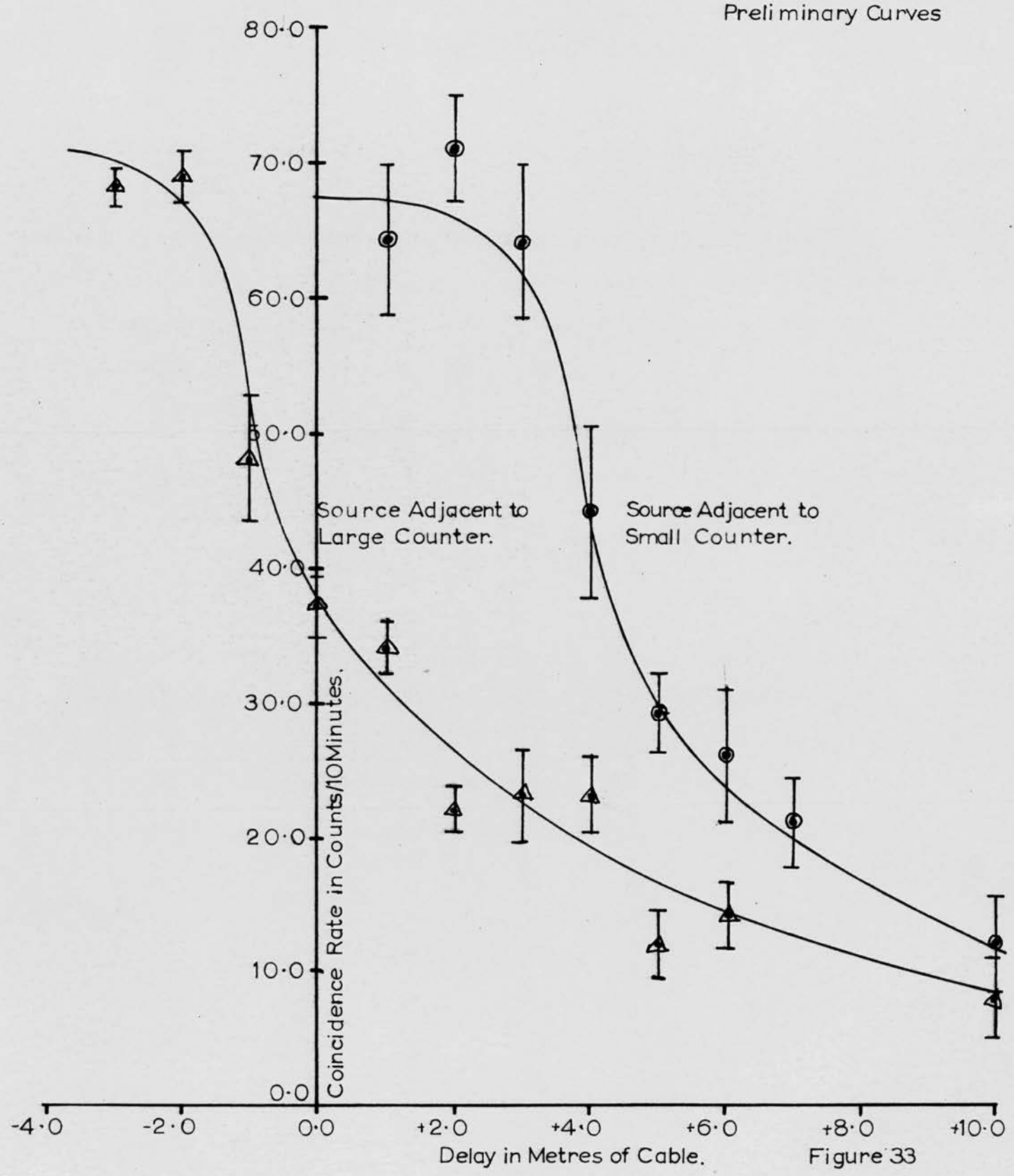

Figure 33

It was found that the range of delay available in the delay line box was in the wrong part of the scale, and it was not possible to include the peaks of both curves. A length of about 5 metres of cable in series with the box was removed and a length of about 1 metre substituted. The effect of this was to allow readings of the delay which were negative with respect to the original ones to be taken (up to -4 metres). This method of adding or subtracting cable in one channel or the other can always be used to bring the range of variation on the box into the desired working range. Subtraction of cable from one channel is, of course, equivalent to addition of the same length of cable to the other side. Only relative delays are of interest. A check on the singlefold counting rates of the two counters was kept, these being measured regularly. It could thus be seen whether or not they were remaining relatively constant.

It was now discovered that reflection of pulses was taking place at the input to the delay line box; as the cable from the counter and the cable in the box were of different characteristic impedance. This was undesirable, and so the original cable between the counter and the box was replaced by an equivalent length of the same type of cable as that in the box (120-Ω). By viewing the channel input pulses on the oscilloscope before and after the change, it could easily be seen that they were much less distorted afterwards. The top of the pulse had previously shown an oscillatory waveform, which was due to the presence of reflections.

Repeat measurements were made for the two delayed coincidence curves. The positions of the curves were essentially the same as before, although the actual counting rates were somewhat greater.

A test was also made to see whether replacing the delay box in its original position between the channel and the coincidence chassis made any difference to the results. There was no essential difference. The box was then again replaced between the small counter and channel input. It was found that the coincidence counting rates were now stable, and could be reproduced after a fairly long period of time, which was not the case before the replacement of the large photomultiplier. The results are shown in Figure 34. The relative shift of one graph with respect to the other was about 4 metres of delay cable, corresponding to a velocity of $(3{\cdot}0 \pm 0{\cdot}5) \times 10^8$ m/sec. This showed that the coincidence unit was operating correctly.

The source was removed and the large counter placed with its axis vertical. It had previously had its axis horizontal, so that the scintillator could cover the largest possible solid angle as seen from the other counter. The separation was still about 3.5 metres.

The singlefold counting rates were 6,200/min. for the large counter and 690/min. for the small counter, the counters counting cosmic rays. The theoretical chance coincidence rate was therefore

$$C = 2 \times 30 \times 10^{-9} \times 690 \times 6200/\text{hour}$$

$$\approx 0.25 \text{ per hour.}$$

One count was observed in a single period of 3 hours, which was in accord with the theoretical value. The object of this was to check the numbers of chance coincidences which could have been caused by cosmic rays in the foregoing experiments. This rate was negligible compared with the true rate.

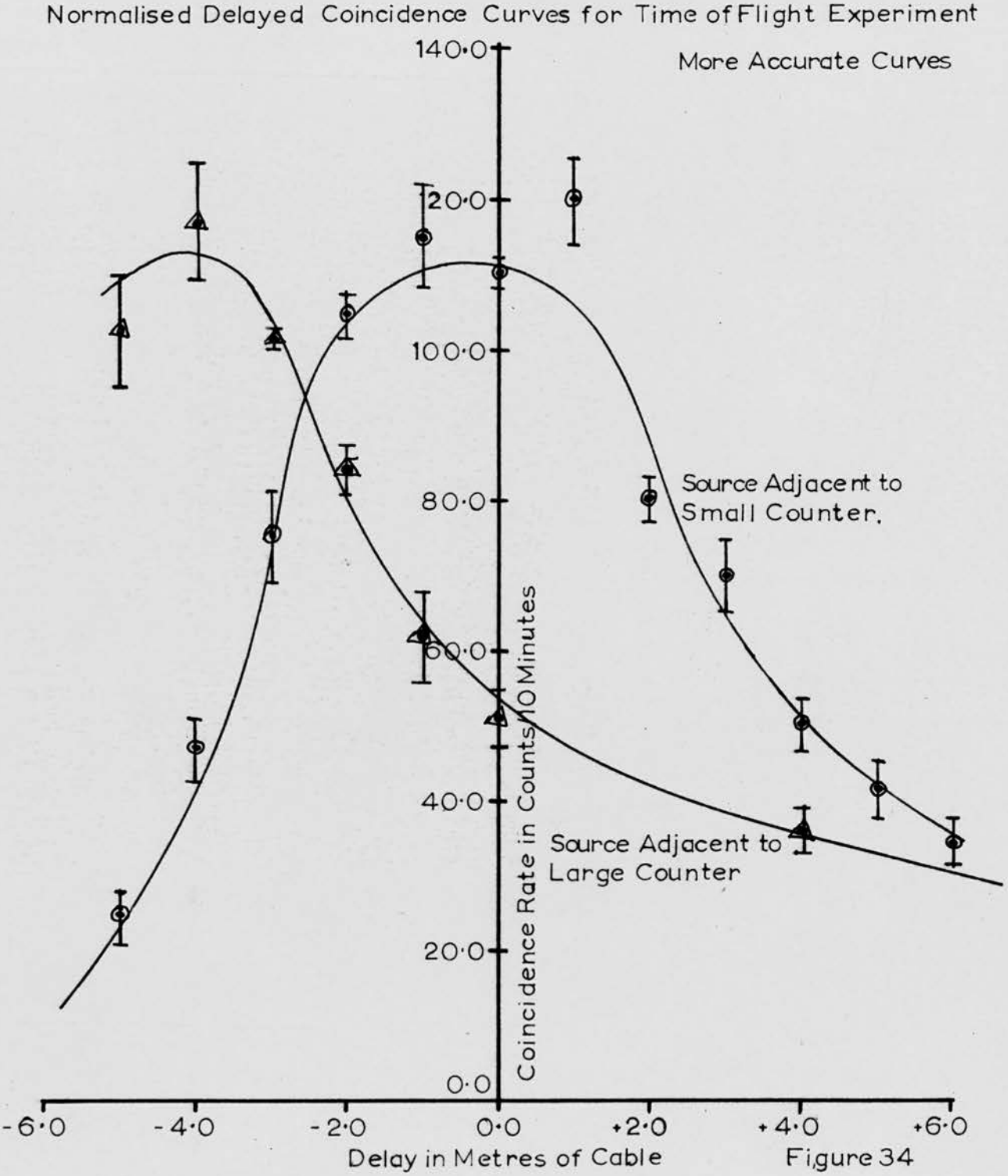
Normalised Delayed Coincidence Curves for Time of Flight Experiment
More Accurate Curves
140·0
120·0
100·0
80·0
60·0
40·0
20·0
0·0
Coincidence Rate in Counts/10 Minutes
Source Adjacent to Small Counter.
Source Adjacent to Large Counter
-6·0
-4·0
-2·0
0·0
+2·0
+4·0
+6·0
Delay in Metres of Cable

Figure 34

8.3. Delayed coincidence curves, using cosmic rays.

The counters were first placed so that the large one was vertically above the small one, at a separation of about 0.35 metres. A delayed coincidence curve was now obtained in the same manner as previously using cosmic rays which passed through both counters in succession. The shape and width of the curve obtained was similar to those obtained with the Co^{60} source. The maximum counting rate was about 45 counts/hour. The curve is given in figure 35.

The vertical separation of the counters was now increased to 1.0 metre. The maximum coincidence counting rate was now about 11.0 counts/hour, with the same singlefold rates as before (6,200 per min. for the large counter and 690 per min for the small one). The vertical separation of the counters was again increased to 1.8 metres, when the maximum coincidence rate was about 5 per hour. The counter E.H.T. voltages were now reduced so that the singlefold counting rates fell to about 4,000 per hour for the small counter and 8,000 per hour for the large one. This did not have any noticeable effect on the coincidence rate confirming, as had been assumed, that the pulses cut out were due to small energy losses in the scintillators, and not to fast particles capable of passing through both counters to give a true coincidence. The particles producing coincidences were mostly fast μ -mesons.

For counting rates of 4000/hr. and 8000/hr. the chance coincidence rate is given by

$$N = 2 \times 30 \times 10^{-9} \times \frac{4000}{3600} \times \frac{8000}{3600} \text{ / sec.}$$

$$= 4.7/\text{year.}$$

Delayed Coincidence Curve for Fast Cosmic Rays (Mostly μ-Mesons)
Passing Through the Two Scintillation Counters

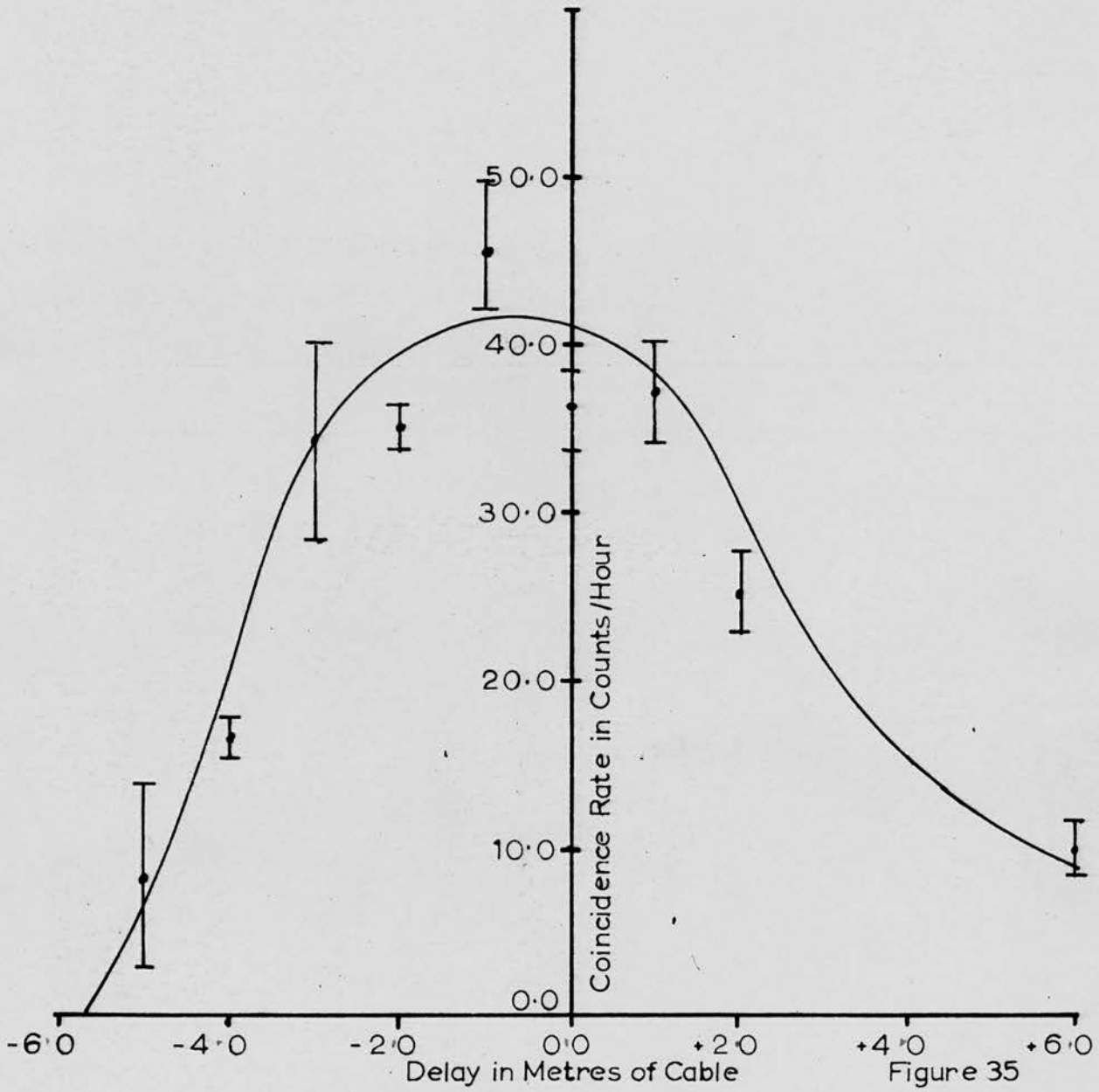

Figure 35

A piece of 120 Ω cable 11 metres in length was now made up. This could be inserted in the side containing the large counter, and would thus be equivalent to removing the same amount from the side containing the small counter. With this length of cable in position, and the delay line box removed from circuit, a coincidence rate of 0 counts in $18\frac{3}{4}$ hours was obtained. As a very slow particle would be required to give a true coincidence ($\beta \sim 0.1$ or 0.2), this showed that there are very few of these particles, as expected. In the above, the delay in the channel containing the large counter was about 60 mμs greater than that in the other channel.

8.4. Summary.

A description of the method of measuring the resolving time of the unit, using a variable delay in one channel, has been given. The results obtained have been shown to be equal to the expected value, as determined by the pulse lengths in the unit (about 20 mμs).

A method of measuring the velocity of atomic particles or γ-rays by the "time of flight" method has been described. This method has been applied to find the velocity of the γ-rays emitted by Co^{60}, a value of $(3.0 \pm 0.5) \times 10^8$ metres per second being obtained. This showed that the circuit was working correctly

Chapter 9.

THE RESPONSE OF THE PLASTIC PHOSPHOR TO COLLISION ENERGY LOSS, AND THE COUNTING EXPERIMENTS WITH THE LARGE COUNTER.

9.1. Introduction.

This chapter contains a discussion of the linearity of response of a plastic phosphor when an ionising particle passes through it. Calculations for the range and specific energy loss of protons, electrons, α-particles and μ-mesons in the NE101 plastic phosphor are also given. The counting experiments performed with the large counter, using cosmic rays and γ-rays are described.

9.2. Consideration of the phosphor response to particles of different energies and different kinds.

9.2.1. Theoretical response of phosphor.

A theory of the dependence of the specific fluorescence of a phosphor, dL/dx, on the specific energy loss by collision dE/dx, was proposed by Birks (1951 b), who gave the equation

$$\frac{dL}{dx} = \frac{A\, dE/dx}{1 + kB\, dE/dx}$$

where A, B and k are constants for a given phosphor. He attributed the non-linearity to the quenching effect of damaged molecules on the emitted photons.

Boreli and Grimeland (1955) made measurements on a plas tic phosphor, and obtained a value for kB of 10.5 cm of air per meV. It will be reasonable to take the same value for the phosphor used here. Using the value for the density of the phosphor of

1.035 gm per cc and that for air at N.T.P. of 0.00129 gm per cc; we obtain a value of kB for the phosphor of 0.013 cm of phosphor per Mev.

In order to apply this theory to the energy losses of different types of particle which pass through or stop in the phosphor, some values of $\frac{dE}{dx}$ for different energies are required. These are given in the following section.

9.2.2. Collision loss $\frac{dE}{dx}$, and range of particles in plastic Scintillator.

(a) Collision loss.

Calculations have been carried out to determine the collision loss and range-energy curves for various particles in the NE101 plastic phosphor. For electrons, a contribution from radiation loss must also be taken into account at high energy.

The basic formula upon which the calculations have been based is:-

$$-\left.\frac{dE}{dx}\right|_{collision} = NZ\phi_0 \frac{3}{4}\frac{z^2}{\beta^2}\left[\log_e \frac{2M\beta^2 W_m}{I^2 Z^2 (1-\beta^2)} - 2\beta^2\right] \quad \text{---(1)}$$

in the usual notation (see Heitler - Quantum Theory of Radiation, p. 368), E is kinetic energy.

For NE101 plastic phosphor:

Density = 1.035 gm per cc.

Composition = 91% Carbon and 9% Hydrogen by weight.

The formula (1) was re-arranged, and values of $NZ\phi_0$ and

$\log_e\left(\frac{2\mu}{IZ}\right)$ computed separately for the Carbon and Hydrogen.

The final results were:-

$$-\left.\frac{dE}{dsc}\right|_{\text{collision}}^{\text{Hydrogen}} = 0.0284\left\{\frac{1}{\beta^2}\left[\left\{\log_e\left(\frac{\beta^2}{1-\beta^2}\right)-\beta^2\right\}+11.40\right]\right\}\text{Mev cm}^{-1}$$

$$-\left.\frac{dE}{dsc}\right|_{\text{collision}}^{\text{Carbon}} = 0.1443\left\{\frac{1}{\beta^2}\left[\left\{\log_e\left(\frac{\beta^2}{1-\beta^2}\right)-\beta^2\right\}+9.60\right]\right\}\text{Mev cm}^{-1}$$

The total collision loss is given by

$$\left(-\left.\frac{dE}{dx}\right|_{\text{collision}}^{\text{Total}}\right)=\left(-\left.\frac{dE}{dsc}\right|_{\text{collision}}^{\text{Carbon}}\right)+\left(-\left.\frac{dE}{dsc}\right|_{\text{collision}}^{\text{Hydrogen}}\right)$$

Corresponding values of β, E and $-\left.\frac{dE}{dsc}\right|_{\text{coll.}}$ for μ-mesons are given in Table 4. A graph of β and $-\left.\frac{dE}{dsc}\right|_{\text{collision}}^{\text{Total}}$ is given in figure 36.

(b) <u>Range-energy curves for heavy particles</u>.

$$\frac{dR}{dE} = \left(\frac{1}{-\frac{dE}{dx}}\right)$$

where R is the range of a particle of energy E. R is found by numberical integration from a graph of E and $\left(\frac{1}{-\frac{dE}{dx}}\right)$. The range of a particle of energy E_t is the area under the graph between E = 0 and E = E_t. Corresponding values of E and R for μ-mesons have been computed. The results are shown graphically in figure 37.

Table 4.

Table of values of E and $\frac{dE}{dx}$ for μ-mesons, protons, α-particles and electrons for given values of β

β	μ-mesons		Protons		α-particles		Electrons	
	E Mev	$-\frac{dE}{dx}$ Mev per cm	E Mev	$-\frac{dE}{dx}$ Mev per cm	E Mev	$-\frac{dE}{dx}$ Mev per cm	E Mev	$-\frac{dE}{dx}$ Mev per cm
0.05	0.106	269.8	0.9417	269.8	3.767	1079.2	0.0005	190.0
0.10	0.528	91.44	4.688	91.44	18.75	365.8	0.0026	73.30
0.15	1.267	46.87	11.26	46.87	45.04	187.5	0.0056	38.68
0.20	2.218	28.85	19.70	28.85	78.80	115.4	0.0107	24.37
0.25	3.485	19.70	30.96	19.70	123.8	78.8	0.0169	16.80
0.30	5.069	14.39	45.04	14.39	180.2	57.56	0.0250	12.36
0.35	7.181	11.01	63.80	11.01	275.2	44.04	0.0347	9.519
0.40	9.610	8.715	85.37	8.715	341.5	34.860	0.0465	7.574
0.45	12.57	7.102	111.6	7.102	446.4	28.408	0.0608	6.185
0.50	16.27	5.909	144.5	5.909	578.0	23.636	0.0787	5.164
0.55	20.91	5.003	185.8	5.003	743.2	20.012	0.101	4.386
0.60	26.40	4.301	234.5	4.301	938.0	17.204	0.128	3.776
0.65	33.37	3.747	296.4	3.747	1186	14.988	0.161	3.294
0.70	42.35	3.303	376.2	3.303	1505	13.212	0.205	2.906
0.75	53.87	2.944	478.6	2.944	1914	11.776	0.262	2.591
0.80	70.44	2.654	625.8	2.654	2503	10.616	0.340	2.339
0.85	94.84	2.422	842.6	2.422	3370	9.688	0.459	2.134
0.90	136.7	2.248	1214	2.248	4856	8.992	0.661	1.979
0.96	377.1	2.145	3350	2.145	13,400	8.580	1.314	1.884
0.99	642.8	2.259	5710	2.259	22,840	9.036	3.111	1.985
0.995	950.0	2.357	8439	2.357	33,760	9.428	4.598	2.081
0.999	2257	2.616	20,050	2.616	80,200	10.464	10.91	2.383

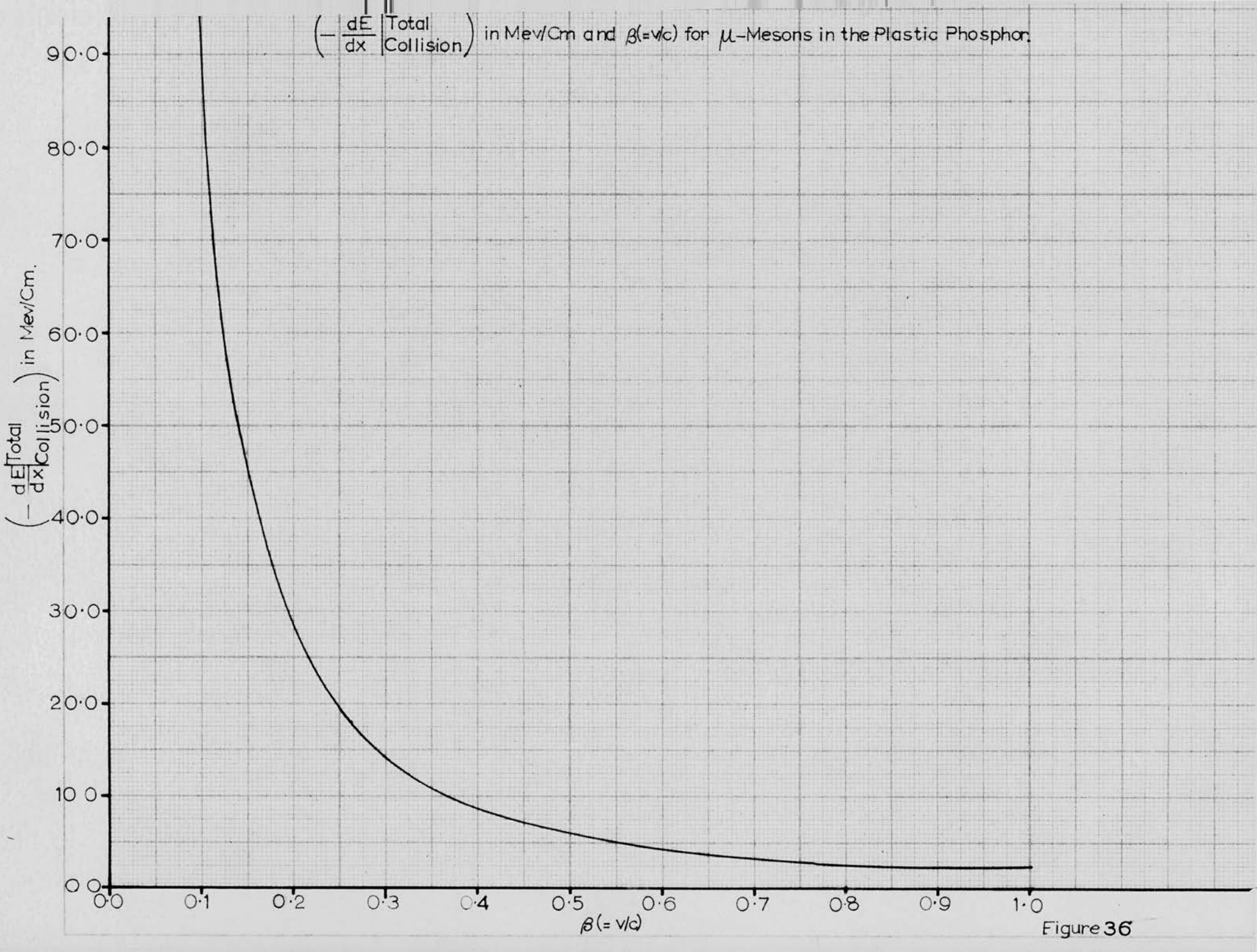
$\left(-\frac{dE}{dx}\middle|\begin{matrix}\text{Total}\\\text{Collision}\end{matrix}\right)$ in Mev/Cm and $\beta(=v/c)$ for μ-Mesons in the Plastic Phosphor.
$\left(-\frac{dE}{dx}\middle|\begin{matrix}\text{Total}\\\text{Collision}\end{matrix}\right)$ in Mev/Cm.
90·0
80·0
70·0
60·0
50·0
40·0
30·0
20·0
10 0
0 0
0·0
0·1
0·2
0·3
0·4
0·5
0·6
0·7
0·8
0·9
1·0
$\beta(=v/c)$

Figure 36

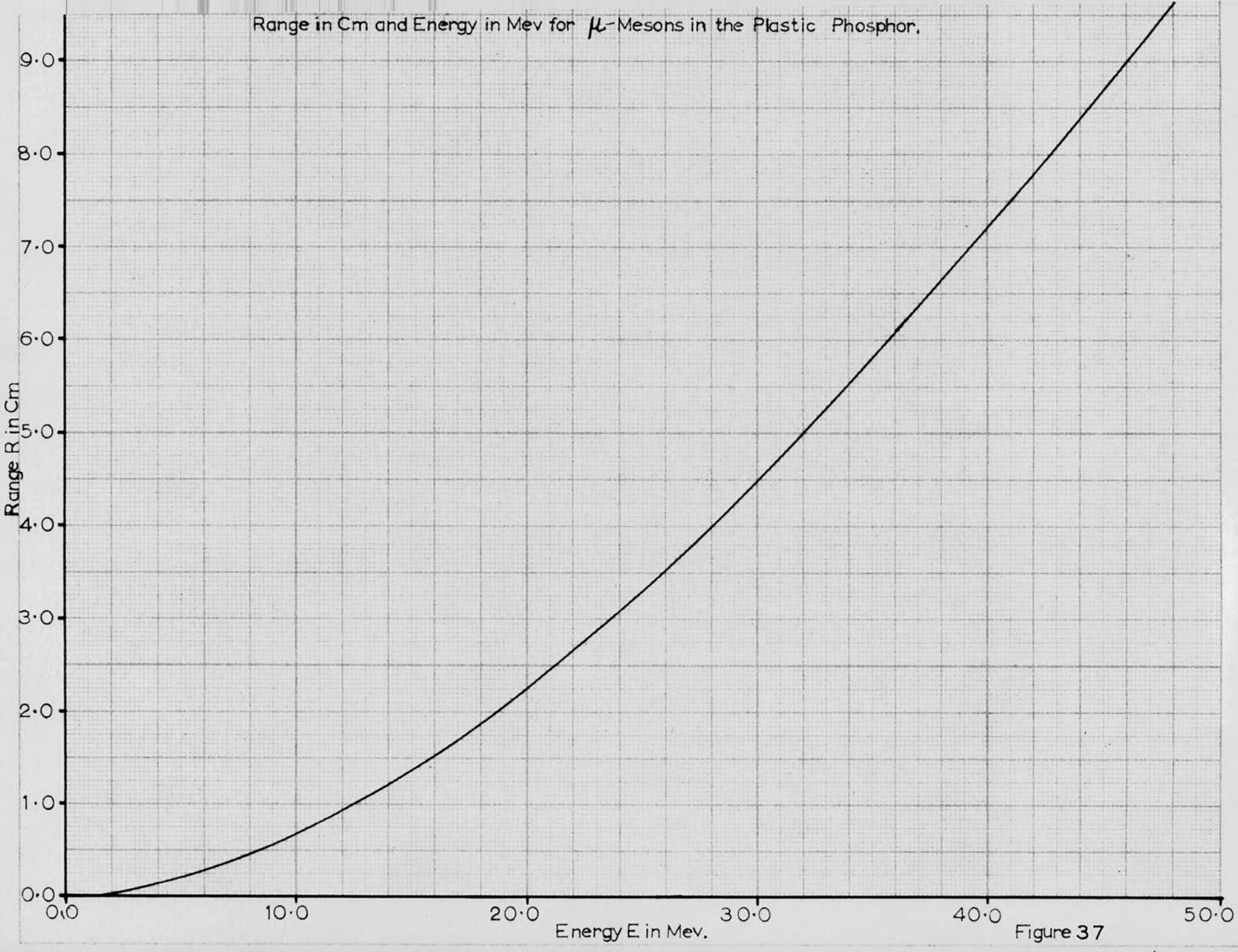
Range in Cm and Energy in Mev for μ-Mesons in the Plastic Phosphor.
Range R in Cm
9·0
8·0
7·0
6·0
5·0
4·0
3·0
2·0
1·0
0·0
0·0
10·0
20·0
30·0
40·0
50·0
Energy E in Mev.

Figure 37

The results for μ-mesons can easily be extended to give the Range-Energy curves for protons and α-particles. We note from equation (1) that for protons, $-dE/dx$ for a given β is the same as for μ-mesons; and for α-particles, $-\frac{dE}{dx}$ is four times the value for μ-mesons

$$\text{Also} \quad (K.E.)_p = \left(\frac{1836}{207}\right) (K.E.)_\mu$$

$$(K.E.)_\alpha = \left(\frac{4 \times 1836}{207}\right) (K.E.)_\mu$$

$$\text{Hence, using } R = \int \frac{dE}{\left(-\frac{dE}{dx}\right)}$$

$$\left.\begin{aligned} R_p &= 8.884\, R_\mu \\ R_\alpha &= 8.884\, R_\mu \end{aligned}\right\} \quad \text{for a given value of } \beta$$

Therefore, to obtain corresponding values (given β) of R and E for protons, we multiply the values of R by 8.884 and E by 8.884. To obtain corresponding values for α-particles, we multiply the values of R by 8.884 and E by 35.54. Range-Energy curves for protons and α-particles are given in figure 38. Values of β, E and $-\frac{dE}{dx}$ are given in table 4.

(c) Range-Energy curves for electrons.

Calculations similar to the above have been performed for electrons up to an energy of about 10 Mev. The energy loss by radiation has been taken into account, but is only a small factor up to the largest energies considered. The Range-Energy curve is given in figure 39, where it will be seen that 10 Mev electrons have a range of the order of 2 inches, so that relatively low-energy

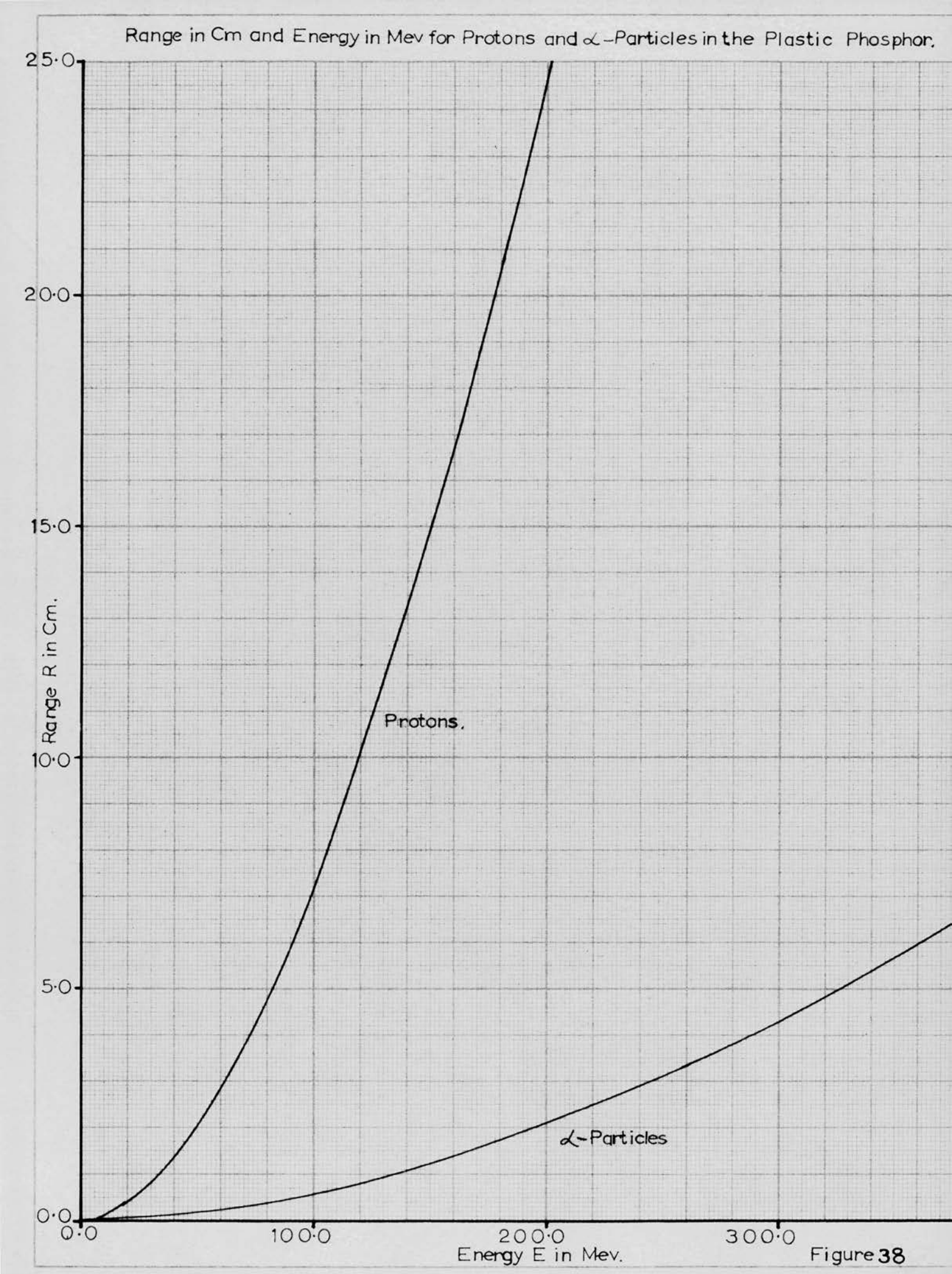
Range in Cm and Energy in Mev for Protons and α-Particles in the Plastic Phosphor.
25·0
20·0
15·0
10·0
5·0
0·0
Range R in Cm.
Protons.
α-Particles
0·0
100·0
200·0
300·0
Energy E in Mev.

Figure 38

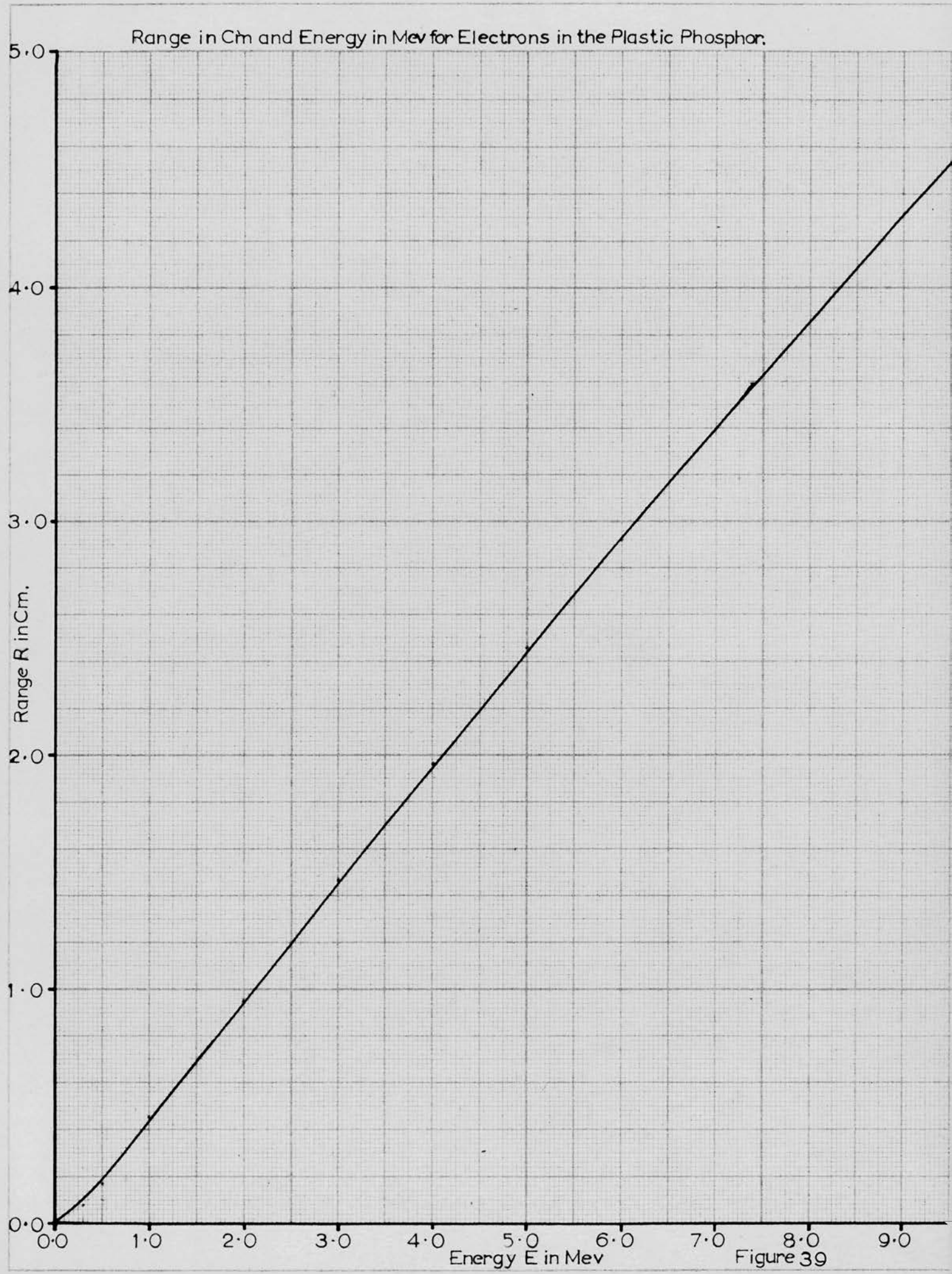
Range in Cm and Energy in Mev for Electrons in the Plastic Phosphor.
5·0
4·0
3·0
2·0
1·0
0·0
Range R in Cm.
0·0
1·0
2·0
3·0
4·0
5·0
6·0
7·0
8·0
9·0
Energy E in Mev

Figure 39

knock-on electrons produced by heavy particles will be able to enter the cloud-chamber. Values of β, E and $-\frac{dE}{dx}$ are given in table 4.

9.2.3. Linearity of response of phosphor to different energy losses.

Using the value of kB from section 9.2.1., we can write:-

$$\frac{1}{A}\frac{dL}{dx} = \frac{dE/dx}{1 + 0.013\frac{dE}{dx}}$$

The response of the phosphor will be linear if $0.013\frac{dE}{dx} \ll 1$. Reference to table 4 shows that considerable non-linearity will be present for α-particles and protons of low or moderate energy, and for μ-mesons of low energy. The response to electrons will be almost linear except at very low energy (less than about 0.5 Mev).

Hence, for electrons of Energy greater than 0.5 Mev, we can write

$$L = \text{constant} \times E \quad \left(-\frac{dE}{dx} \text{ small}\right)$$

and for α-particles of Energy less than about 100 Mev

$$L = \text{constant} \times R \quad \left(-\frac{dE}{dx} \text{ large}\right)$$

For fast μ-mesons passing right through the phosphor without losing an appreciable fraction of their total energy $-dE/dx$ is constant and small, so that the light output is given by

$$L = A\left(-\frac{dE}{dx}\right) \times l$$

where l is the path length in the phosphor.

This is in agreement with Bowen and Roser (1951, 1952) who investigated the response of anthracene to cosmic ray μ-mesons, and found a linear response at relativistic velocities. The

energy loss for μ-mesons at minimum ionisation (β = 0.96) passing vertically through the phosphor and having a path length in it of 2 inches is referred to henceforward as I_{min}, and is equal to about 10 Mev.

A graph of dL/dx and dE/dx, showing the results obtained using anthracene crystals by various workers up till 1956 is given by Brooks (1956). Experimental values for electrons, protons and α-particles are shown. A good fit to the theoretical curve defined by the equation above is obtained. Brooks also gives curves for L and E obtained from the same results. The curve for electrons is linear as expected from theory, while those for the other particles are non-linear and in accord with the theoretical curves. They have been obtained by numerical integration of curves of $\frac{1}{A}\ \frac{dL}{dx}$ and residual range for each type of particle.

Curves of L and E can be obtained for the NE101 phosphor by the method mentioned above. Corresponding values of $\frac{dE}{dx}$ and R can be found by using the range-energy curves, together with the values of E and $\frac{dE}{dx}$ given in table 4; to select pairs of values which apply to the same energy. The curves show that an 80 Mev proton stopping in the phosphor would give an output corresponding to about 5 I_{min}, while a 200 Mev α-particle would give an output of about 7 I_{min}. If the phosphor response was linear, outputs of 8 I_{min} and 20 I_{min} respectively would be obtained. The ranges are both about 5 cm.

From the above results it can be noted that if a star is produced in the phosphor, a large amount of energy can be

dissipated by secondary particles stopping in it giving a large output pulse.

For inorganic phosphors the value of kB is much less than for organic phosphors. Thus for NaI (Tℓ), measurements by Taylor et al (1951) show that the response curves for electrons, protons and deuterons are all coincident, while only the response for α -particles is appreciably non linear, being about 60% of that for the other particles at 10 Mev.

9.3. Pulse height-frequency distribution curves for large scintillator for γ -rays and μ -mesons.

9.3.1. Distribution for Rd Th γ-rays.

A small Rd Th source was contained in a collimator made of lead blocks, as used for the Co^{60} source (section 8.2.3.) Rd Th emits a γ-ray with an energy of 2.62 Mev. γ -rays of this energy incident on the phosphor give rise to:-

(a) Photoelectrons of energy 2.62 Mev.

(b) Electron pairs of total kinetic energy 1.6 Mev.

(c) Compton recoil electrons of maximum energy 2.4 Mev.

In addition, any scattered photon which had produced a Compton recoil could then produce a pair or a photoelectron (or another Compton electron), if it had sufficient energy and the scintillator was sufficiently large.

In a small phosphor of low atomic number, and with photons of this energy, the Compton cross section is very much greater than that for the other two processes. This would give rise to a broad peak of electron energies near 2.4 Mev. In a large phosphor each scattered photon is likely to be re-scattered and finally to

produce a photoelectron, so that the total photon energy is released and the electron energies in this case are peaked about the photon energy (2.62 Mev) and there is no Compton edge. The phosphor used was sufficiently large (5 inches in diameter and 2 inches thick) for those incident photons which are backscattered to lose their total energy in it. At this energy the majority of the scattered photons will be backscattered.

The γ -rays were incident along a diameter of the phosphor. The output of the pulse amplifier was fed to a five-channel pulse amplitude analyser, which was used with a channel width of 1 volt. The spectrum obtained showed a peak at 21 volts and it was assumed that this peak corresponded to an energy of 2.62 Mev.

These measurements were done while the writer was working with Davies(1957), and the peak obtained is given in his thesis. A similar curve was obtained for γ -rays from Cobalt 60 which is also given by Davies. This had a peak at a voltage about half that for the Rd Th curve.

9.3.2. The Cosmic ray spectrum.

The Rd Th source was now removed. The axis of the counter remained vertical and the amplifier gain was reduced by a factor of eight (18 db) by means of the attenuator. A similar curve was now obtained when the source was not present, due to the passage of fast cosmic ray μ -mesons through the phosphor, the counting rate being much smaller in this case. The spectrum was first obtained using the 5-channel analyser. A repeat measurement was made as a test of the single-channel analyser, a similar curve being obtained with a peak at the same voltage. This curve is given in

figure 40. This curve had a peak at a voltage (~10V) approximately half that for the source. Thus the energy loss for these mesons was assumed to be equal to 2.62 x 8 x $\frac{1}{2}$ Mev; = 10.5 Mev; for μ -mesons having a path length of 2 inches in the phosphor.

Calculations are given in section 9.2.2. for the energy losses of various charged particles in the plastic phosphor. For a fast μ -meson at minimum ionization (β = 0.96) having a path length of 2 inches (5 cm) in the phosphor, the computed energy loss was 10.9 Mev. This was in good agreement with the value of 10.5 Mev for the cosmic ray peak showing that the light output in the phorphor for these mesons is proportional to energy loss; at least up to 10 Mev. The width of the peak was due to statistical fluctuations in the counter system and to μ-mesons and other particles; mainly electrons having path lengths in the phosphor different from 2 inches.

Taking the pulse height at the peak as equivalent to I_{min} the energy loss of a μ-meson at minimum ionization passing vertically through the phosphor; the analyser bias could then be set to any desired value. The amplifier attenuator could be kept constant, or reduced by a known factor to extend the scale.

9.4. Detection of showers occurring in lead.

9.4.1. General introduction.

In the previous section, a distribution curve is given showing how the number of pulses in a given range of pulse heights varies with the magnitude of the pulse. A maximum occurs at 21 volts 10·5 due to the fast singly charged cosmic ray particles, mostly

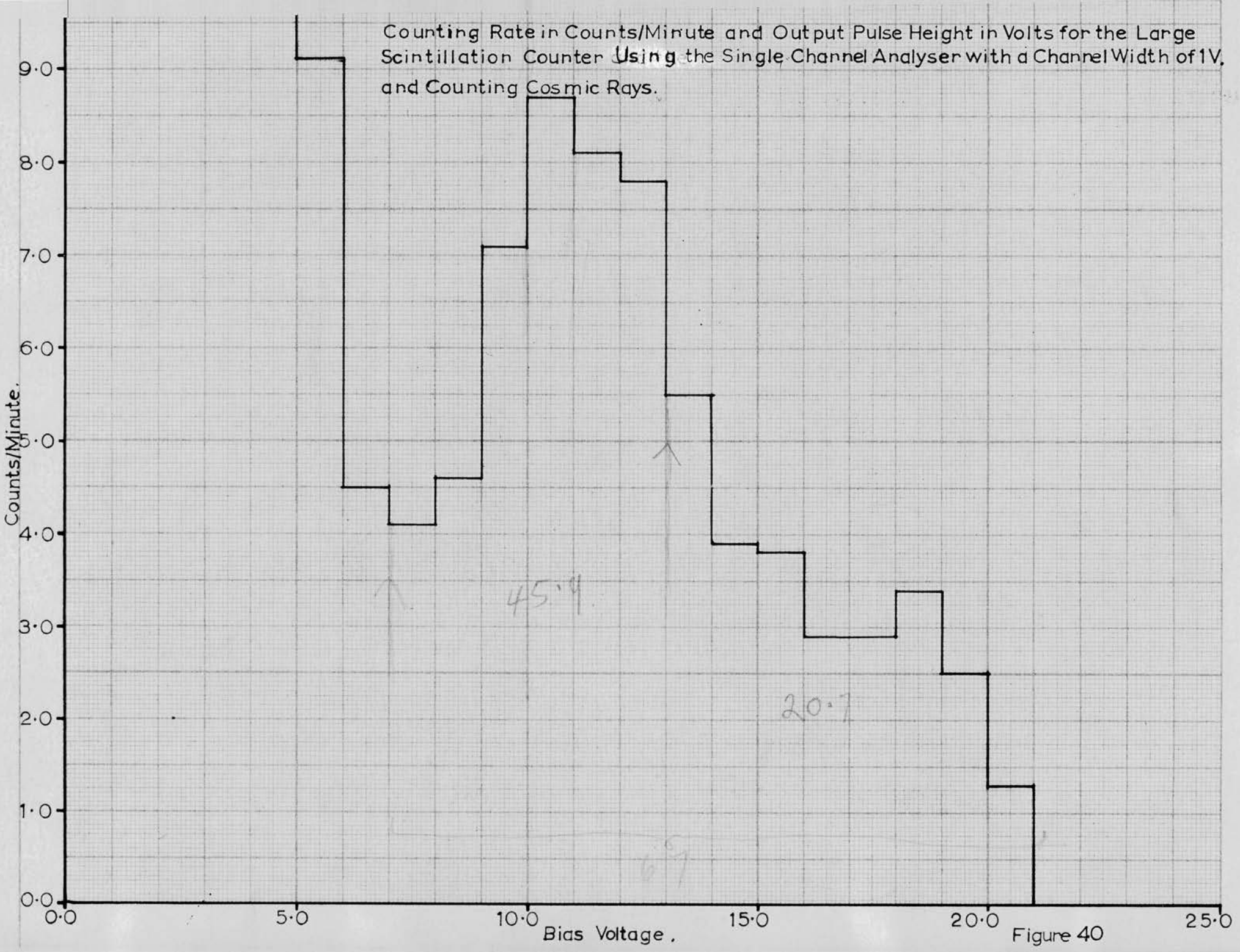
Counting Rate in Counts/Minute and Output Pulse Height in Volts for the Large Scintillation Counter Using the Single Channel Analyser with a Channel Width of 1V, and Counting Cosmic Rays.
9·0
8·0
7·0
6·0
5·0
4·0
3·0
2·0
1·0
0·0
Counts/Minute.
0·0
5·0
10·0
15·0
20·0
25·0
Bias Voltage.
45·9
20·7

Figure 40

electrons and μ-mesons passing vertically through the scintillator. Confirmation of this has been obtained by counting the number of 2-fold coincidences between pulses from the scintillator and a tray of Geiger counters placed beneath. A new curve was obtained showing a maximum at the same pulse height, even when the Geiger tray is shielded by several cm. of lead. It will be convenient in what follows to identify this maximum with energy loss rather than pulse height. A fast μ-meson passing vertically through the scintillator will lose, on the average, 10.5 Mev. This figure for velocities greater than 0.96 c. is practically independent of velocity if high energy transfers to electrons are neglected. Its value for velocity equal to 0.96 c is a minimum and this quantity equal to I_{min} will be used as a unit rather than pulse height.

As mentioned previously, the curve tails off gradually on the high voltage side of the maximum. There are several reasons why this is so; (i) straggling (in some cases the μ-meson may produce an energetic 'knock-on' electron), (ii) a fraction of the particles pass through the scintillator at an angle to the vertical, (iii) evaporation stars are produced by nucleons and π-mesons and (iv) showers.

At sea-level, the star rate should be between 1 and 5 per hour in the scintillator. Of these, about 10% will be energetic stars in which π-mesons are produced. The counting rate of pulses greater than 5 I_{min} is 6 per hour, of which not more than half can be due to evaporation stars unassociated with any fast secondary particles.

The assumption that an appreciable fraction of these large pulses are due to cosmic ray showers has been successfully verified, by measuring the counting rate at a fixed discriminator bias under varying thickness of lead. These results will be described in the following section.

The first counter experiments on the production of showers in lead were done by Rossi (1933), using three Geiger counters in a triangular arrangement.

The curve of shower rate against thickness of lead showed a maximum at about 1.5 cm of lead, thereafter decreasing slowly with increasing thickness of lead and eventually returning approximately to the rate for no lead. Such a curve is called a Rossi curve. The experiment was repeated by many other workers, among them Auger et al (1936), similar curves being obtained.

The results were interpreted by assuming that the cosmic radiation contains a hard component, capable of penetrating large thicknesses of matter, and a soft component which is easily absorbed. If the soft component produces numerous showers in thin layers of lead, which are then absorbed if the thickness is greater, the maximum observed is to be expected. The slow decrease in shower rate is ascribed to the hard component, which produces fewer showers but which is much more penetrating. The finite count for zero lead thickness is due to showers produced above the apparatus.

9.4.2. Experimental Rossi curve.

An experiment was done, using the large scintillation counter instead of a Geiger coincidence arrangement, to see whether a

curve similar to those obtained by Rossi and other workers could be obtained. Lead of varying thickness was used, from 0 to 18 cm. The amplifier output went to the single channel analyser, which was set to a channel width of 4 I_{min} to 6 I_{min} (see section 9.4.1.). Channel output pulses were counted for the various amounts of lead, the gain of the system remaining constant throughout. A curve very similar to that obtained by Rossi, and having a maximum at 1.5 to 2 cm of lead was obtained. As pulses due to single particles could be eliminated by a suitable bias, a singlefold system could be used. The curve obtained is shown in figure 41. A similar curve, but with a less well defined maximum, was obtained when a channel width of 3 - 5 I_{min} was used, as more non-shower events could now be counted.

This curve confirms the view that an appreciable fraction of the large pulses are due to cosmic ray showers, of which there are a number of different types. In an attempt to identify the type of shower responsible for the large pulses, the scintillator was mounted above a cloud chamber. Several different arrangements were used to trigger the cloud chamber, namely; (i) scintillation counter in coincidence with one tray of Geiger counters, (ii) scintillator alone and (iii) two scintillators in coincidence. These results are rather difficult to set down, mainly because at sea-level the showers are not usually of one particular type only but a mixture. In the following chapter, the photographs obtained with each arrangement will be discussed and finally an attempt is made to sum up the situation as a whole.

Thickness of Lead in Mm and Counting Rate in Counts/Minute for Electron Showers Produced in Lead; Using the Large Scintillation Counter, and the Single Channel Pulse Height Analyser with a Channel Width from 40-60 Volts (4-6 $I_{min.}$).

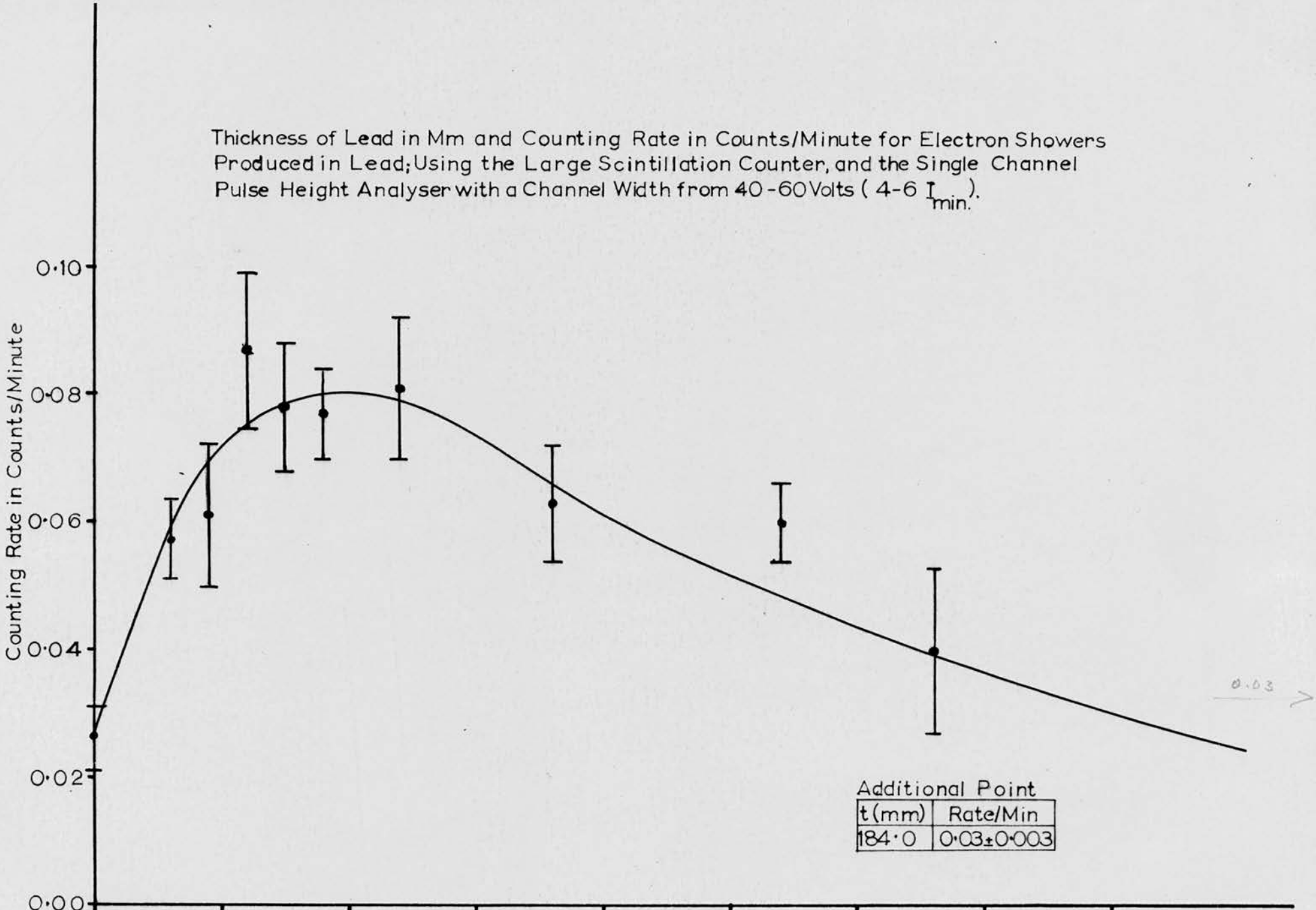

Additional Point

t (mm)	Rate/Min
184·0	0·03±0·003

Figure 41

Chapter 10.

THE CLOUD-CHAMBER WITH COUNTER-CONTROL.

10.1. General introduction.

Photographs were taken with several different arrangements of counters.

After considering the results obtained from counting only, it would seem that the large pulses, greater than 4 I_{min}, could be accounted for by the following:-

(a) Showers produced initially by high energy photons or electrons in the material above the counter. These are known as 'Cascade' or 'Soft' showers.

(b) Showers produced when a single heavy particle, mostly μ-mesons, transfers sufficient energy to an electron. These are known as "Knock-on" showers.

(c) Showers produced by nucleons or π-mesons in a single nuclear interaction. The secondary particles in these penetrating showers are mostly π-mesons.

(d) Evaporation stars produced by nucleons or π-mesons, in which no fast secondary particles appear, but which contain only protons and α-particles emitted with energies ranging up to several hundred Mev. Proton recoils can also be included in this.

(e) Fast single particles travelling in a direction inclined to the vertical and possibly accompanied by a small number of electrons. These are called "side showers".

These events will be considered in more detail below.

(a) Cascade showers

If a high energy electron or photon is incident on a dense absorber, a cascade shower can be produced. As the thickness of the absorber is increased, the number of shower particles leaving it at first increases to a maximum and then decreases again. This is the process producing the peak in the Rossi curve (see section 9.4.)

A cascade shower is dependent upon two different processes for its growth. These are the production of photons by high-energy electrons (Bremostrahlung) and the creation of electron pairs by photons. It will be seen, therefore, that the sum of these two processes can lead to an electron-photon cascade process if the energy of the initial electron (or photon) is sufficiently large. Theoretical treatments of this process have been given by numerous workers, and it will be useful to use some figures published by Bhabha and Chakrabarty (1948) to find the number of emergent electrons produced in a lead plate of given thickness by an incident electron of a given energy.

To do this we must know the characteristic cascade units for the material concerned. These are the characteristic length l_o, which is approximately equal to the mean free path of a photon before pair creation takes place; and the critical energy E_c, at which the energies of the electrons and photons have become too small, so that no more pair creation can take place. These units depend on the material concerned. For lead, Heitler (Quantum Theory of Radiation - O.U.P. - 3rd Edition, p. 391)

gives $\ell_0 = 0.51$ cm and $E_c = 14\ mc^2$.

The lead plate in the chamber is between 2.0 cm and 2.5 cm in thickness, and can conveniently be taken as having a thickness equal to $4\ \ell_0$. Table 5 shows corresponding values of E_0, the energy of the primary electron, and N the number of shower particles produced by it. The probability for the production of cascade showers in the phosphor, which is mostly carbon of density ~ 1 and has a thickness $< 0.25\ \ell_0$; can be found from the references quoted to be very small (< 1.7 particles for a primary energy of 30 G.ev.)

(b) Knock-on showers

A heavy particle passing through matter can produce one or more "knock-on" electrons. The theoretical results have been quoted by Rossi and Greisen (1941) and the following theory is taken from this reference.

Let $\chi(E,E')dE'dx$ be the probability for a particle of mass μ, charge ± 1 and energy E, traversing a thickness dx, to transfer an amount of energy between E' and E' + dE' to a free electron. The function χ is called the differential collision probability. We can measure dx in gm per sq cm.

Classical theory gives the following expression known as the Rutherford formula, which is valid for small values of E', i.e. small compared with E'm, the maximum energy transferred in a head-on collision:-

$$\chi(E,E')dE' = \frac{2C\mu_e}{\beta^2}\ \frac{dE'}{(E')^2}$$

Here, $C = \pi N_A \frac{Z}{A} r_o^2$ where N_A is Avogadro's number.

Table 5.

The number of cascade shower electrons produced in the lead plate of thickness 2 cm by a primary electron of energy E_o.

E_o Mev	N
85	0.52
234	1.90
603	6.00
1660	15.6
4900	36.8
12,300	76.9
32,400	149
102,000	272
246,000	468

Computed from figures published by Bhabha and Chakrabarty - Physical Review Vol. 74, p. 1361, (1948).

For particles with a spin of $\frac{1}{2}$, (μ-mesons) Bhabha (1938) has given:-

$$(E,E')dE' = \frac{2C\mu_e}{\beta^2}\frac{dE'}{(E')^2}\left[1-\beta^2\frac{E'}{E'_m}+\frac{1}{2}\left(\frac{E'}{E+\mu}\right)^2\right]$$

where again E'_m is the maximum transferable energy to the electron by the incident particle. It can be shown that

$$E'_m = 2\mu_e\left(\frac{\beta^2}{1-\beta^2}\right)$$ providing the momentum of the incident particle is $\ll \mu^2/\mu_e c$. μ and μ_e being the rest mass energies of the particle and electron respectively. For a μ-meson, this quantity is equal to 20 Gev/c. As long as $E' \ll E'_m$, the classical formula gives the same result as the quantum-mechanical one, and will be used here.

The number of knock-on electrons per unit length having kinetic energy $> E'$ is given by

$$N(>E) = \int_{E'} \chi(E,E')dE$$

In most cases, the upper limit for this integral can be taken as E'_m as defined above.

Some values of the function $N(>E')$ are given in Table 6, referring to μ-mesons passing through lead and through the scintillator. The fourth column refers to the minimum energy, E_{min} which the μ-meson must have to produce a knock-on electron of energy E'. In other words, these probabilities refer only to μ-mesons having energy $\gg E_{min}$.

In general, μ-mesons will not normally produce many electrons in passing through a 2 cm. thick lead plate.

Table 6.

The number $N(>E')$ of knock-on electrons of energy $>E'$ produced in the phosphor, and in the lead plate, by a μ-meson of energy large compared with E_{min}.

E' (Mev)	$N(>E') \times 10^2$ Phosphor - 5 cm	$N(>E') \times 10^2$ Lead Plate-2 cm	E_{min} GeV
10.0	4.3	13.8	0.30
100.0	0.43	1.38	1.0
200.0	0.22	0.69	1.4
400.0	0.11	0.35	2.0
600.0	0.07	0.23	2.4
1000.0	0.04	0.14	3.1

(c) Penetrating showers.

Penetrating showers are the result of an interaction between a high energy nucleon or a π-meson and an atomic nucleus. Fast secondary particles are produced, mainly $\pi^{\pm}$, and π^{0} mesons in nearly equal numbers. In addition, a number of slow nuclear particles are also present. The π^{0} mesons decay very rapidly into two photons owing to their very short half lifetime which is less than 10^{-14} sec.

The interaction length for shower production is about 100 gm cm^{-2}, but only if the energy of the incoming particle is at least several GeV. For energies less than 1 GeV and above threshold, there is only a small probability of producing more than one π-meson. The cross-section for capture of π-mesons of energy not greater than several hundred Mev is still about 100 gm cm^{2}, the capture resulting in an evaporation star of low energy nuclear particles.

At very high energies, other types of mesons may also be produced.

The showers are difficult to identify in the cloud chamber. If more than three particles produce back to a common origin and if they produce no large showers in the lead plate, it is assumed that they are penetrating particles. However, these photographs always show many electron tracks due to the small electron showers produced by photons resulting from the decay of the π^{0} mesons.

(d) Stars

In addition to showers of the three types mentioned, large

signals can also be produced by stars which are formed in the phosphor and which do not have any fast secondary particles with sufficient energy to leave the phosphor.

According to Page (1950), light nuclei such as carbon and oxygen do not give many stars with more than about six prongs. Also, a large proportion of the prongs are due to α-particles. The Range-energy curve for α-particles (figure 38) shows that the range of a 200 Mev α-particle in the scintillator is only about 2 cm, so that large amounts of energy can be dissipated in the phosphor itself without producing any visible secondary particles. Also, the range of a 50 Mev proton is again about 2 cm, so that the total energy of protons of this and lower energies produced in stars will often be absorbed in the phosphor. The output pulse heights produced by these particles, especially the α-particles, are not proportional to the energy loss because of the non-linearity of the phosphor, discussed in section 9.2. Hence, the output pulse produced by a 200 Mev α-particle stopping in the phosphor will not be about 20 I_{min} but only about 8 I_{min}. For a 100 Mev α-particle it will be about 2.5 I_{min} and for a 50 Mev proton about 3 I_{min}.

Stars may be induced either by uncharged particles (mainly neutrons) or by charged particles (protons). Page considers that the majority of stars having energies of less than about 200 Mev are produced by neutrons. It is thus reasonable to assume that a large proportion of stars will produce a signal as large as 5 I_{min}, as this will only be equivalent to about two protons of energy 50 Mev each.

The number of stars which will be produced in the phosphor per hour can be calculated from an expression given by Page. She gives an expression for the number of stars dn_r formed in the atoms of the element r per day, in 1 cm^2 of emulsion of thickness dx. The element r is considered to be one of the constituents of the emulsion there being N_r atoms per cc. If n_o is the total flux of star-producing particles per cm^2 per day and σ_r the cross section for star production, then

$$\frac{dn_r}{n_o} = N_r \sigma_r \, dx.$$

Making the reasonable assumption that the expression can be applied to carbon atoms in the phosphor and taking σ_r as equal to the geometrical cross-section of the carbon nucleus and n_o as 28 particles/cm^2/day at sea level as given by Page; the number of stars per hour in the large phosphor comes to about 5.3/hour. At a counting rate 5/hour, corresponding to an energy loss $5\ I_{min}$ we can therefore expect that at least some of the counts are due to stars of this energy.

In this investigation it appears later that this figure is too high, unless some of these stars are associated with a shower produced near the apparatus. When the counting rate is set to 5/hour, certainly, at least 40% of the photographs show evidence of some kind of shower.

(e) Other causes of large scintillations

If we consider the large phosphor, fast particles travelling at a large angle to the vertical can lose energy of up to about

2.5 I_{min} owing to the increased path length in the phosphor. If such a particle produces a knock-on electron in addition, signals as great as 3 I_{min} may be produced. The number of pulses as great as 5 I_{min} due to such a process will be small as it will correspond to knock-on electrons of a total energy of 25 Mev even when the particle is travelling at a large angle to the vertical.

It can be concluded that the maximum contribution to signals of about 5 I_{min} and greater is made by stars, and by the types of shower already discussed.

10.2. The photographs.

10.2.1. The large scintillator and geiger counters in coincidence.

The first counter control system used to trigger the cloud chamber consisted of the large scintillator immediately on top of the cloud chamber, together with a tray of geiger counters beneath the chamber. The two outputs were fed to the slow coincidence unit described in section 4.6.

For all the photographs, the bias at the large scintillator output was between 5 I_{min} and 6 I_{min} corresponding to a singlefold counting rate of between about 5/hour and 2/hour. The doublefold rate was much less, being only about 0.5/hour to 0.2/hour. The difference was due to the geometry of the system, as many showers would not contain any particles passing through a Geiger counter. Also, stars in the scintillator with sufficient energy to produce an output pulse of 5 - 6 I_{min} would not always have any secondary particles leaving the phosphor.

The majority of the photographs (about 70) were taken with about 4 cm of lead above the Geiger counter tray to prevent the counters being triggered by low-energy electrons. Most of these photographs were taken before the lead plate was inserted in the chamber, so that it cannot be determined whether or not any of the showers contain penetrating particles. From the photographs taken with this system after the lead plate was fitted, penetrating particles are present in some of the showers. The proportion of showers in these photographs varied from about 70% to about 90% depending on the singlefold counting rate of the scintillation counter. The 90% yield corresponded to a bias of about 6 I_{min} and a coincidence rate of about 0.2/hour.

Some photographs were taken with about 4 cm of lead immediately underneath the phosphor, in addition to the 4 cm above the Geiger counters. Of eight photographs taken consecutively with this arrangement, seven contained showers, the average waiting period being about four hours.

This work was done while the writer was working with Davies and the results are more fully described in his thesis (Davies (1957)). The photographs taken with the counter arrangements discussed in the later sections of this chapter were taken by the writer only. As examples of all the types of shower described here were obtained later in the other runs, no photographs of this run will be given.

10.2.2. The large scintillator only.

It was suspected that a fairly large proportion of the singlefold counts from the scintillation counter at a counting rate of 2/hour were due to showers. As the singlefold counting rate was eight or ten times greater than the coincidence rate for the experiments on the previous section, a shower yield of 10% or 15% with the large scintillator only would still be as good as a shower yield of 100% with the coincidence circuit, the rate of shower production being about the same in each case.

Photographs were now taken with the large scintillator immediately above the chamber, no lead being present. The output pulses from the counter-amplifier went to the single channel pulse height analyser (see Chapter 5). The pulses to trigger the cloud-chamber were taken from the analyser differential output. The reason for this was that showers of the type in which we are interested contain only a relatively small number of particles. Hence, if the acceptable pulse height is restricted to a small range, say from 4 I_{min} to 6 I_{min}, pulses due to events such as extensive showers produced above the apparatus will not trigger the cloud chamber. As the chamber was still non-automatic at this stage, only relatively small numbers of pictures were taken. Sixty-one pictures were taken with the above system, the pulse heights used being in the interval 5 I_{min} to 6 I_{min} for most of them. The counting rate varied between about 2/hour and 4/hour, and 21 showers were obtained which was a yield of $\sim$ 35%. Of these showers, 16 (26%) contained more than 5 particles. The details are given in Table 7.

Tables

Table 7 - Statistics for photographs obtained using large scintillator only, no lead being present.

Number of photographs (excluding blanks)	61
Percentage of showers or events	35%
Counting rate	2 - 4/hour
Shower rate	0.6/hour

Table 8 - Statistics for photographs obtained using large and small scintillators in coincidence with the slow coincidence system.

Number of photographs	25
Percentage of showers or events	24%
Counting rate	2 - 3/hour
Shower rate	0.5 - 0.7/hour

Table 9 - Statistics for photographs obtained using large and small scintillators in coincidence with the fast coincidence system.

Number of photographs	320
Percentage of single penetrating particles	30%
Percentage of other events	7%
Counting rate	5/hour
Shower rate	0.3 - 0.5/hour

Table 10 - Statistics for photographs obtained using small scintillator only, with lead above the counter.

Number of photographs	120
Percentage of single penetrating particles	10%
Percentage of other events	10%
Counting rate	2/hour
Shower rate	0.3/hour

Examples of the various types of shower discussed in section 10.1 were obtained in this run. A large number of photographs showed cascade showers, many of which multiplied further in the lead plate. The original cascade showers were largely produced by nuclear interactions in the roof of the building or higher up in the atmosphere, in which π_0 mesons were produced and then decayed to give photons. These photons then initiated a cascade shower as explained in section 10.1(a).

An example of photograph which includes a cascade shower is shown in Plate 1. The shower is locally produced, as the tracks in the upper part of the chamber project back tc a point lying in the phosphor. The thickness of the phosphor is only a quarter to an eighth of a radiation length, so that the most likely method of production was from a high-energy nuclear interaction involving the production of several high energy π^0 mesons. These then decayed, giving high energy photons which produced the cascade. The core of the shower would then contain the tracks of other penetrating particles from the interaction, but it is not possible to be sure of this as the shower is too dense. The photographs also includes tracks due to low energy electrons.

A very high energy photon can produce a shower of several particles even in a thickness of a fraction of a radiation length.

As cascade showers are often produced by the γ -rays resulting from the decay of π^0 mesons formed in nuclear interactions, it is to be expected that a photograph will often show a cascade shower,

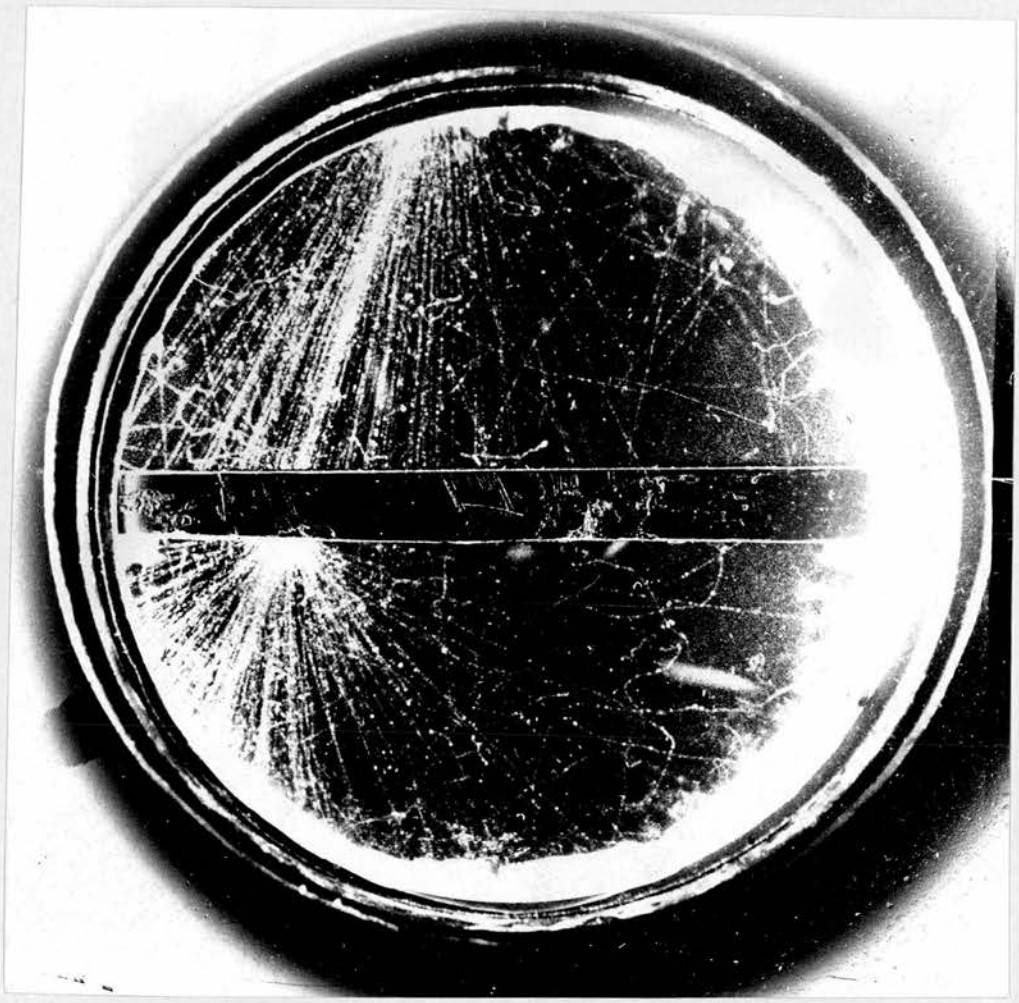

Plate 1.

See text, page 139.

probably with a secondary interaction in the lead plate and accompanied by one or more penetrating particles. Such showers have been observed by many workers using arrangements of Geiger counters for shower detection. Several examples were found in this run (about 25% of the shower yield) which contained at least one penetrating particle in addition to the electron shower. An example of one of these showers is shown in Plate 2, in which the penetrating particle is marked.

Penetrating showers in which the photographs only showed the tracks of a small number of particles were also obtained. The photographs of showers of this type obtained in this run were not of good quality, and a photograph is shown in Plate 8 of such a shower obtained in a later run (Section 10.2.3.(b)). The photograph is discussed in that section. It is likely that showers containing penetrating particles and electrons are those produced near to the chamber, while those with penetrating particles only are produced higher up, so that the cascade shower has died out by the time the chamber is reached.

Plate 3 shows a large shower most probably produced by a high-energy particle travelling at a large angle to the vertical. This was incident on the side of the lead plate or on one of the metal parts of the chamber. The inclination to the vertical of the tracks in the chamber make it likely that incident particle was travelling horizontally or nearly so, and the number of tracks indicates that it was of very high energy.

10.2.3. <u>The large and small counters in coincidence</u>.

Photographs were taken with the two counters in coincidence

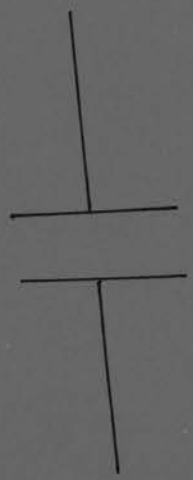

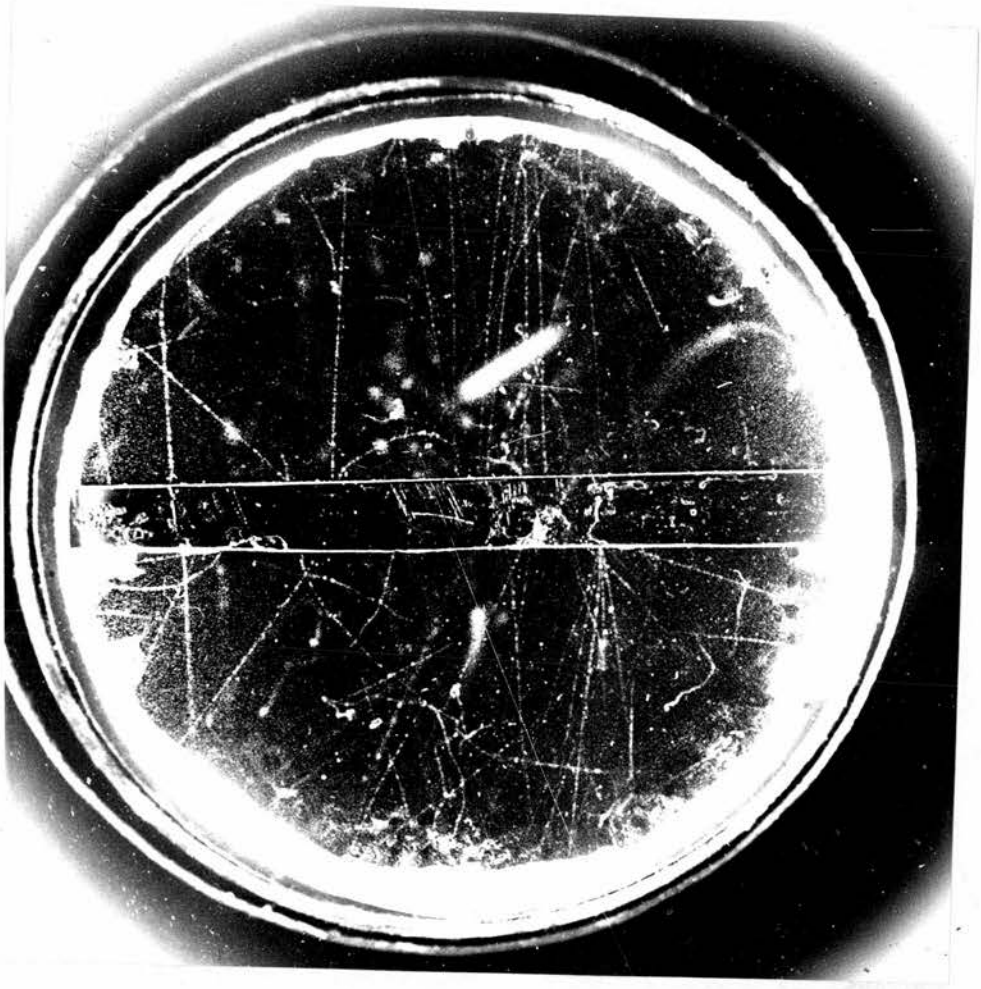

Plate 2.

See text, page 140.

Plate 3.

See text, page 140.

both with the original slow coincidence system and with the fast coincidence system.

(a) Photographs taken with the original slow coincidence system

For these photographs the two scintillators were placed directly above the cloud chamber with the large one immediately above the small one. About twenty-five photographs were taken with this system, of which six showed showers a yield of about 24%. As two of these showers were obtained at one end of the run and four at the other, with a run of about 15 pictures in between with no showers and very little else, it is suspected that the true shower counting rate may have been higher than 24% and that some of the blank photographs taken during this period may have been due to poor photography, or to spurious triggering of the chamber by electrical pick-up. The discriminator biasses for both channels were about 2 I_{min} in the above. The counting rate was 2 - 3 an hour.

Two photographs were obtained with biasses of 4 I_{min} and 5 I_{min} on the large counter and 1 I_{min} on the small counter. Both of these were showers. It was considered that a coincidence system of shorter resolving time and having the counters separated by a much greater distance would probably be more satisfactory. No photographs from this run are reproduced as better examples of the same types of showers were obtained elsewhere. Table 8 shows the results

(b) Photographs taken with the fast coincidence system.

The two counters were placed above the cloud-chamber for this run. The small counter was immediately on top of the chamber.

The large counter was outside the cloud chamber hut, and vertically above the small one, the separation being about 1.65 metres. This large separation ensured that only particles travelling vertically or at a small angle ($< 3^{\circ}$) to the vertical could produce a genuine coincidence due to the same particle passing through both counters. Coincidences would also be produced by electrons associated in showers, different members of the showers passing through the two counters. Due to the small resolving time the number of chance coincidences was very small (see section 8.3.)

The bias levels in the two channels were arranged so that all the single fast particles passing through the two phosphors would be able to record coincidence. In order to ensure this, the counting rate in channel 1 (small counter) was made about 4000/hour and that in channel 2 (large counter), about 8000/hour. As the intensity of the penetrating component of the cosmic radiation is about 0.01 particles/cm^2/sec/[illegible] these will all be counted when the counting rate of the small counter (area 26 sq. cm) is greater than 10,000/hour and that of the large counter (area 120 sq cm) is greater than 4,500/hour. This was satisfied by the values given above. The coincidence counting rate at the separation of 1.65 metres was about 5 counts per hour.

About 320 photographs were taken with this arrangement at a rate of 5/hour. Inspection of the photographs obtained showed that a large number of them ($\sim$ 30%) had single penetrating particles which passed through the two scintillators and then through the lead plate in the cloud-chamber. The majority of these single particles will be μ-mesons. An electron having

sufficient energy to penetrate the plate without appreciable loss of energy as shown by the straightness of the tracks on the two sides of the plate, would normally produce a small cascade shower (see Table 5), so that the particles are unlikely to be electrons. A typical example of one of these tracks is shown in Plate 4.

In addition to the single particles, about 7% of the photographs showed events of other types including showers and interactions in the lead plate. Some of these are shown in Plates 5 - 9. This counting rate for events corresponded to $\sim$ 1 event per 4 hours, which is of the same order of magnitude as for the singlefold counting system, although the events selected by the new system are of a more interesting type.

Plate 5 shows an event in which three interactions are produced in the lead plate, probably by electrons. It is believed that this is part of a penetrating shower produced in the ceiling above the chamber. There is evidence of a small number of penetrating particles crossing the chamber having the same general direction.

Plate 6 shows another shower. In this case the tracks extend throughout the cloud chamber and the shower is a mixed one containing electrons and possibly penetrating particles. The track marked 1 at the left hand side of the chamber is possibly that of a heavy particle.

The event shown in plate 7 is probably a μ -meson deviated due to multiple scattering in the lead plate. The track above the plate appears to be somewhat more lightly ionising than the one beneath the plate, although it is not possible to say whether

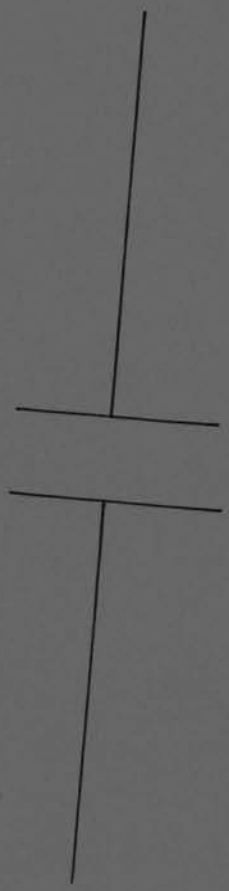

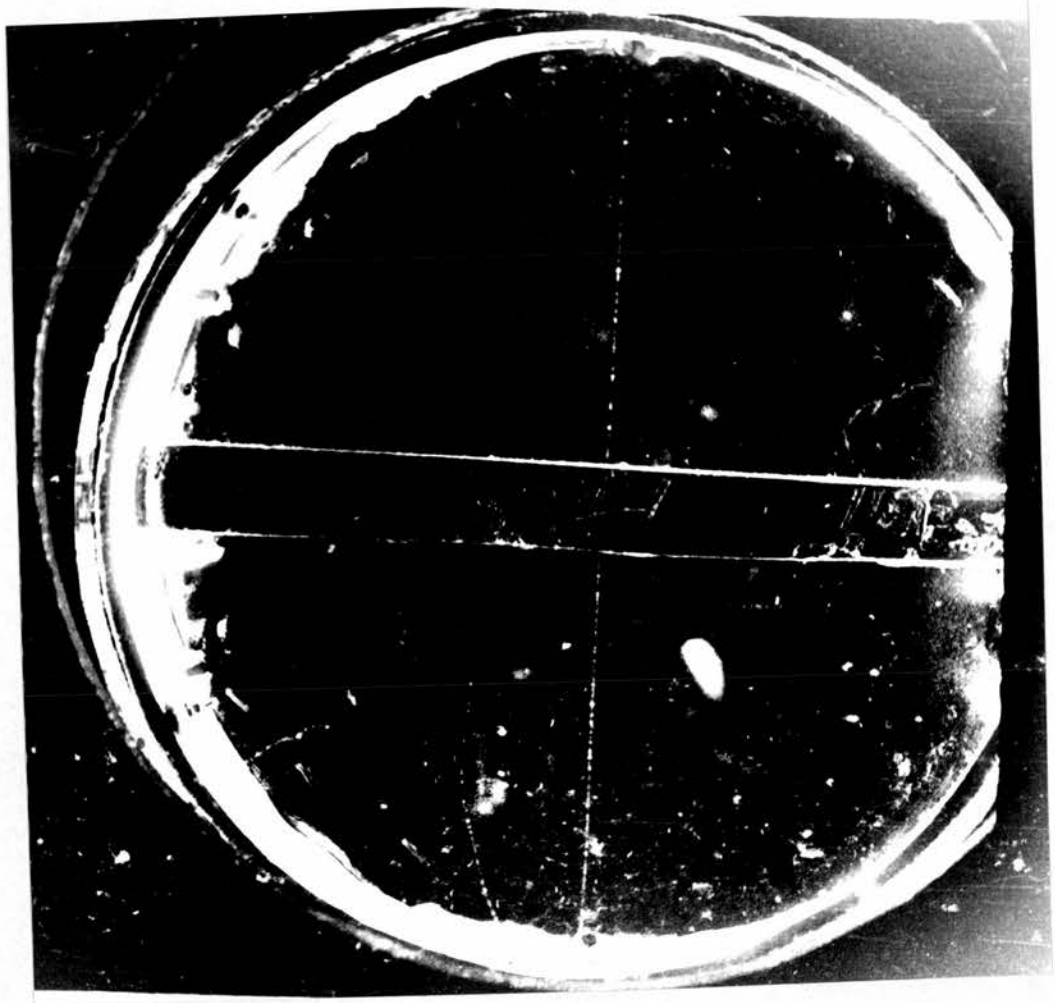

Plate 4.

See text, page 143.

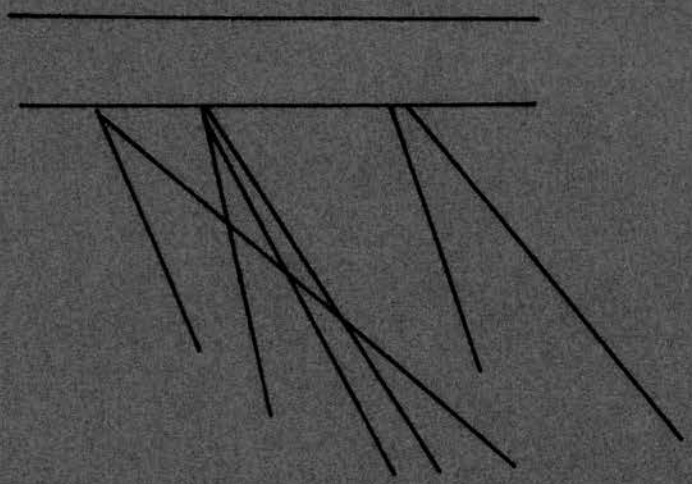

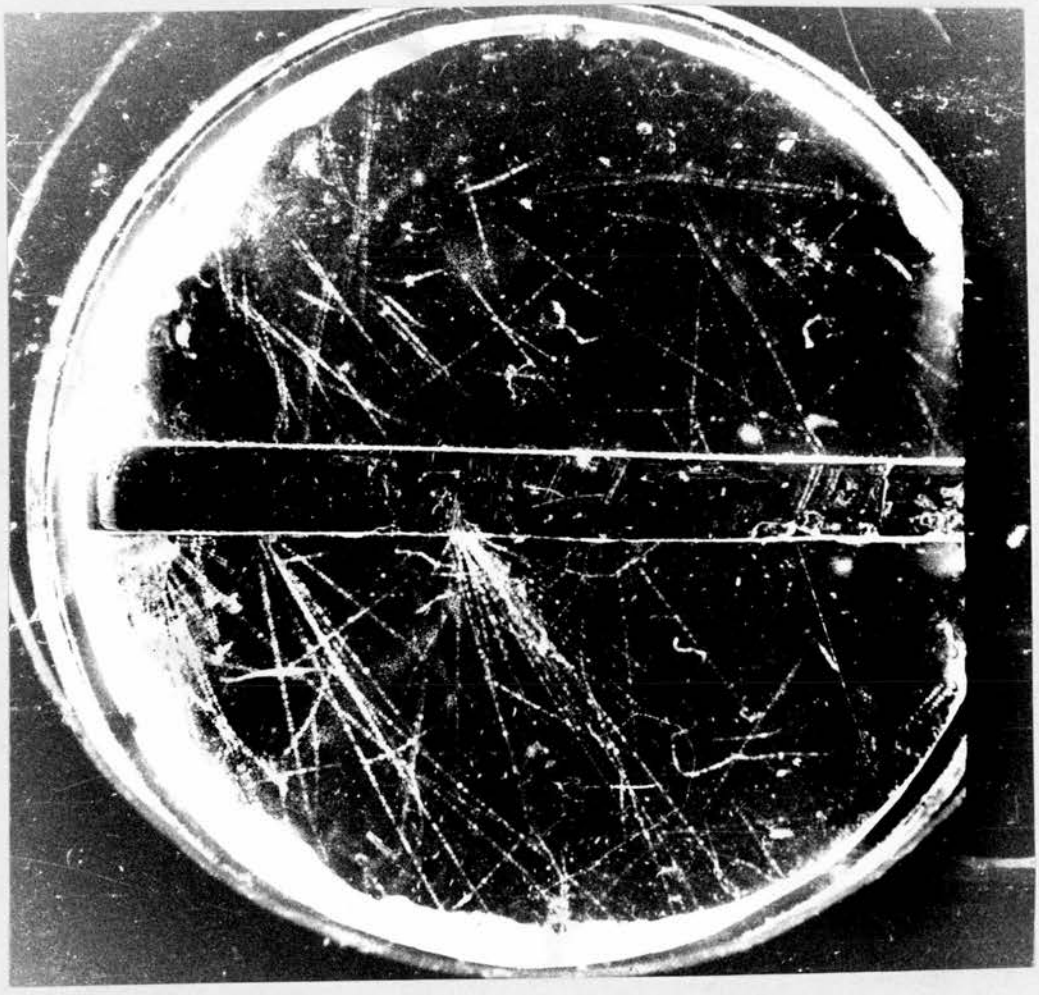

Plate 5.

See text, page 143.

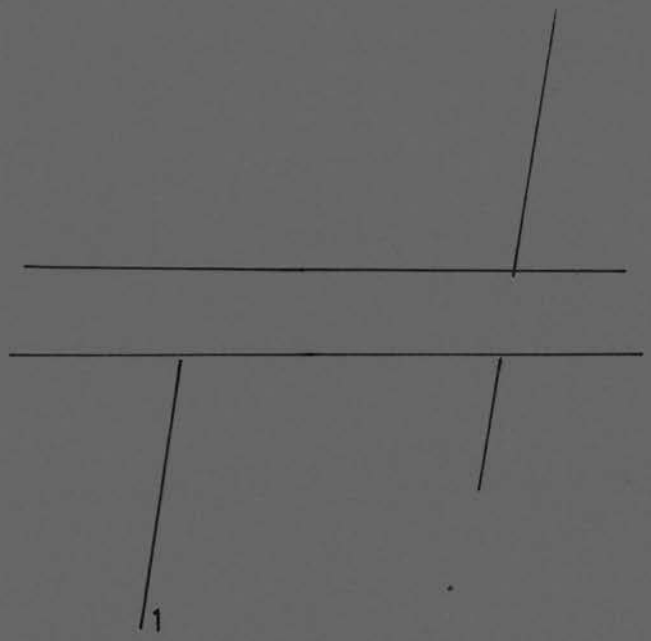
1

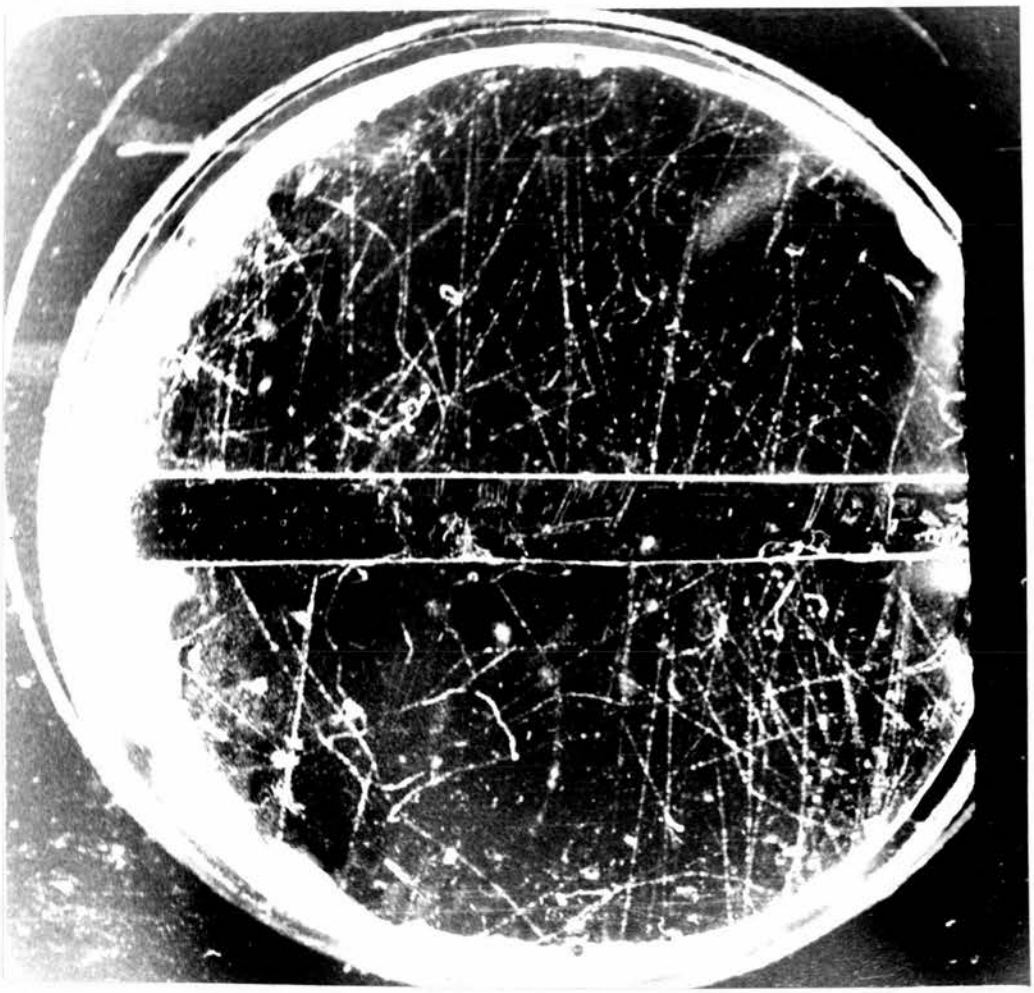

Plate 6.

See text, page 143.

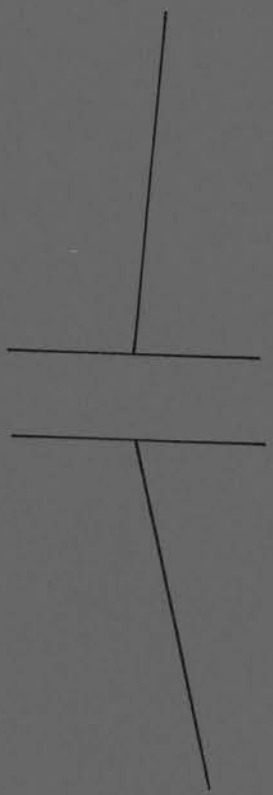

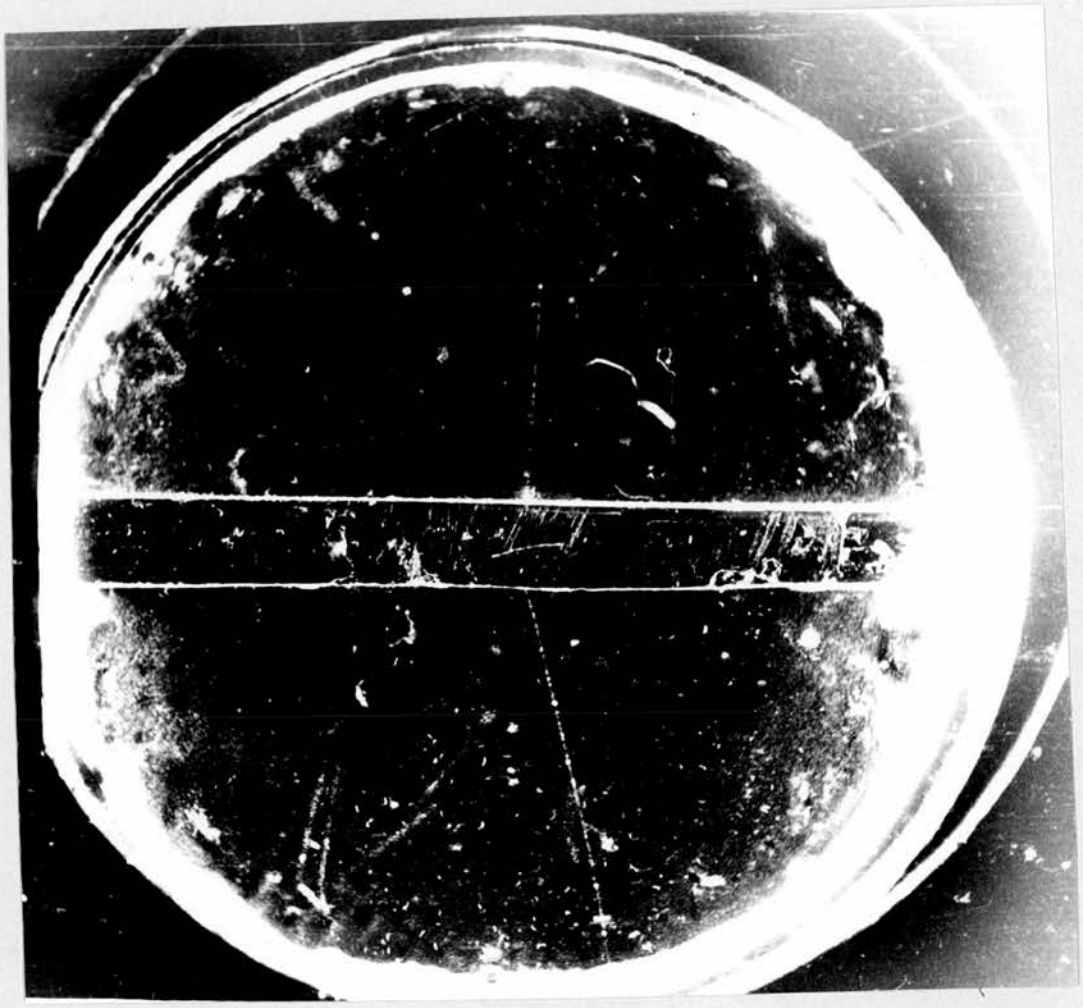

Plate 7.
See text, page 143.

this is in fact the case, or whether the two tracks were differently illuminated.

Plate 8 shows a small penetrating shower in which one of the primary particles produces a star in the lead plate. The particle on the left passes straight through the plate, emerging in its initial direction. The particle on the right produces the interaction, in which four associated tracks can be seen.

A shower containing penetrating particles is shown in Plate 9, in which the tracks of the penetrating particles are indicated. These tracks are approximately parallel, which shows that the event was produced at a considerable height above the apparatus.

A summary of the numbers of single particles and events obtained during this run is given in Table 9.

10.2.4. Photographs taken with the small counter only, with 15 cm of lead above the counter.

Some lead was placed above the small counter, with the counter immediately above the chamber. It was hoped that secondaries from interactions in the lead which only covered a small area would be selected by the counter. A small counter should be better than a large one, as there is then a bias in favour of events which result in the dissipation of a large amount of energy in a small volume, rather than events such as extensive air showers or other electron showers which can dissipate a large amount of energy in a large volume.

About 120 photographs have been taken with this arrangement to date, at a counting rate of about 2/hour or about 6 I_{min}. About 10% show showers or other events and an additional 10% show single penetrating particles at various angles to the vertical. The

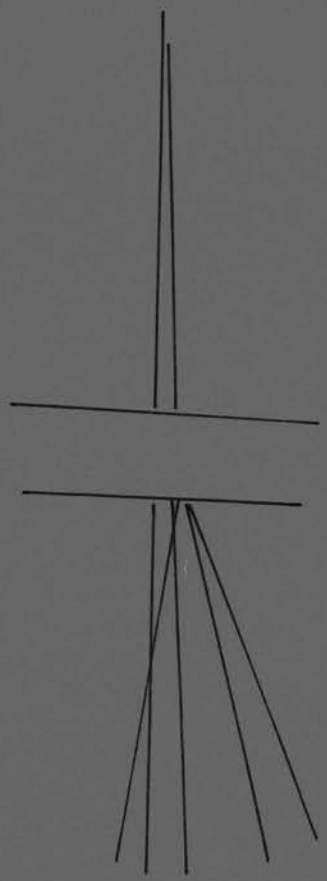

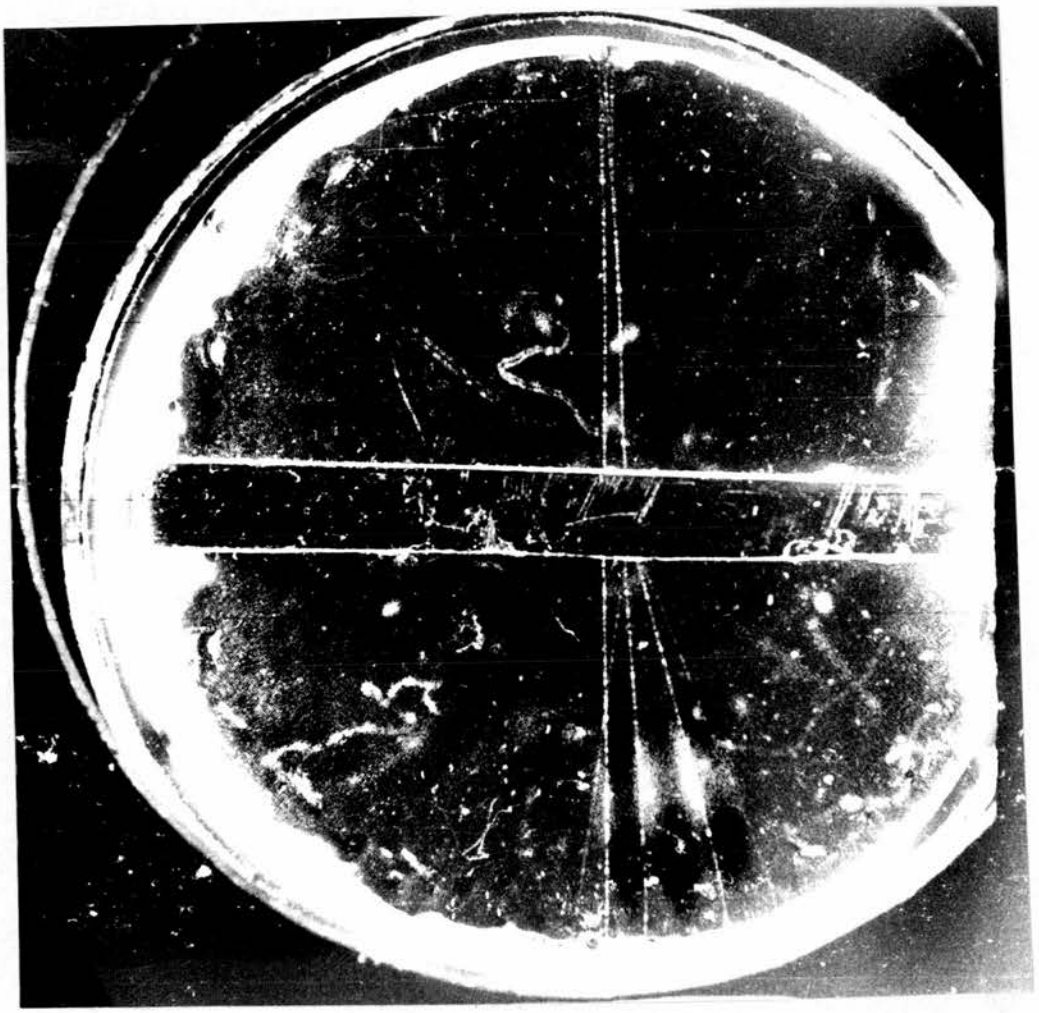

Plate 8.

See text, page 144.

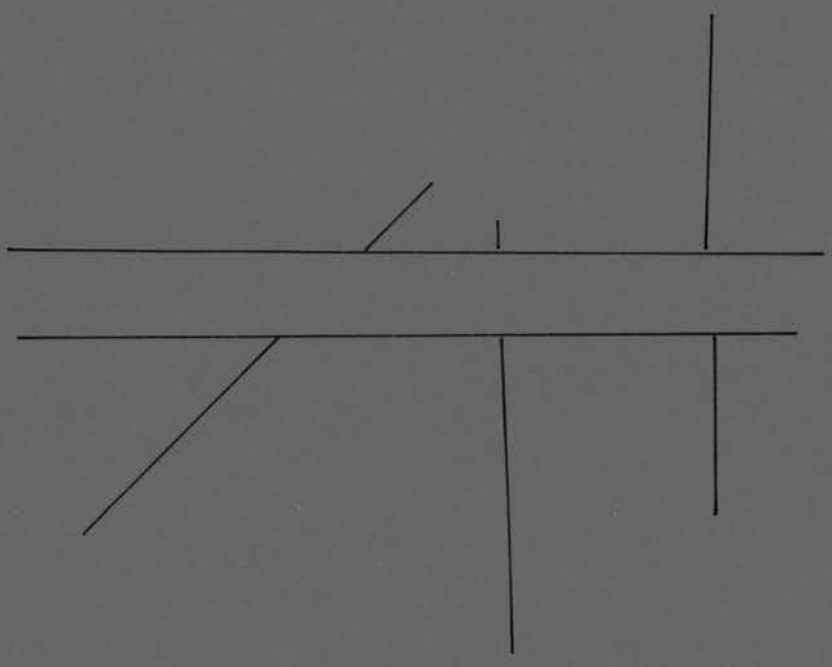

Plate 9.

See text, page 144.

photographs showing no events are due to either particles which pass through the phosphor at such an angle that they do not enter the chamber, or to stars produced in the phosphor with no fast secondary particles.

Plates 10-12 show photographs taken with this arrangement. Plate 10 shows a small penetrating shower containing two nearly parallel tracks of particles which pass through the lead plate. The quality of this photograph is poor, and the two halves of the chamber have been given different exposures in order to obtain a reasonable contrast. The reason for the bad quality is that the chamber sensitive volume was suffering from vapour depletion and required the addition of more alcohol.

Plate 11 shows a penetrating shower which produces an interaction in the lead plate. The track indicated is that of a heavy particle. This photograph was taken during the same overnight run as Plate 10, and evidence of vapour depletion can be seen in the top part of the chamber.

The event in Plate 12 is probably a star produced in the lead plate by one of the particles seen above the plate. The other particle and the track beneath the plate are then secondary particles from this star.

Table 10 gives a summary of the statistics of this run.

10.3. Conclusions.

The cloud chamber photographs can be said, generally speaking, to confirm the results described in earlier sections. The results using the fast coincidence system with bias levels $\sim I_{min}$ on each counter showed that single penetrating particles can then be

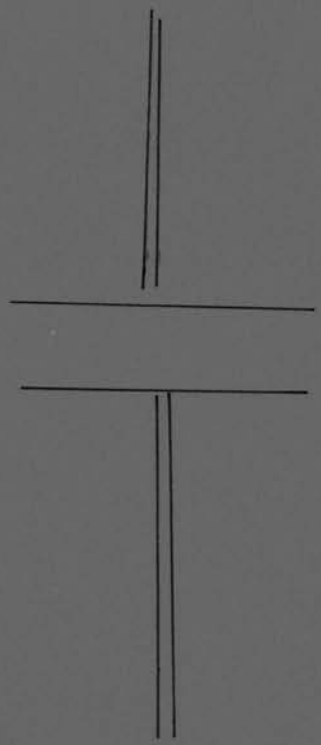

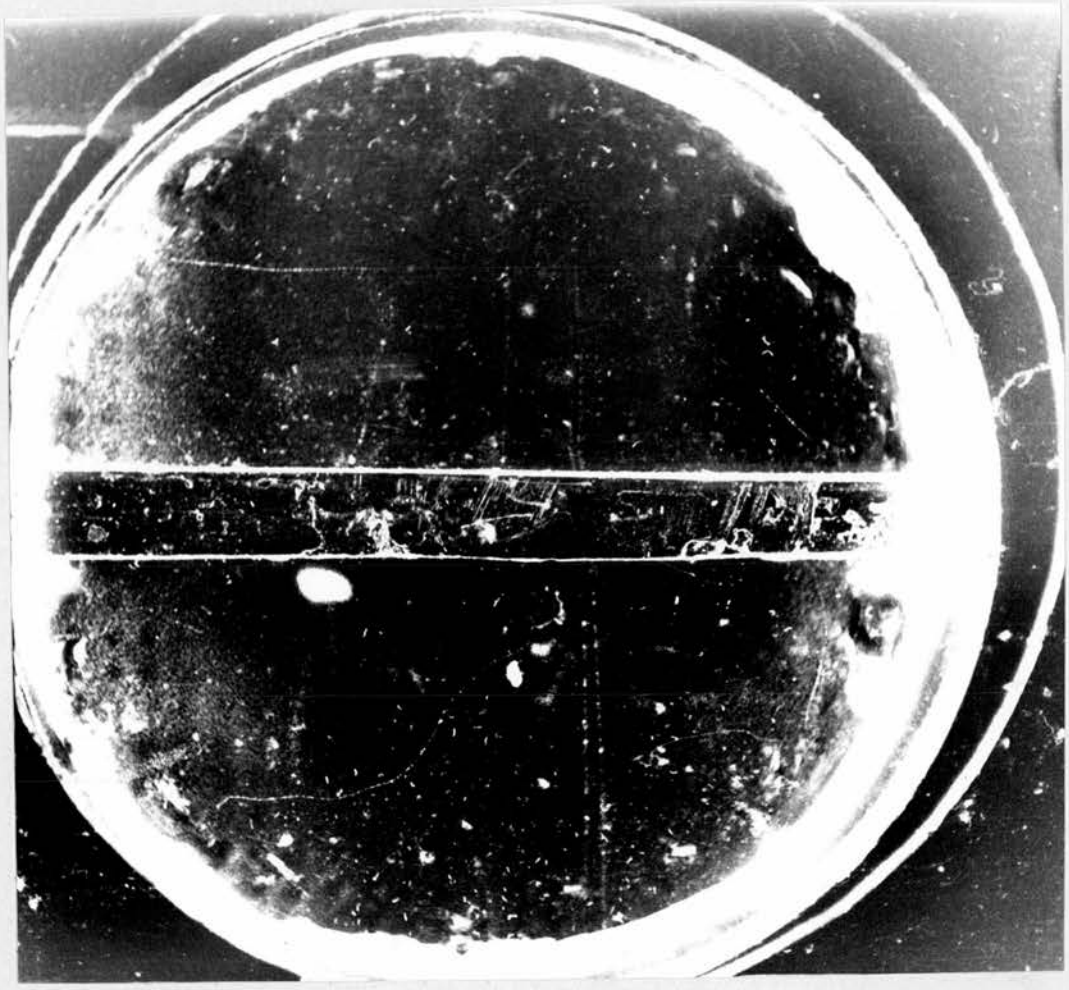

Plate 10.

See text, page 145.

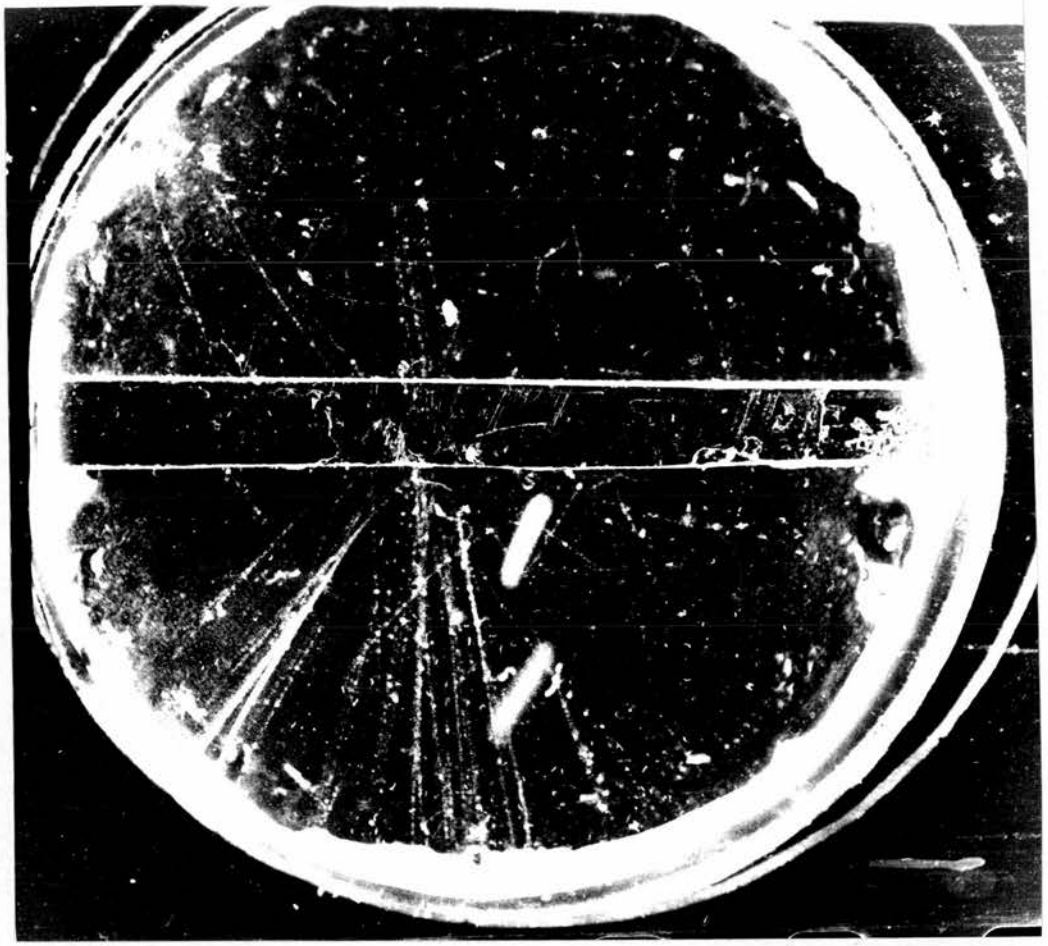

Plate 11.

See text, page 145.

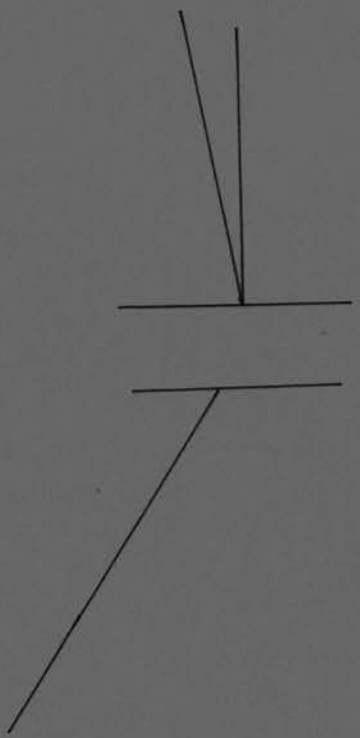

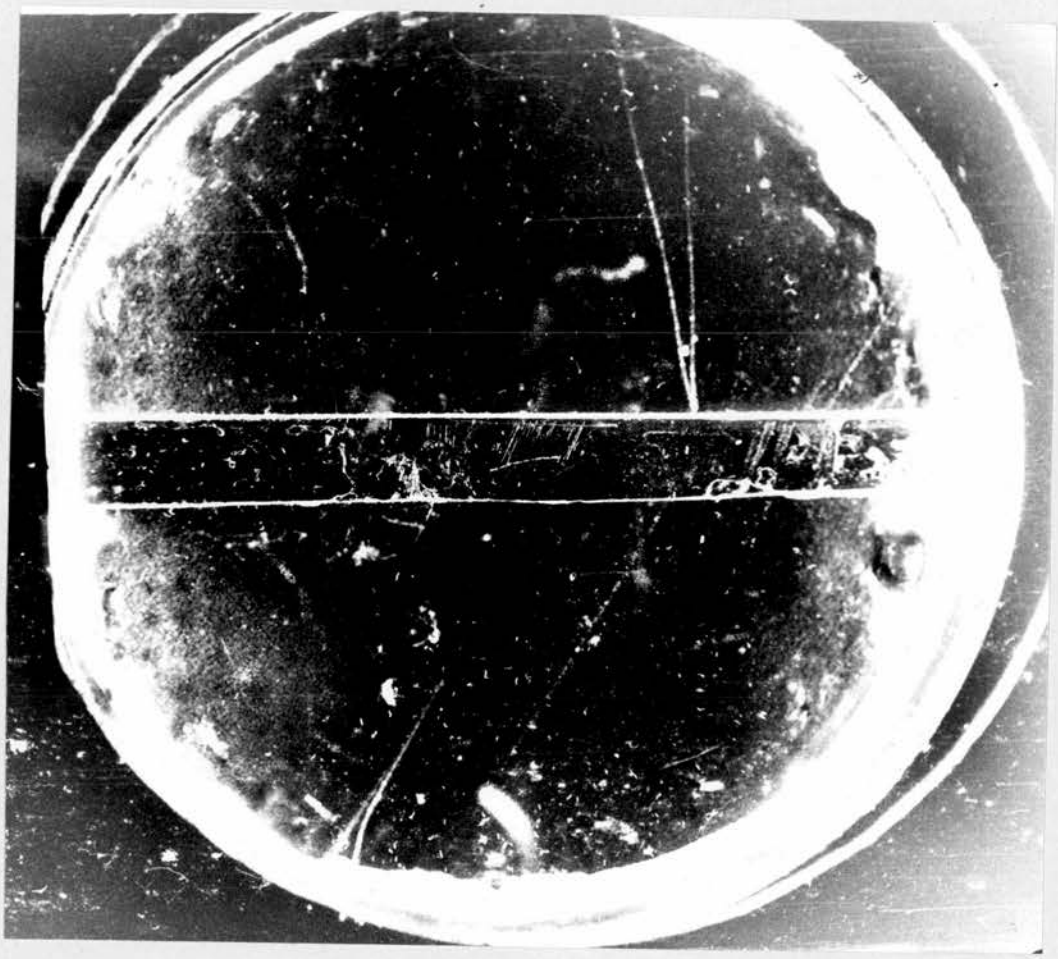

Plate 12.

See text, page 145.

selected, most of which are μ-mesons as they pass through the lead plate with little loss of energy.

With a discriminator bias of 5 or 6 I_{min} and a counting rate of about 2 per hour, 25 to 40% of the photographs taken with the single scintillator show showers of one kind or another. Completely blank photographs occur only in about 20% of the cases and these probably represent evaporation stars in the scintillator, caused by either low energy protons or neutrons. This is much smaller than that expected from the results obtained with nuclear emulsions i.e. about 5/hour. This figure was obtained by assuming that 28 nuclear particles per cm^2 per day in this energy range fall on the scintillator. Most of these must be neutrons. It is known from work with a randomly controlled chamber that not more than 4 of these particles can be protons. In addition, to explain the results here, in only a few cases can a star occur in the scintillator which is not associated with a number of other charged particles.

Of the other photographs, it can be said with certainty that they all show convincing evidence that the large scintillations are connected with some cosmic ray event. The spurious background must be negligible. Although the linearity of the scintillator with energy loss cannot at present be tested above 10 Mev, it has been shown that as the discriminator bias is increased, denser and denser showers are obtained. Although about 10-15% of the photographs show tracks of penetrating particles, not many penetrating showers can be traced back to the scintillator. As might be expected at sea-level, and in the basement; in those showers

containing penetrating particles, and, in fact nearly all the showers of any kind which were obtained, very few single events occur. It can be imagined that even if one nuclear particle strikes the building, several interactions will take place and the tracks in the chamber come not from one single event but from several related events. In some of these "untidy" showers, the penetrating particles have lost the direction of the incident particle and although produced as π -mesons, many of them enter the chamber as μ -mesons having decayed on the way to the chamber.

It is difficult to assess the efficiency of this system. A simple 4-fold coincidence system using Geiger counters had previously been in use at Aberystwyth. The counting rate of this system was about 1/hour. Not more than 20% of the photographs taken showed any evidence of penetrating particles other than μ -mesons. The present system compares favourable with this even when only one counter is used, and little or no absorber is present. It should be possible with this system to study small showers.

Pure electron showers do not provide much background. The majority of the electron showers observed on these photographs appear to be associated with penetrating particles; either coming indirectly from π^0-decays or 'knock-on's' by π or μ -mesons. A small number of large air showers were observed; photographs showing some hundreds of parallel tracks with an even larger number of low energy electrons of energy less than 1 Mev.

At high altitudes, this system should give good results. An efficient arrangement would consist of a number of small, dense scintillators such as NaI crystals, each covered by its own

photomultiplier. The advantage of using smaller crystals say only 2 cm. diameter would arise from the fact that this should bias in favour of stars. The range of most evaporation particles would be less than the crystal diameter. On the other hand, a large pulse could only be given by a relatively dense shower of fast particles. A large liquid or plastic scintillator placed within the chamber, in coincidence with the NaI scintillators would only be useful if it adequately covered the whole chamber.

ACKNOWLEDGEMENTS

I wish to thank Professor N. Feather, F.R.S. for the use of the facilities of his laboratory.

I am very much indebted to Dr. G.R. Evans, F.R.S.E. for suggesting the subjects for this thesis and for much helpful advice and encouragement throughout the course of the work.

I am grateful to Dr. R.A. Donald for his help in printing some of the plates for this thesis.

I also wish to acknowledge the valuable help given by Mr. A. Headridge and his staff in the construction of apparatus.

I am indebted to the Department of Scientific and Industrial Research for the award of a Research Studentship throughout the course of this work.

References

(1) Ascoli (1952) - R. Ascoli - Nuovo Cimento 9, 610 (1952).

(2) Barford and French (1955) - N.C. Barford - Review Paper - Proceeding of Conference on Cloud Chamber and Associated Techniques - London 1955.

(3) Bay (1951) - Z. Bay - Rev. Sci. Inst. 22, 397, (1951)

(4) Bell (1954) - R.E. Bell. - Annual Review of Nuclear Science 4, 101, (1954).

(5) Bhabha (1938) - H.J. Bhabha - Proc. Roy. Soc. 164, 257, (1938).

(6) Bhabha and Chakrabarty (1948) - H.J. Bhabha and S.K. Chakrabarty Phys. Rev. 74, 1361, (1948).

(7) Binder (1949) - D. Binder - Phys. Rev. 76, 856 (1949).

(8) Birks (1951a) - J.B. Birks - J. Brit. I.R.E. 11, 209 (1951).

(9) Blumenfeld and Lederman (1954) - H. Blumenfeld, E.T. Booth and L.M. Lederman - Rev. Sci. Inst. 25, 1220 (1954).

(10) Boreli and Grimeland (1955) - F. Boreli and B. Grimeland - Il Nuovo Cimento 2, 336, (1955).

(11) Bowen and Roser (1951) - T. Bowen and F.X. Roser - Phys. Rev. 82, 284 (1951).

(12) Bowen and Roser (1952) - T. Bowen and F.X. Roser - Phys. Rev. 85, 992 (1952).

(13) Brooks (1956) - F.D. Brooks - Progress in Nuclear Physics 5, 252 (1956).

(14) Butler et al (1950) - C.C. Butler, W.G.V. Rosser and K.H. Barker - Proc. Phys. Soc. 63A, 145 (1950).

(15) Chang and Rosenblum (1945) - W.Y. Chang and S. Rosenblum - Phys. Rev. 67, 222 (1945).

(16) Cleland and Jastram (1951) - M.R. Cleland and P.S. Jastram - Phys. Rev. 84, 271, (1951).

(17) Cockcroft and Walton (1932) - J.D. Cockcroft and E.T.S. Walton - Proc. Roy. Soc. (Lond.) 137A, 229 (1932).

(18) Collinge et al (1956) - B. Collinge, A.W. Merrison and D. Eccleshall - J. Sci. Inst. 33, 72 (1956).

(19) Davies (1957) - D.N. Davies - Ph.D. Thesis - University of Wales (1957).

(20) Emigh (1954) - C.R. Emigh - Rev. Sci. Inst. 25, 221 (1954).

(21) Fischer and Marshall (1952) - J. Fischer and J. Marshall - Rev. Sci. Inst. 23, 417 (1952).

(22) Gaerttner and Yeater (1949) - E.R. Gaerttner and M.L. Yeater - Rev. Sci. Inst. 20, 588 (1949).

(23) Garlick and Wright (1952) - G.F.J. Garlick and G.T. Wright - Proc. Phys. Soc. 65B, 415 (1952).

(24) Garwin (1953) - Garwin R.L. - Rev. Sci. Inst. 24, 618 (1953).

(25) Gillette (1950) - R.H. Gillette - Rev. Sci. Inst. 21, 294 (1950).

(26) Goldwasser and Nicolai (1955) - E.L. Goldwasser and V.O. Nicolai - Proceedings of London Cloud Chamber Conference (1955).

(27) Hazen (1942) - W.E. Hazen - Rev. Sci. Inst. 13, 247 (1942).

(28) Howland et al (1947) - B. Howland, C.A. Schroeder and J.D. Shipman - Rev. Sci. Inst. 18, 551 (1947).

(29) Luckey and Weil (1952) - D. Luckey and J.W. Weil - Phys. Rev. 85, 1060 (1952).

(30) MacIntyre (1949) - W.J. MacIntyre - Phys. Rev. 76, 312 (1949).

(31) Moody (1952) - N.F. Moody - Electronic Eng. 24, 214 (1952).

(32) Morton (1952) - G.A. Morton - Nucleonics 10, 39 (1952).

(33) Newton (1950) - T.D. Newton - Phys. Rev. 78, 490 (1950).

(34) Park (1956) - E.C. Park - J. Sci. Inst. 33, 257 (1956).

(35) Post and Schiff (1950) - R.F. Post and L.I. Schiff - Phys. Rev. 80, 1113 (1950).

(36) Raffle and Robbins (1952) - J.F. Raffle and E.J. Robbins - Proc. Phys. Soc. 65B, 320 (1952).

(37) Robinson (1953) - E. Robinson - Proc. Phys. Soc. 66, 73, (1953).

(38) Rochester (1946) - G.D. Rochester - Proc. Roy. Soc. 187, 464 (1946).

(39) Rossi (1933) - B. Rossi - Z. Physik 82, 151 (1933).

(40) Rossi and Greisen (1941) - B. Rossi and K. Greisen - Rev. Mod. Phys. 13, 240 (1941).

(41) Rutherford (1919) - E. Rutherford - The London, Edinburgh and Dublin Phil. Mag. and J. Sci. 37, 581 (1919).

(42) Salvini (1951) - G. Salvini - Il Nuovo Cimento 8, 798 (1951).

(43) Strauch (1953) - K. Strauch - Rev. Sci. Inst. 24, 283, (1953).

(44) Swank (1954) - R.K. Swank - Ann. Rev. Nuc. Sci. 4, 111 (1954).

(45) Taylor et al (1951) - C.J. Taylor, W.K. Jentschke, M.E. Remley, F.S. Eby and P.G. Kruger - Phys. Rev. 84, 1034 (1951).

(46) Walker et al (1956) - J. Walker, G. Tagliaferri, J.C. Bower and D.W. Hadley - J. Sci. Inst. 33, 113 (1956).

(47) Wells (1952) - F.H. Wells - Nucleonics 10, 28 (1952).

(48) Williams (1939) - E.J. Williams - Proc. Roy. Soc. 172A, 194 (1939).